

Caveolae-mediated phagocytosis of biomaterial surface structures by human osteoblasts

Dissertation
zur
Erlangung des akademischen Grades
doctor rerum naturalium (Dr. rer. nat.)
der Mathematisch-Naturwissenschaftlichen Fakultät
der Universität Rostock

vorgelegt von

Caroline Mörke

geb. am 30.01.1989 in Teterow

Rostock, März.2016



Datum der Einreichung: 21.03.2016

Datum der Verteidigung: 15.07.2016

Gutachter:

Prof. Dr. J. Barbara Nebe,
Universitätsmedizin Rostock, Zentrum für Medizinische Forschung, AB Zellbiologie

PD Dr. Sergei Kuznetsov,
Universität Rostock, MNF, Institut für Biowissenschaften

Prof. Dr. Jan de Boer
University of Twente, Institute for Biomedical Technology and Technical Medicine, Department of Tissue Regeneration

Content list

Abbreviation list.....	1
1. Introduction.....	3
1.1 Motivation	3
1.2 Anatomy and function of human bone	4
1.3 Biomaterials	7
1.4 Cell-biomaterial interaction	10
1.5 Actin cytoskeleton.....	12
1.6 Endocytosis and caveolae-mediated phagocytosis.....	13
1.7 Signaling cascades and energy requirements during phagocytosis.....	16
2. Material and Methods.....	20
2.1 Materials	20
2.1.1 Reagents.....	20
2.1.2 Buffers/Solutions	21
2.1.3 Kits/Assays/Antibodies.....	22
2.1.4 Consumable materials	25
2.1.5 Laboratory instruments	26
2.2 Methods.....	27
2.2.1 Titanium surface preparation	27
2.2.2 Surface functionalization with plasma polymerized allylamine (PPAAm)	28
2.2.3 Osteoblast cell lines and cell culture experiments	29
2.2.4 Real time-qPCR for mRNA expression analyses.....	31
2.2.5 Protein quantification.....	32
2.2.6 Protein localization via immunofluorescence staining.....	34
2.2.7 Cholesterol quantification and staining.....	35
2.2.8 Cav-1 transfection	35
2.2.9 ATP and ADP measurement	36
2.2.10 Mitochondrial activity.....	36
2.2.11 Reactive oxygen species (ROS) determination.....	37
2.2.12 Live cell imaging	38
2.2.13 Confocal laser scanning microscopy.....	38
2.2.14 Cell morphology analysis.....	39

2.2.15 Statistical analysis	39
3. Results.....	40
3.1 Cell phenotype and cytoskeleton organization on micro-pillars	40
3.2 Osteoblast-specific functions on the micro-pillars	43
3.3 Caveolae-mediated micro-pillar phagocytosis	44
3.4 Micro-particle uptake by human MG-63 osteoblasts	55
3.5 Phagocytosis – ATP and ROS.....	60
3.6 Endocytic and raft proteins, $\beta 1$ -integrin and integrin-associated signaling proteins	63
3.7 Attempted phagocytosis – Signaling molecules.....	67
3.8 Inflammation response of MG-63 osteoblast towards the micro-pillared textures	72
3.9 Micro-pillar coating with plasma-polymerized allylamine (PPAAm)	74
3.10 Attempted phagocytosis on rough stochastic surfaces	78
4. Discussion.....	80
4.1 Nucleus deformation and actin organization on micro-pillars	81
4.2 Caveolae-mediated phagocytosis of the surface-fixed micro-pillars	82
4.3 Micro-particle internalization and inflammatory response	86
4.4 Phosphatidylinositol lipids and their binding protein AnnexinA2	88
4.5 Integrins and integrin-mediated signaling.....	90
4.6 Cell-material surface contact establishment.....	91
4.7 Stochastic rough surfaces and commercial implant designs	93
5. Summary.....	96
Zusammenfassung.....	97
References.....	98
Appendix.....	I
Acknowledgements.....	I
Statutory declaration	II
Publications and Lectures	III

Abbreviation list

3D	3 dimensional
ADP	adenosine diphosphate
ALP	alkaline phosphatase
AKT	protein kinase B
AMPED	2-amion-2-methyl-1,3-propandiol
AnxA2	annexin A2
Arf6	ADP-ribosylation factor 6
Arp2/3	actin related protein 2/3
ATCC	American Type Culture Collection
ATP	adenosine triphosphate
BMP	bone morphogenic protein
BSA	bovine serum albumin
BSP	bone sialo protein
Cav-1	caveolin-1
Cat	catalase
CD	cluster of differentiation or classification determinant
CDC42	cell devision control protein 42
Co	control
Col1	collagen type I
DAPI	4',6-diamidino-2-phenylindole
DCF	2',7'-dichlorofluorescin
DCF DA	2',7'-dichlorofluorescin diacetate
DMEM	Dulbecco's modified Eagle medium
DMSO	dimethylsulfoxide
DNA	deoxyribonucleic acid
DRIE	deep reactive-ion etching process
ECM	extracellular matrix
ER	endoplasmic reticulum
ERK 1/2	extracellular signal-regulated kinase 1/2
FACS	fluorescence activated cell sorting
FAK	focal adhesion kinase
FAK(pY397)	autophosphorylated focal adhesion kinase at its Tyrosine397
FCS	fetal calf serum
Fig	figure
FITC	fluorescein isothiocyanate
FN	fibronectin
G-actin	globular actin
GAPDH	glyceraldehyde 3-phosphate dehydrogenase
GFP	green fluorescent protein
GSK3	glycogen synthase kinase 3

hFOB	human primary fetal osteoblasts
hOB	human primary osteoblasts
HRP	horseradish peroxidase
IκB	inhibitory protein of κB
JC-1	5,5',6,6'-tetrachloro-1,1',3,3'-tetraethylbenz-imidazolyl-carbocyanine iodide
IL	interleukin
IQR	interquartile range
LAMP	lysosome-associated membrane glycoproteins
MFI	mean fluorescence intensity
NFκB	nuclear factor κB
OCN	osteocalcin
OPN	osteopontin
P-1x1x1	1x1x1 μm geometrical micro-pillared titanium surfaces
P-2x2x5	2x2x5 μm geometrical micro-pillared titanium surfaces
P-3x3x5	3x3x5 μm geometrical micro-pillared titanium surfaces
P-5x5	5x5x5 μm geometrical micro-pillared titanium surfaces
PBS	phosphate-buffered saline
pCav-1	phosphorylated caveolin-1
PI(4,5)P ₂	phosphatidylinositol-4,5-bisphosphate
PI(3,4,5)P ₃	phosphatidylinositol-3,4,5-trisphosphate
PI3K	phosphatidylinositol 3-kinase
PPAAm	plasma polymerized allylamine
PRX2	thioredoxin peroxidase
PVDF	polyvinylidene fluoride
Ref	planar titanium reference surface
RhoA	Ras homolog family member A
RGD	arginine-glycine-asparagine amino acid sequence
ROCK1	Rho-associated kinase
ROS	reactive oxygen species
RNA	ribonucleic acid
rpm	revolutions per minute
RT	room temperature
SDS	sodium dodecyl sulfate
SDS-PAGE	sodium dodecyl sulfate polyacrylamide gel electrophoresis
SEM	scanning electron microscopy
siRNA	short interfering RNA
SOD	superoxide dismutase
TCPS	tissue culture polystyrene
Ti-CB	corundum-blasted titanium
Ti-P	polished titanium
TRITC	tetramethylrhodamine
xg	gravitational force
Y	tyrosine

1. Introduction

1.1 Motivation

Defects and inflammation of bone and joints affect several million people worldwide annually. At a time of steadily increasing lifespans, associated with rising requirements on body parts, temporarily and permanent implants undertake the body parts functions and enable their maintenance and consequently also the preservation of the patient's life quality. In 2008, 159,000 hip arthroplasties as well as 146,000 knee arthroplasties were performed in Germany. In comparison to 2004, this represents an increase of 15% for the hip and 33% for the knee arthroplasties [1]. The numbers for the first implanted hip and knee arthroplasties were constant until 2013, but accompanied by an increase in implant revision operations [2]. First cell-biomaterial interactions are pivotal for the acceptance and ingrowth of an implant and despite increasing studies; these complex reactions are not completely understood. Therefore, detailed analyses of the based cellular mechanisms during the first implant ingrowth phase are necessary for the optimization and improvement of the integration as well as acceptance of implants.

Today's biomaterials should not only be inert and biocompatible, they should also be bioactive, so in other words promote and stimulate the regeneration of the surrounding tissue. The surface topography in micro- as well as nanometer range was shown to influence cellular processes, such as cell adhesion, spreading, migration, proliferation, as well as extra-cellular matrix protein production. All these cellular processes are crucial for the first cell-biomaterial interaction and for the first phase of implant ingrowth [3-6].

Previous studies with stochastically rough structures demonstrated enhanced cell adhesion, whereas the cell spreading and proliferation was reduced, accompanied by altered integrin expression and actin cytoskeleton organization [7;8]. These findings led to assumptions of cell structure - cell function dependencies, as well as the ability of the cells to perceive their underlying surface topography. The cellular responses induced by topography variables such as, heights, sharp edges, or roughness are not exactly ascertained.

For the evaluation of the impact of the surface topography on the cell behavior, a defined geometrically designed topography was used. This model implant topography, having a micro-pillared structure, has the advantage of constant repetitive dimensions and facilitated the analysis of topography-induced cellular processes during the initial cell-biomaterial contact. This micro-pillar topography induced a rearrangement of the actin cytoskeleton in osteoblasts into clustered local spots around the pillar edges instead of stress fiber arrangement normally found on planar surfaces.

The resulted cell architecture alteration decreased the synthesis of the extra-cellular matrix (ECM) proteins collagen type I (Col1) and bone sialo protein (BSP), accompanied by a reduced $\beta 3$ -integrin expression, the adhesion receptor for BSP [9]. In addition, the synthesis of the ECM protein fibronectin (FN) was significantly disturbed after 24 h, but after all the phosphorylation state of central signaling proteins, e.g. protein kinase B (AKT) and glycogen synthase kinase 3 (GSK3) remained unaltered on the micro-pillars [10].

Finally, the modes of action of this typical surface-mimicry of the cell's actin of the underlying geometry were still unexplained. The present thesis should enlighten the topography-induced cell architecture and behavior changes of osteoblasts. Additionally, the gathered knowledge provides a new insight into the interaction of osteoblasts with structured biomaterials and the improvement of bioactive implants.

1.2 Anatomy and function of human bone

Bone is a highly organized, metabolic active rigid tissue, which provides structural support for the body in form of the skeleton. The skeleton consists of more than 200 bones and provides protection of vital internal organs. It serves as a reservoir for minerals, such as calcium and phosphate, and regulates the maintenance of these minerals homeostasis, as well as acid-base balance. Bone is formed out of the mesenchyme tissue. In addition, it permits movement and locomotion by providing levers for the muscles. The bone marrow provides the environment of hematopoiesis, meaning the production of cellular blood components [11].

Bone is a heterogeneous composite material consisting of a mineral inorganic phase (70%, mainly compounded by hydroxyapatite ($\text{Ca}_{10}(\text{PO}_4)_6(\text{OH})_2$)), an organic phase (20%), as well as 10% water. The organic phase contains predominantly (90%) collagenous proteins, other non-collagenous proteins and proteoglycans [12]. The collagenous proteins are mostly composed of collagen type I (Col1) with trace amounts of types III and V [11]. Col1 is a unique triple helical molecule forming fibrillar lattices, which provide elasticity of the tissue, stabilizing the ECM, as well as supporting and templating the initial mineral deposition [12]. To the non-collagenous proteins appertain among others osteocalcin (OCN), fibronectin (FN), alkaline phosphatase (ALP) and bone sialo protein (BSP), all categorized as glycoproteins. They were produced by the osteoblasts during their maturation into osteocytes, as well as from osteocytes themselves. Because of this specific expression, they were used as functional markers for the osteogenesis. Some of the non-collagenous proteins, e.g. FN and BSP, contain the integrin-binding arginine-glycine-asparagine amino acid sequence (RGD-sequence), which conveys the ability of the ECM protein to offer binding sites for the integrin cell surface receptors.

This integrin-mediated binding is the basis of many cell attachment and adhesion activities. Whereas the other non-collagenous proteins without integrin-binding sites have different functions than adhesion mediation, e.g. OCN release is part of the bone-turnover signaling cascade [13] and ALP plays a role in the calcification of the bone matrix [11]. BSP also acts as an initiator for the mineralization by triggering the agglomeration of hydroxyapatite [13].

Bone tissue is constituted of three different cell types: the bone-forming osteoblasts, the bone-resorbing osteoclasts and osteocytes. The last are the most commonly found cells in mature bones.

Osteoblasts evolve out of mesenchymal stem cells, regulates besides the bone forming also the bone metabolism and the genesis of osteoclasts. Osteoblasts produce and secrete the collagenous as well as non-collagenous proteins of the organic bone matrix, which is called osteoid. Subsequently, the incorporation of calcium phosphate compounds achieves the mineralization of the osteoid. Completely embedded and integrated osteoblasts into the bone matrix undergo differentiation into osteocytes. Osteocytes and their processes reside inside bone spaces (called lacunae osseae). Via their long cytoplasmic extensions, osteocytes can reach into tiny canals called canaliculi ossei, which are used for exchange of nutrients with the vascular system [13]. Osteocytes are linked metabolically and electrically through gap junctions. As terminally differentiated osteoblasts, the osteocytes synthesize much less matrix proteins compared with osteoblasts. During the differentiation of the osteoblasts from pre-osteoblasts to osteocytes, the osteoblast marker proteins were variously expressed, see **Fig. 1**.

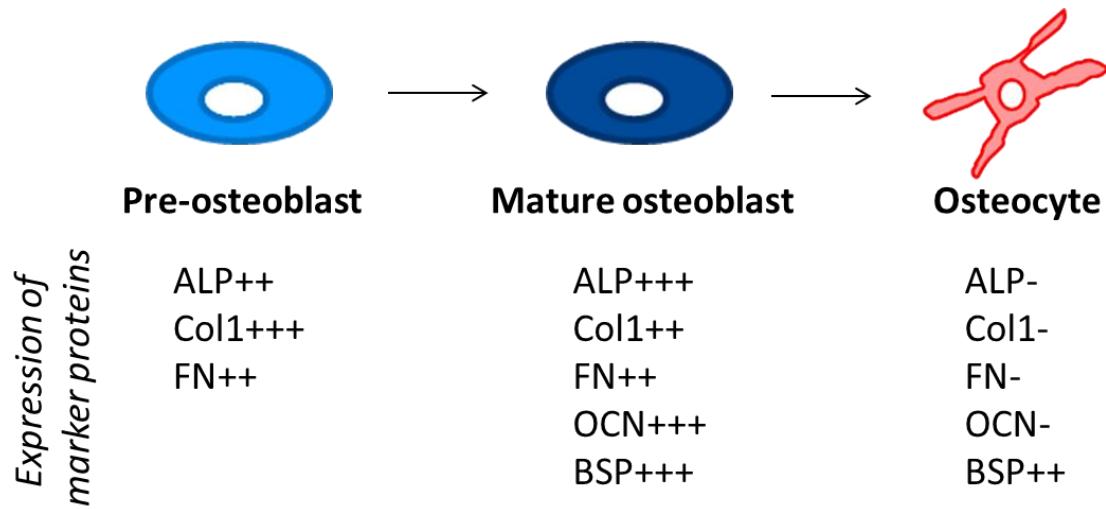


Figure 1: Schematic illustration of the sequential expression of marker proteins during the osteoblast differentiation. Adapted after Figure 1 in [6]. ALP: alkaline phosphatase; BSP: Bone sialo protein; Col1: collagen type-I; FN: Fibronectin; OCN: Osteocalcin; +++: very high expression; ++: high expression; -: low to no expression.

The bone-resorbing osteoclasts are polynucleated cells and derived from mononuclear precursor cells of the monocyte-macrophage (haematopoietic) lineage. Binding of osteoclasts to the bone matrix causes them to become polarized with the bone resorbing surface, developing a ruffled border, which is formed when acidified vesicles are transported via microtubules to fuse with the membrane [11]. The ruffled border vesicles released from the lysosome contain beneath acids (lactic and citric acid), also hydrolytic enzymes (members of the matrix metalloproteinases and cathepsin), which enables the resorption of the mineralized bone matrix [13].

Bone remodeling is the process by which bone is renewed to maintain bone strength and mineral homeostasis by releasing calcium and phosphate. It is a dynamic lifelong mechanism involving the removals of old bone and replacement with newly synthesized bone matrix, also preventing the accumulation of bone micro-damages [11].

Bone remodeling is sequentially carried out composed of tightly coupled, bilateral regulating groups of osteoclasts and osteoblasts. The remodeling process is arranged in four phases: resorption, reversal, formation and mineralization [13]. Resorption involves the recruitment and activation of mononuclear osteoclast precursors at the bone surface and fusion of multiple mononuclear cells to form multinucleated preosteoclasts. Preosteoclasts bind to the bone matrix and form annular sealing zones around bone-resorbing compartments. They develop into osteoclasts and secrete hydrogen ions via the acid-containing vesicles into the resorbing compartments to lower the pH, which helps mobilize bone material. For the digestion of the organic matrix, osteoclasts release hydrolytic enzymes from their lysosomes. Resorption phase is completed after the osteoclasts undergo apoptosis. In the resulted resorption cavities, osteocytes were released from the bone and preosteoblasts are recruited to begin new bone formation by synthesizing and secreting of matrix proteins. Osteoblasts also regulate mineralization of the newly formed bone matrix by releasing vesicles containing calcium and phosphate, as well as enzymes that destroy mineralization inhibitors. With the mineralization, the bone remodeling process is finished and endures up to four months [11]. This means for a healthy human approximately 5-10 % bone replacement each year. Regulation of bone resorption and formation influenced by numerous autocrine and paracrine factors, such as parathyroid hormone, calcitonin and estrogen. A dysbalance between bone resorption and formation can result in pathologic changes, e.g. accelerated bone resorption, accompanied with loss of bone density and fracture predisposition during osteoporosis [13].

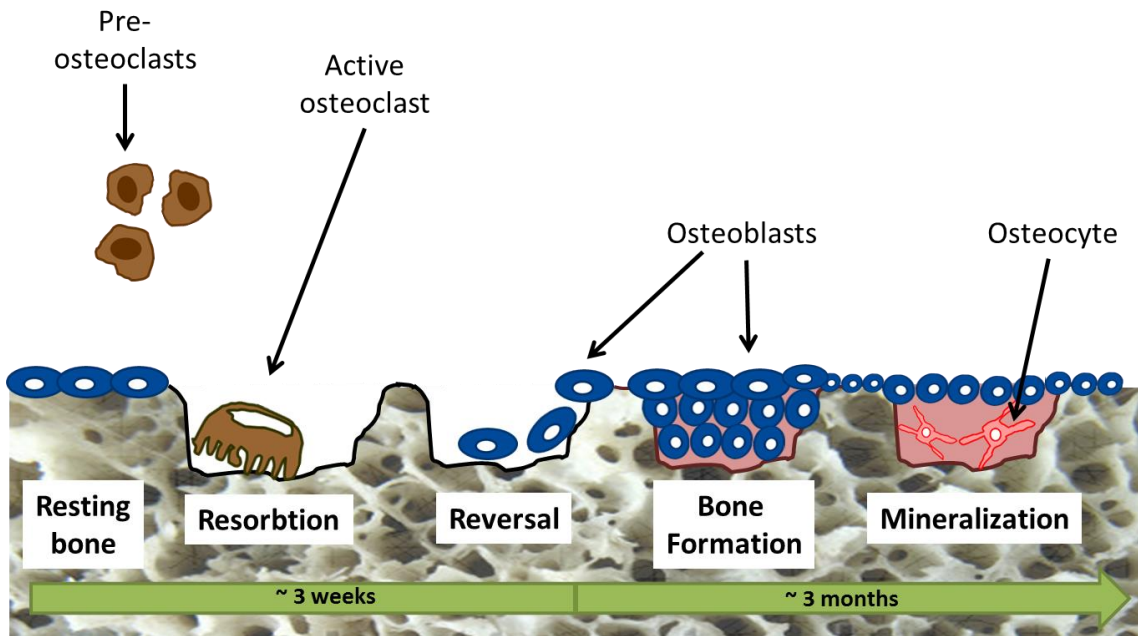


Figure 2: Schematic illustration of the bone remodeling process. Active osteoclasts resorb the bone and subsequently accumulation of osteoblasts achieves bone remodeling and regeneration. Adapted and modified after Figure 1 in [14].

1.3 Biomaterials

Biomaterials are natural or synthetic materials, as well as composites, which are intended to interface with biological systems for an unlimited time to treat or replace a tissue, organ or function of the human body [15]. Current applications not only include functional displacement and supportive scaffolds for guided cell or tissue growth, but also drug delivery systems and external communicating devices.

Considering the enormous advancements, developments of medical treatments and technologies, i.e. drug delivery including nanoparticle treatments, electromagnetically stimulation systems or tissue engineering, the definition was extended by D.F. Williams in 2009 [16]: „*A biomaterial is a substance that has been engineered to take a form which, alone or as part of a complex system, is used to direct, by control of interactions with components of living systems, the course of any therapeutic or diagnostic procedure, in human or veterinary medicine.*” Now the diagnostic medicine including the temporal substitute or medical measuring tools are involved and linked to biomaterials.

The direct contact and consequently physical, chemical and biological interactions of biomaterials with biological systems demand high requirements towards the biomaterial to accomplish its functionality and time stability. Therefore, the biomaterial has to be biocompatible, consequently accepted and tolerated by the body, and should not evoke an inflammatory response resulting in function loss or ultimately a

rejection of the implant. Biomaterials are supposed to have functional similarity to their natural replacement depending on the medical application, thus they also have to fulfill mechanical and technical requirements as well. For the replacement of the hard-tissue, such as bone, in hip and knee prosthetics, high mechanical loadability and rigidity are demanded. On the other side, for soft-tissue biomaterials, e.g. vascular prostheses, a specific elasticity and permeability are crucial to maintain the exchange of components with the surrounding tissue [17].

Considering the steadily increasing importance of biomaterials in the medicine, interaction and stimulation of the surrounding tissue cells are requested for triggering the regeneration of the tissue [18]. The retention time in the body is also a relevant aspect for the biomaterials properties. Permanent implants should have durability for several years and stay in the body ideally for the rest of the patient life, constantly maintaining its function. Hence, it has to have a certain biostability, biological and chemical inertness, to elude unnecessary consecutive and reversion operations.

The number of bone implants to replace and restore the function of damaged or diseased tissue is steadily increasing and because of the high life expectations, the number of reversion operation rises as well. The needed function and application site of the biomaterial define the technical requirements of the used material. Therefore, different materials are used depending on the application. Calcium phosphate, polymer and collagen-hydroxyapatite composites are employed in non-loadbearing sites of the bone, because of their moderate mechanical properties. Metals, such as titanium and its alloys, are used as orthopedic implants because of their high mechanical strength and stability. Titanium is a longstanding established biomaterial utilized in hard-tissues, not only because of its mechanical stability but also because its corrosion resistance and positive physical properties. A nanometer-thick titanium oxide layer is naturally formed in the present of oxygen. This passivation layer alters the physical materials properties, such as increasing the hydrophilicity and therefore facilitating a better protein absorption as well as cell attachment resulting in enhanced interaction with the tissue [19]. Functionality and interaction between biomaterials and cells are decisive for the medical success of the implant, which can be influenced by topographical surface modifications. The interface between biomaterials and cells are important for the stimulation of cell adhesion, spreading, proliferation and differentiation of the cells, which accelerates the implant ingrowth as well as anchorage, known as osseointegration, and finally, the medical success. A successful osseointegration depends also on the “race for the surface” [20] between cells and bacteria, so that an enhanced initial cell-biomaterial interaction reduces an inflammatory response. A biomaterial can be functionalized via topographical, but also chemical surface modification [21].

Topographical modification of biomaterial surfaces offers a huge potential for new implant design strategies and topography-induced cell physiology changes are subjects of intensive research [3-10;22;23].

Cells are able to recognize surface topographies in micron as well as nanometer size and adapt their cellular behavior [24-26]. Micron-scale topography has been reported to induce changes in cell adhesion, morphology, motility and gene expression [25]. Cells can sense nano-topographies with their filopodia down to 10 nm [27]. Despite intensive research, the principles of cellular responses to surface topography are not completely understood. Because many variables influence cellular interactions to surface structures, general cell behavior principles for nano- and micro-topography could not be established [6]. In order to increase the surface contact as well as the mechanical fixation of the implant with the bone tissue, most manufacturers modify the titanium surfaces by blasting with silica, aluminia, glass or titanium particles and create irregular stochastic rough surfaces [26]. Surface profiles of stochastic rough surfaces are shown in **Fig. 3**. Rough surfaces showed an increased osseointegration compared to polished smooth surfaces because of increased cell attachment and adhesion [28;29]. Correlations between the roughness of these stochastic titanium surfaces and cellular functions in MG-63 osteoblasts were found, e.g. increased cell adhesion and differentiation, but decreased cell growth and disturbed actin organization as well as expression of integrin receptors [7;8;30].

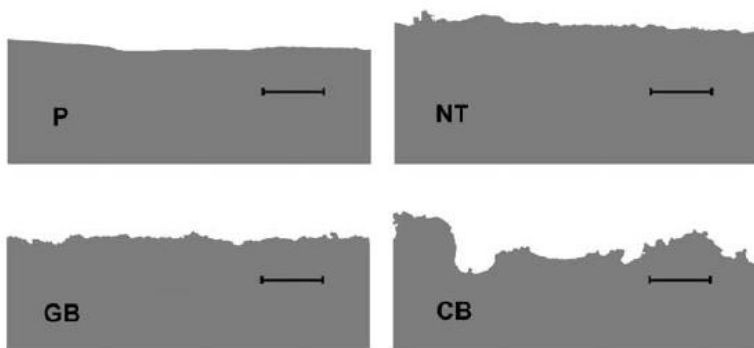


Figure 3: Cross-section images of structured titanium samples demonstrating the depth profile. P: polished; NT: non treated; GB: glass blasted; CB: corundum blasted; bar 20 µm.
Figure was taken out of [6].

Chemical etching is commonly used after the blasting or machining process to further increase the complexity of the surface micro-structure [29]. Interventions to change the surface roughness often produce changes in the adsorbed proteins conformation and concentration. Numerical calculations predict an altered adsorption behavior of proteins near edges and spikes, which may influence subsequent cellular adhesion, spreading and migration [31;32]. Most studies were performed with these stochastic surface models. With growing technical innovations, regularly distributed topographies ranging from micron to nano-scale dimensions can be produced via lithographic or etching processes, such as deep reactive ion etching [3;24].

Another way, to modify implant surfaces, is via chemical surface functionalization by putting an additional layer on the implant. For once, this includes a layer of adsorptive proteins, such as Col1, bone morphogenetic proteins (BMPs), FN or peptide sequences containing the RGD integrin-binding motif [33-35]. Furthermore, physical plasma derived surface functionalization are also a component of research. On surfaces coated with low pressure plasma polymerized allylamine (PPAAm), MG-63 osteoblast showed enhanced cell adhesion and spreading [36]. Surface treatment with an atmospheric pressure plasma jet, e.g. working with argon-oxygen gas, had not only increased cell spreading, but was also able to destroy and eliminate bacterial biofilms [37,38].

1.4 Cell-biomaterial interaction

Adhesion to an ECM is critical for the survival of connective tissue cells, such as osteoblasts and their precursors, which determines their cell growth and responses, e.g. cell spreading, proliferation and differentiation. When cells approach an implant material, they will only adhere to adsorbed ECM proteins from the blood or serum and not to the bare material [33;35;39]. This first cellular attachment, adhesion and spreading will influence the cells capacity to proliferate and to differentiate in contact with the material and is grouped into the first phase of cell-biomaterial interactions [34]. In consequence, the cell adhesion is the deterministic process in cell-biomaterial interaction involving the anchorage of the cells with the biomaterial surface [35]. This complex process includes various biological components, such as the cell membrane and cytoskeletal proteins, which are connected to a functional unit (focal adhesions) and covers different phases. It starts with the rapid attachment phase, where short-term events like physicochemical linkages, e.g. van der Waals and ionic forces, between the cells and the materials promote interactions. Continuing with the longer term active adhesion phase, which involves biological molecules such as ECM proteins interacting with integral cell membrane proteins (integrins) for building the focal adhesions by recruiting adapter proteins (e.g. vinculin, paxillin) and the cytoskeletal polymerization machinery. The focal adhesion induces signal transduction, resulting in the regulation of gene expression [34]. Cell spreading is a process related to adhesion and involves similar extracellular proteins, e.g. vitronectin and FN, which are required for the formation of the intracellular focal adhesions [33,35].

Cell adhesion as well as spreading at adsorbed ECM proteins on a biomaterial surface, is mediated by integrins, a transmembrane receptor, involved in cell-ECM and cell-cell adhesion [40]. Among integrins also selectines, syndecans, immunoglobulins and cadherins are receptors for cell-ECM and cell-cell interactions.

Osteoblasts express cadherins, syndecans and integrins, whereas integrins are the most important for adhesion [34]. But syndecans also act as co-receptors in $\beta 1$ -integrin-mediated cell adhesion [41]. Integrins are heterodimers, consisting of a non-covalently associated α - and β -subunit [40]. Both transmembrane subunits contain a large extracellular domain, which bind to specific amino acid sequences of ECM proteins, e.g. RGD (arginine-glycine-aspartic acid) motif, and mostly short cytoplasmic domains involved in activation of intracellular signaling. 18 α - and 8 β -subunits with 24 different combinations have been reported to date, whereas 12 integrins includes the $\beta 1$ -subunit [42]. $\beta 1$ -integrin represents the predominant adhesion receptor in osteoblasts. Upon ligand binding, integrin associates with the actin cytoskeleton and cluster together to form focal adhesions. Focal adhesions are multifunctional protein complexes more than 200 nm in size, mediating besides cell-ECM adhesion also force transmission, cytoskeletal regulation and signaling [43]. They are dynamic structures containing various different molecules including scaffolding, structural proteins, kinases and phosphatases [44]. Transmembrane integrins bind to the ECM with their extracellular side and adapter proteins such as talin, vinculin and paxillin are recruited to the cytoplasmic side of the integrins in focal adhesions. These adaptor proteins are co-localized with kinases and phosphatases, e.g. focal adhesion kinase (FAK), transducing the signals to the nucleus for regulation of gene expression [43]. So, focal adhesions function as structured links between the ECM and the cytoskeleton [40]. Integrins transmit information about the ECM environment via the kinases and phosphatases in signaling cascades resulting in modified gene expression and cell physiology [34]. This integrin-mediated sensing of the ECM composition as well as topography is called “outside-in” signaling of the bi-lateral transmission [45]. Thus, integrins function as mechanotransducers of extracellular signals that determine subsequent cellular processes, such as cell adhesion, spreading, migration and consequently also cell survival, proliferation and differentiation [40;44;45].

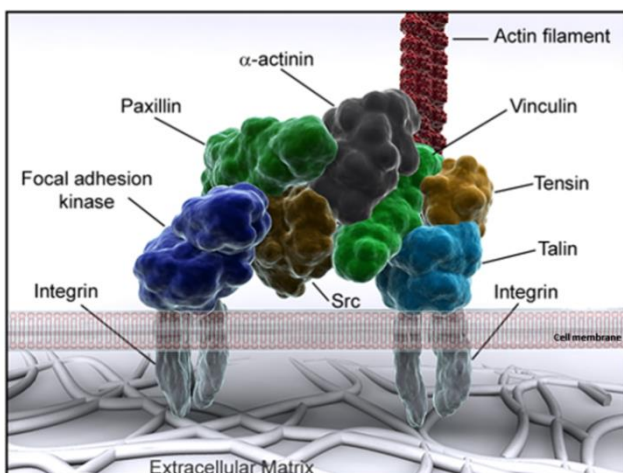


Figure 4: Schematic illustration of the focal adhesion complex. The cell is connected with their environment via the focal adhesion complex, which involves signal transduction from the cell membrane located integrin receptors via the adaptor proteins (e.g. vinculin, focal adhesion kinase or paxillin) to intracellular structures, such as the actin cytoskeleton. Image modified after [46].

Inflammation processes play an important role for the implant osseointegration, not only during the acute inflammatory response triggered in the early periods after injury to initiate tissue repair but also because osteoblasts themselves can produce and secrete cytokines that control inflammation [47]. These pro-inflammatory cytokines, e.g. receptor activator of nuclear factor κ B ligand (RANKL), Interleukin (IL) 1 and 6, regulate osteoclast activation and differentiation; therefore contribute to higher bone resorption [11]. Cytokine production is necessary for regulation of the healing process, but an imbalanced pro-inflammatory response after biomaterial implantation can compromise the implant success. Various stimuli, including orthopedic materials, were reported to induce pro-inflammatory cytokine production in osteoblasts [47]. Especially, phagocytosable wear debris released from the biomaterial stimulate the osteoblasts to produce pro-inflammatory cytokines resulting in bone resorption and implant osseolysis. Nuclear factor κ B (NF κ B) is the predominant regulator of transcriptional activation of inflammatory cytokines and particle challenged osteoblasts showed an activation of the transcription factor NF κ B [48;49].

1.5 Actin cytoskeleton

The actin filaments are one of three cytoskeletal polymers, besides the microtubules and the intermediate filaments. All three are organized into networks controlling the shape and mechanics of eukaryotic cells. They resist deformation and can reorganize in response to externally applied forces, which influence cell morphology and spreading [50]. Actin is the most abundant structural protein, and actin filaments (F-actin), in form of a twisted helix, are generated by adenosine triphosphate (ATP)-dependent polymerization of monomeric globular actin (G-actin). The spatiotemporal F-actin formation is tightly regulated, e.g. by Ras homolog family member A (RhoA, a GTPase that regulates stress fiber formation) and Rock1 (a protein serine/threonine kinase and major downstream effector of RhoA). Forming a network by branching of new nucleated actin filaments is initiated by the actin related protein 2/3 (Arp2/3) complex, which is controlled by the GTPases cell devision control protein 42 (CDC42) [50]. Longer unbranched F-actin networks form actin stress fibers, spanning through the cell and have contact to focal adhesions at least at one end [51]. Actin polymerization orchestrates also the focal adhesions assembly at the cell periphery, resulting into spreading of the cell. Cortical actin microfilaments at the inner face of the cell membrane cause membrane protrusions to form lamellipodia, which test the substrate for adhesive sites. In migrating cells the lamellipodia, or the thinner, but longer form called filopodia, mark the leading edges. Actin stress fiber linkage with activated integrin is not only associated with cell spreading and movement, but also triggers cell-specific intracellular signaling cascades regulating cell proliferation,

differentiation and gene expression. In conclusion, the actin cytoskeleton is a central and essential component in many cell physiological processes [35].

1.6 Endocytosis and caveolae-mediated phagocytosis

Endocytosis is the energy-using uptake of extracellular material into cells by engulfing them in membrane vesicles. It is an active transport form in which cells take up molecules as well as nutrients. Phagocytosis is a special form of endocytosis involving the actin-dependent internalization of large cargos with sizes >0.5 µm [52]. There are mainly three forms of endocytosis: (i) clathrin-mediated endocytosis, where the triskelion-shaped protein clathrin is involved in forming clathrin-coated vesicles, (ii) caveolae-mediated endocytosis and (iii) clathrin and caveolae-independent endocytosis including macropinocytosis, ADP-ribosylation factor 6 (Arf6)-dependent and flotillin-dependent endocytosis. Clathrin- and caveolae-mediated endocytosis are the predominantly applied forms, whereas the clathrin-mediated endocytosis is involved in the uptake of nano-sized cargos smaller than 200 nm [53].

Endocytosis has many functions, among others it controls the composition of the plasma membrane and controls the response of cells with their environment interaction [54]. Consequently, the composition of the plasma membrane is crucial for the endocytosis process. Cell membranes are composed of phospholipid bilayers with embedded proteins, a complex mixture of cholesterol, various glycerolphospholipids as well as sphingolipids. Sphingolipids have longer and more saturated carbon-atom chains, these distinct biophysical properties enable the lipids to behave differently in a monolayer. Glycerolphospholipids show a mobile fluid phase, whereas sphingolipids have a more tightly packed organization because of a stronger lateral cohesion of the longer saturated acyl chains [55]. Phosphatidylinositols belong to the group of glycerolphospholipids because of their unusually large inositol headgroups. They are rapidly metabolized by phosphorylation of the inositol at the positions 3,4 and 5 [56], this phosphorylated inositols have an important role in the regulation of cell movement [53]. During endocytosis, phosphoinositides experience a sequential turnover. Phosphatidylinositol-4,5-bisphosphate ($\text{PI}(4,5)\text{P}_2$) is located in nascent endosomes and is converted by phosphatidylinositol 3-kinase (PI3K) to phosphatidylinositol-3,4,5-trisphosphate ($\text{PI}(3,4,5)\text{P}_3$) in the late engulfment phase [57], see **Fig. 5**. $\text{PI}(4,5)\text{P}_2$ and $\text{PI}(3,4,5)\text{P}_3$ can bind and increase the activity of proteins that modify membrane chemistry and the actin cytoskeleton [53], e.g. the cytosolic protein annexin A2 (AnxA2), which can bind to $\text{PI}(4,5)\text{P}_2$ and is involved in endocytic membrane dynamics, as well as actin cytoskeleton recruiting during phagocytosis. Specific lipid clustering in the cell membrane, such as micro-domain formation rich in cholesterol and $\text{PI}(4,5)\text{P}_2$, are triggered by AnxA2. It not only organizes but also stabilizes lipid micro-

domains, in conjunction with the underlying actin cytoskeleton, because of its actin-binding ability [58]. During phagocytosis, thus the uptake of a solid cargo, a controlled movement of the plasma membrane shaped by the surface to ingest, is driven by the actin cytoskeleton. Actin is concentrated as discrete patches in the advancing cups and forms a belt (ring)-shape band that moves outward over the cargo [53], see also **Fig. 5**. After engulfment, the cargo is localized in an internal vesicle called phagosome, which subsequently fuses with the lysosome, a membrane-bound cell organelle. The lysosome is involved in nutrients digestion, secretion processes and plasma membrane repair [52;53].

CD68, a lysosome-associated membrane glycoprotein (LAMP) family member, is involved in lipid uptake and play an important role in phagocytosis and lysosomal traffic. It was found predominately localized to phagosomal and lysosomal compartments. The expression of CD68 correlate with the activation of professional phagocytic cells, known as macrophages [59], but CD68 was also localized in vesicles of phagocytized titanium particles in osteoblasts [60], making CD68 suitable as marker protein for phagocytosis analysis in osteoblasts as well.

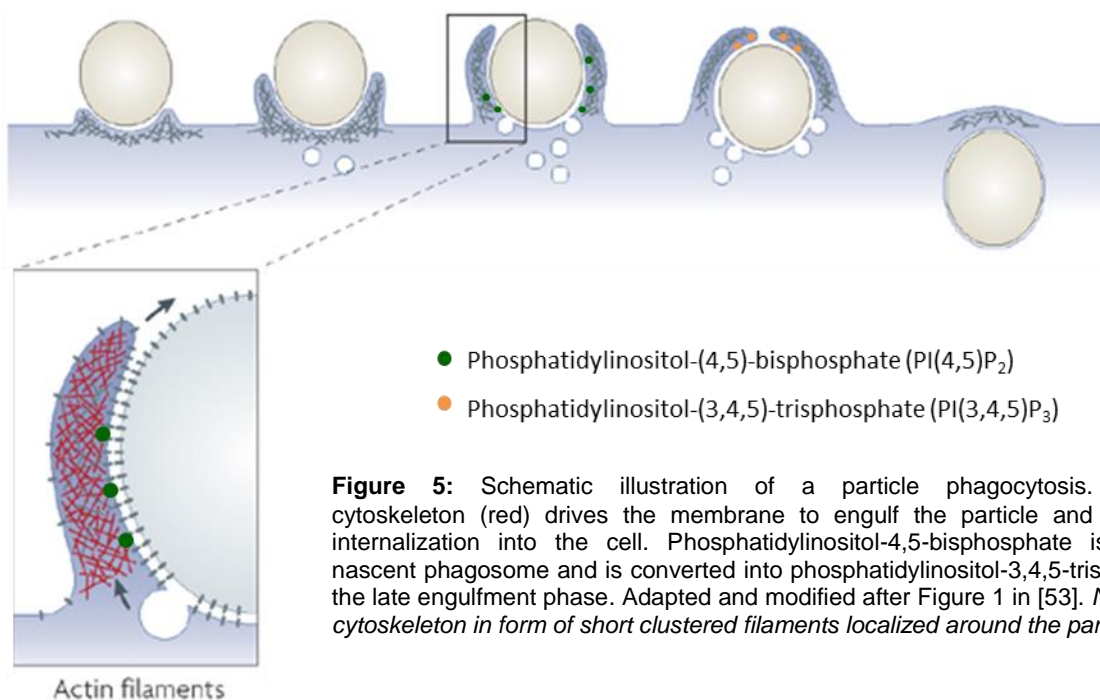


Figure 5: Schematic illustration of a particle phagocytosis. The actin cytoskeleton (red) drives the membrane to engulf the particle and enables the internalization into the cell. Phosphatidylinositol-4,5-bisphosphate is located in nascent phagosome and is converted into phosphatidylinositol-3,4,5-trisphosphate in the late engulfment phase. Adapted and modified after Figure 1 in [53]. Note the actin cytoskeleton in form of short clustered filaments localized around the particle.

Caveolae are 50-80 nm in diameter, cholesterol- and sphingolipid-rich plasma membrane invaginations considering a subdomain of plasma membrane micro-domains, which are called lipid rafts. In the caveolae/lipid raft micro-domains, multiple signaling molecules have been localized, which are involved in various cellular processes, including phagocytosis [61;62] and the transduction of cell surface signals [63]. The raft-dependent/caveolae-mediated phagocytic pathway is regulated by diverse cellular components including caveolin-1 (Cav-1), cholesterol and the actin cytoskeleton, as well as AnxA2 [62;64]. Cholesterol and Cav-1 depletion disrupts the structure of caveolae.

Cav-1 is the major component of caveolae. It binds to 1-2 cholesterol molecules of lipid raft domains and is essential for the formation and stabilization of caveolar vesicles [61]. Cav-1 is synthesized as integral membrane protein in the endoplasmic reticulum (ER). At the ER, Cav-1 goes through a first stage of oligomerization and is then transported to the Golgi complex, forming a newly synthesized protein pool not associated with lipid raft membrane domains. When Cav-1 associates with lipid raft domains, it becomes detergent-resistant and organized into higher-order oligomers, the characteristic form of the surface pool of Cav-1. **Fig. 6** illustrates how Cav-1 is inserted into the caveolar membrane. The N- and C-termini of the protein face the cytoplasm and a “hairpin” intermembrane domain is embedded within the membrane bilayer. The C-terminal domain is close to the intermembrane domain, modified by palmitoyl groups and inserts into the lipid bilayer. The scaffolding domain is a highly conserved region of caveolin and interacts with cholesterol through conserved basic and bulky hydrophobic residues (marked in **Fig. 6** with red circles) [64].

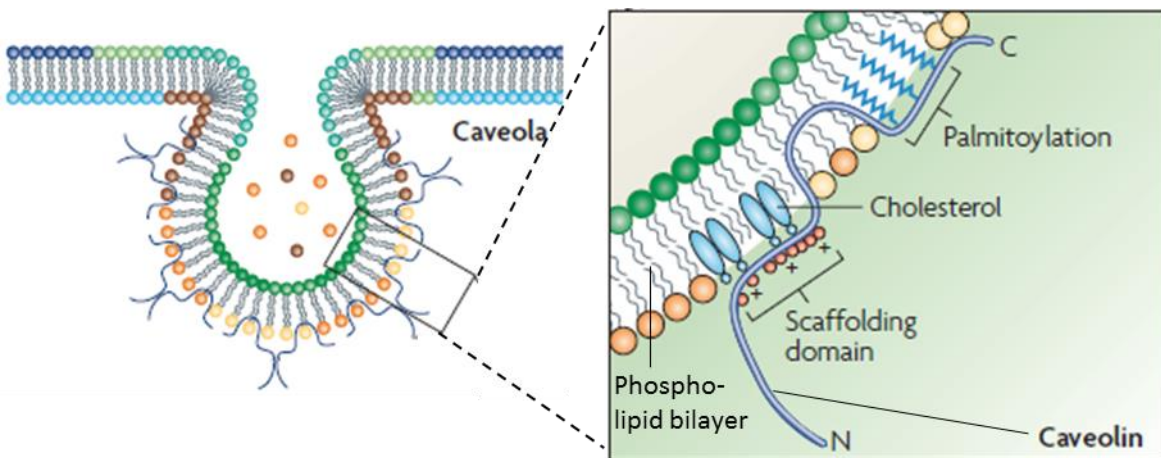


Figure 6: Schematic illustration of the caveolae composition, especially the position of the intermembrane protein caveolin-1 (Cav-1) in the cholesterol enriched plasma membrane regions. Image modified after Figure 1 in [64].

1.7 Signaling cascades and energy requirements during phagocytosis

The regulation of the phagocytic process involves complex signaling pathways including the extracellular signal-regulated kinase 1/2 (ERK1/2) and nuclear factor κ B (NF κ B) pathways. These are implicated in exterior mechanical and force regulation, beneath their function in cell growth, differentiation and stress response. NF κ B plays also a role in inflammation [3;61;65]. The transcription factor NF κ B is found inactive and bound to the inhibitory protein of κ B (I κ B) in the cytoplasm. After activation signals, such as cytokines or stress response, the NF κ B-I κ B-complex gets phosphorylated by the I κ B-kinase and tagged for proteasomal degradation. Free NF κ B translocates into the nucleus and regulates gene expression of over 150 genes [66].

Phagocytosis is a process involving cell mobility or migration around the internalized cargo. Like reported above in the chapter endocytosis, the PI3K is crucial for the phagocytic engulfment, but also for cell adhesion and migration [56]. This highlights the tightly linked signaling cascades between the phagocytosis, cell adhesion and migration. Consequently, also integrins and the focal adhesions with their signaling cascades participate in a phagocytic process [67], starting with the autophosphorylation of FAK at its Tyrosine397 (FAK(pY397)) after interaction of integrins within focal adhesions. This autophosphorylation provide binding sides for Src kinases and other signaling molecules. After the binding to FAK(pY397), Src kinase switch into an active state by autophosphorylation of its Y419 (Src(pY419)), and transphosphorylates FAK, mediates paxillin recruitment and maturation of focal adhesions, as well as connecting them with the actin cytoskeleton. Src-family kinases are needed for focal adhesions turnover and migration, but also for Cav-1 phosphorylation and internalization processes [50]. Cav-1 can be phosphorylated at its Tyrosin14 by Src kinases. The Tyrosin14 phosphorylation of Cav-1 (pCav-1) is required for the recruitment of Cav-1 to the focal adhesions, where Cav-1 associates with β 1-integrins and links the integrins to Src family kinases, which regulates in conjugation with FAK focal adhesions turnover, migration and proliferation [68;69].

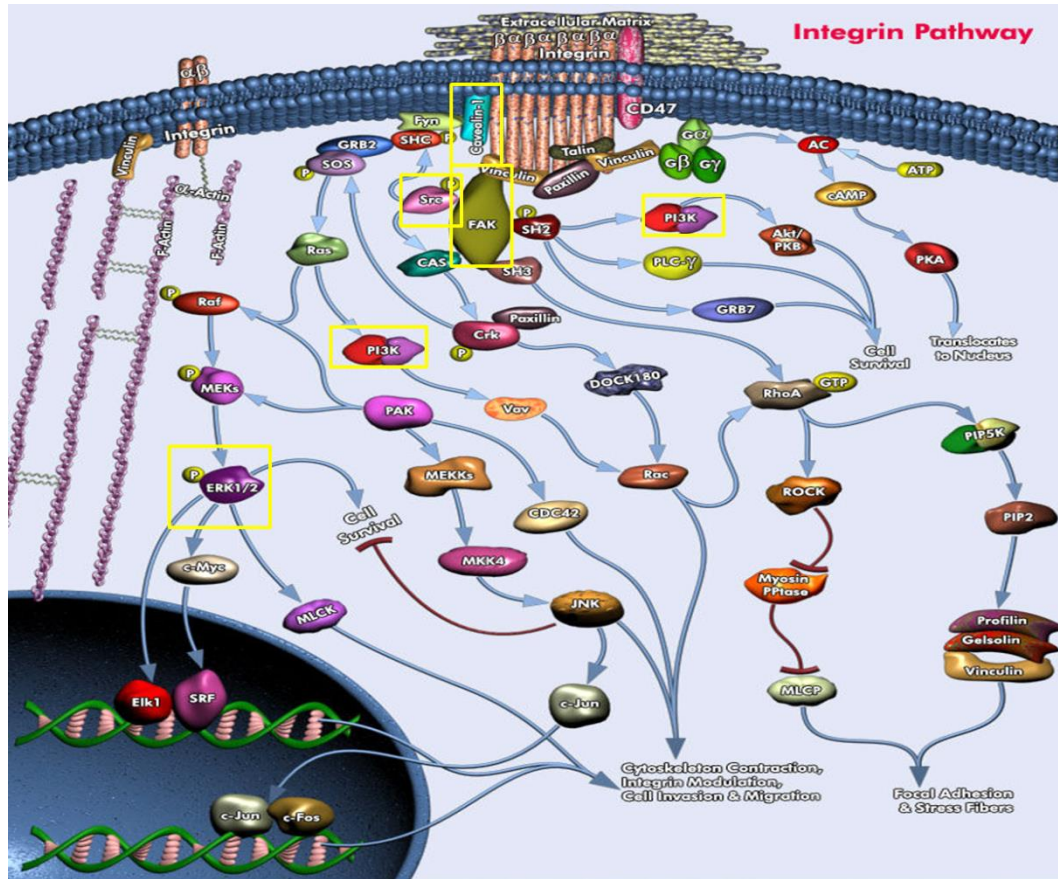


Figure 7: Schematic illustration of the integrin-mediated signaling pathways. In this thesis investigated signaling proteins the extracellular signal-regulated kinase 1/2 (ERK 1/2), focal adhesion kinase (FAK), Src kinase (Src) and phosphatidylinositol-3 kinase (PI3K) as well as caveolin-1 were marked with yellow boxes [70].

Cells as living matter are able to generate metabolic energy, which is required for the maintenance of various cellular functions including phagocytosis, where cells expend energy for the active engulfing movement and internalization [71;72]. The major energy producing pathways in eukaryotic cells are the glycolysis and mitochondrial oxidative phosphorylation, whereas the oxidative phosphorylation is responsible for supplying over 95 % of the total adenosine triphosphate (ATP) requirements. ATP is a coenzyme transporting and transferring chemical energy within the cell [73]. There exists a precise dynamic balance between the production of ATP and the reactions, which utilize ATP. This means, that a higher need for ATP cause an immediate increase in the rate of its synthesis, coupled with the changes in the mitochondrial membrane potential.

The in the inner mitochondrial membrane located ATPases pumps protons across the inner mitochondrial membrane and creates an electro-chemical gradient, the mitochondrial membrane potential. This is in turn used by the ATPase to generate ATP. Mitochondrial membrane potential is an important index of the cells

bioenergetics state, because it is precisely regulated to cope with the energy needs of the cell and directly changes depending on it. In conclusion, metabolic high active cells, such as fast-growing or cancer cells, exhibit a higher mitochondrial membrane potential [74;75]. In addition, oxidative phosphorylation also involves the transport of electrons through a series of protein complexes in the mitochondria. This can cause only partially reduced oxygen or water molecules by a one-electron reduction, resulting in reactive oxygen species (ROS) generation [65].

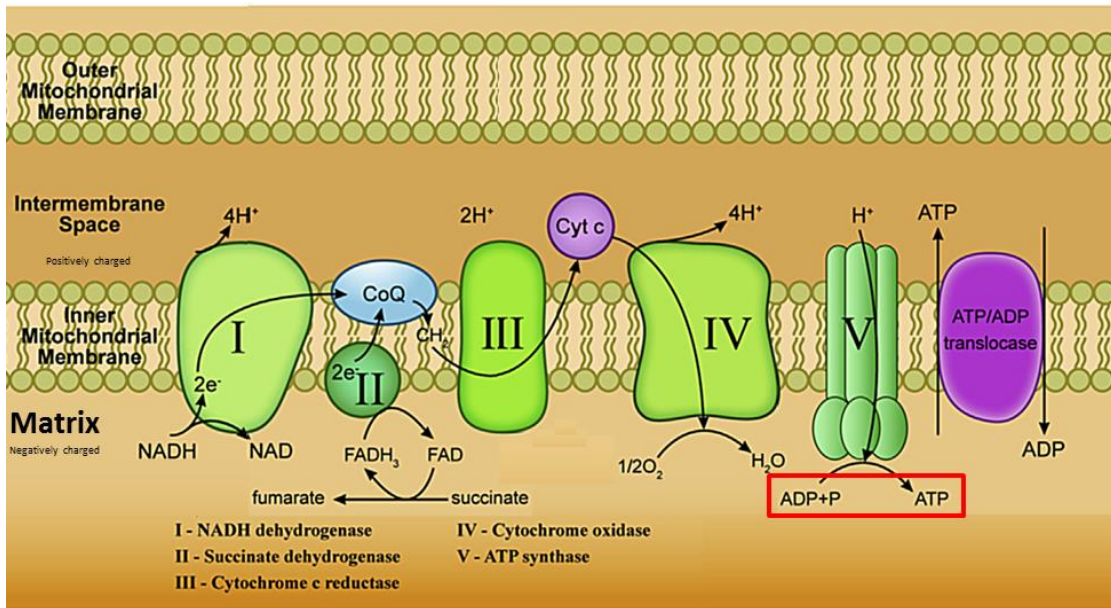


Figure 8: Schematic illustration of the inner mitochondrial membrane including the enzymes participating in the oxidative phosphorylation, hence the ATP production and mitochondrial membrane potential generation. Modified after Figure 8b in [76].

ROS are molecules and ions of oxygen that have an unpaired electron caused by one-electron reduction, which rendered them extremely reactive. They include the superoxide anion (O_2^-), hydrogen peroxide (H_2O_2) and hydroxyl radical (OH^-) [75]. ROS play an important role as mediators in signaling processes, but during stress response, the ROS levels can increase dramatically and damage cell components, e.g. damage of DNA, oxidation of unsaturated fatty acids in lipid and amino acids in proteins. Under most physiological conditions generated ROS are rapidly eliminated by ROS-scavenging enzymes, such as catalases, peroxidases and superoxide dismutases.

Superoxide dismutases convert the superoxide anion (O_2^-) to hydrogen peroxide (H_2O_2) and oxygen (O_2), whereas catalase and peroxidases eliminate the toxic hydrogen peroxide by transforming it into water

(H₂O). Hydroxyl radical (OH[•]) gets eliminated by reactions with antioxidants like glutathione or by oxidizing lipids or amino acids [65].

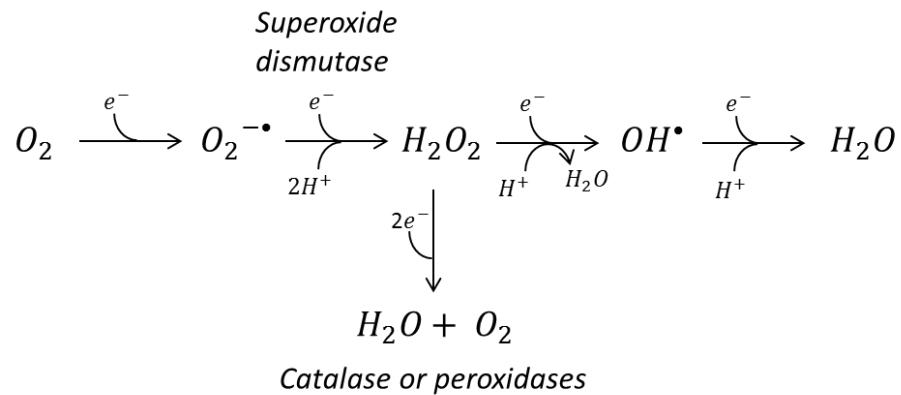


Figure 9: Formation as well as elimination of reactive oxygen species (ROS) by the ROS-scavenging enzymes superoxide dismutase, catalase and peroxidases. O₂: oxygen, e⁻: single electron, H⁺: proton, O₂^{•-}: superoxide anion, H₂O₂: hydrogen peroxide, H₂O: water, OH[•]: hydroxyl radical.

2. Material and Methods

Used chemicals/reagents, assay kits, antibodies, media/ buffer, consumable materials, as well as laboratory instruments with the company information are listed in this chapter. Chemicals/ reagents, as well as antibodies were purchased from the respective companies with the degree of purity *pro analysi*. The distilled water (*A.bidest.*) was taken from the in-house installation.

2.1 Materials

2.1.1 Reagents

5,5',6,6'-tetrachloro-1,1',3,3'-tetraethylbenzimidazolyl-carbocyanine iodide (JC-1)	Life Technologies GmbH, Darmstadt, GER
4',6-diamidino-2-phenylindole (DAPI)	Sigma-Aldrich Co. LLC., St. Louis, MO, USA
Acetic acid (CH ₃ COOH)	Sigma-Aldrich Co. LLC., St. Louis, MO, USA
Aqua bidest. RNase free	Carl Roth GmbH & Co. KG, Karlsruhe, GER
β-Mercaptoethanol	Merck KGAA, Darmstadt, GER
Bovine Serum Albumin (BSA)	Serva Electrophoresis GmbH, Heidelberg, GER
CAV1 siRNA AM16708	Ambion Life Technologies GmbH, Darmstadt, GER
CellLight™ Actin-GFP BacMam 2.0	Life Technologies GmbH, Darmstadt, GER
Collagen Type I Rat Tail	BD Biosciences, Bedfort, MA, USA
Control siRNA AM4613	Ambion Life Technologies GmbH, Darmstadt, GER
Dimethylsulfoxide (DMSO)	Merck KGAA, Darmstadt, GER
DNase	Macherey-Nagel GmbH & Co KG, Düren, GER
Dulbecco's modified Eagle medium (DMEM)	Life Technologies GmbH, Darmstadt, GER
Dulbecco's PBS (1x)	Sigma-Aldrich Co. LLC., St. Louis, MO, USA
Dulbecco's PBS (1x) without Ca/Mg	PAA Laboratories GmbH, Pasching, A
Ethanol	Zentralapotheke, University Rostock, GER
FACS FLOW	BD Biosciences, Erembodegem, BE
FACS Rinse	BD Biosciences, Erembodegem, BE

FAST RED VIOLET LB Salt	Sigma-Aldrich Co. LLC., St. Louis, MO, USA
Femto Dura West Signal	Thermo Scientific, Darmstadt, GER
Fetal Calf Serum (FCS)	Merck KGAA, Darmstadt, GER
Filipin III	Sigma-Aldrich Co. LLC., St. Louis, MO, USA
Fluoroshield	Sigma-Aldrich Co. LLC., St. Louis, MO, USA
Glycerol	Merck KGAA, Darmstadt, GER
Gentamycin 40 mg/ml	Ratiopharm GmbH,Ulm, GER
Glutardialdehyde solution 25 %	Merck KGAA, Darmstadt, GER
Methanol	J.T. Baker, Deventer, NL
MG-63 Transfection Reagent	Altogen Biosystems, Las Vegas, NV, USA
MitoSOX™	Thermo Scientific, Darmstadt, GER
Naphtol AS-MX, phosphate	Sigma-Aldrich Co. LLC., St. Louis, MO, USA
Sodium chloride	Sigma-Aldrich Co. LLC., St. Louis, MO, USA
Paraformaldehyde	Sigma-Aldrich Co. LLC., St. Louis, MO, USA
Phalloidin-tetramethyl-rhodamine	Sigma-Aldrich Co. LLC., St. Louis, MO, USA
Random Primer	Invitrogen AG, Carlsbad, CA, USA
Sodium dodecyl sulfate (SDS)	Merck KGAA, Darmstadt, GER
Skim milked powder	Carl Roth GmbH & Co. KG, Karlsruhe, GER
Superscrip®II Reverse Transcriptase	Invitrogen AG, Carlsbad, CA, USA
TaqMan® Universal PCR Master Mix	Applied Biosystems, Darmstadt, GER
Tris	Carl Roth GmbH & Co. KG, Karlsruhe, GER
Triton-X 100	Merck KGAA, Darmstadt, GER
Trypsin-EDTA (0,05 %)	PAA Laboratories GmbH, Pasching, A
Tween-20	Sigma-Aldrich Co. LLC., St. Louis, MO, USA

2.1.2 Buffers/Solutions

ALP staining solution	100 mM AMPED 0.1 % Naphtol AS MX 0.1 % FAST RED VIOLET LB Salt Aqua dest.
-----------------------	--

Collagen type I solution	200 µg/ml rat tail collagen type I 0.1 % CH ₃ COOH Aqua dest.
Laemmli buffer	62.5 g Tris 5 mg EDTA 10 % Glycerol 2 % SDS 2 % β-Mercaptoethanol
Western blot wash buffer (TBS-T, pH 7.4)	4.84 g (10 mM) 2.32 g NaCl (10 mM) 4 ml Tween 20 (0.1 %) Aqua dest. ad 4l
Electrophoresis buffer (pH 8.3)	25 mM Tris 192 mM Glycerol 0,1 % SDS
Transfer buffer (pH 8.3)	25 mM Tris 192 mM Glycerol 20 % Methanol
ATP/ADP master mix	45.8 µl ATP/ADP assay buffer 0.2 µl ATP/ADP Probe 2.0 µl ATP/ADP Conventer 2.0 µl Developer-Mix

2.1.3 Kits/Assays/Antibodies

Kits

ADP colorimetric/fluorometric assay kit	Abcam, Cambridge, MA, USA
ATP colorimetric/fluorometric assay kit	Abcam, Cambridge, MA, USA
Bio-Rad Protein Assay	Bio-Rad Laboratories GmbH, Munich, GER
Cell Lysis Kit	Bio-Rad Laboratories GmbH, Munich, GER

DCF-DA cellular ROS detection assay kit	Abcam, Cambridge, MA, USA
NucleoSpin®RNA II kit	Macherey-Nagel GmbH & Co KG, Düren, GER
TaqMan® gene expression assays for:	Applied Biosystems, Darmstadt, GER
actin-related 2/3 complex subunit 4 (ARPC4) (Hs00896783_m1)	
alkaline phosphatase (ALP) (Hs00758162_m1)	
caveolin-1 (Cav-1) (Hs00971716_m1)	
cell division control protein 42 (CDC42) (Hs00918044_g1)	
collagen type I (Col1) (Hs0016404_m1)	
extracellular signal-regulated kinase 1/2 (ERK1/2) (Hs01046830_m1)	
fibronectin (FN) (Hs00900054_m1)	
glyceraldehyde 3-phosphate dehydrogenase (GAPDH) (Hs99999905_m1)	
nuclear factor κB (NFκB) (Hs00765730_m1)	
osteocalcin (OCN) (Hs01587813_g1)	
phosphatidylinositol 3-kinase (PI3K) (Hs01046353_m1)	
Ras homolog gene family member A (RhoA) (Hs00357608_m1)	
Rho kinase 1 (ROCK1) (Hs01127699_m1)	

Luminex assays

Human Oxidative Stress Magnetic Bead Panel (H0XSTMAG-18K)	Merck KGAA, Darmstadt, GER
catalase (Cat)	
superoxide dismutase 1&2 (SOD1, SOD2)	
thioredoxin peroxidase (peroxiredoxin 2: PRX2)	
MILLIPLEX MAP Kit for Cell Signaling human	Merck KGAA, Darmstadt, GER
focal adhesion kinase (FAK) (pY397)	
FAK(pY861)	
MILLIPLEX MAP Human Src Family Kinase Kit	Merck KGAA, Darmstadt, GER
Src (pY419)	
MILLIPLEX MAP Kit for Human Bone	Merck KGAA, Darmstadt, GER
Magnetic Bead Panel	
osteoprotegerin (OPG)	
osteocalcin (OCN)	
osteopontin (OPN)	

Luminex Screening assay
interleukin 6 (IL6)

R & D Systems Inc. (Minneapolis, MN,
USA)

Antibodies - Western Blot

Annexin A2 (rabbit polyclonal; 1:1,000)
BSP-2 (rabbit polyclonal; 1:500)
Caveolin-1 (rabbit polyclonal ;1:1,000)
CD68 (rabbit polyclonal; 1:300)
Collagen Type I (rabbit polyclonal; 1:3,000)
ERK 1/2 (rabbit polyclonal)
FAK (mouse polyclonal; 1:1,000)
Fibronectin (rabbit monoclonal; 1:1,000)
NF κ B p65 (mouse polyclonal; 1:1,000)
PI3K p85 α (rabbit polyclonal; 1:1,000)
Src (mouse monoclonal; 1:2,000)
Tyr14 phosphorylated caveolin-1
(rabbit monoclonal; 1:1,000)
GAPDH (mouse polyclonal; 1:1,000)

Anti-rabbit IgG, HRP-linked
(goat polyclonal; 1:5,000)
Anti-mouse IgG, HRP-linked
(horse polyclonal; 1:5,000)

New England Biolabs GmbH, Frankfurt/Main, GER
Acris Antibodies GmbH, Herford, GER
New England Biolabs GmbH, Frankfurt/Main, GER
Proteintech Group Inc., Chicago, IL, USA
Rockland Immunochemicals, Limerick, PA, USA
New England Biolabs GmbH, Frankfurt/Main, GER
BD Transduction, Franklin Lakes, NJ, USA
Sigma-Aldrich Co. LLC, St. Louis, MO, USA
Santa Cruz Biotechnologies Inc., Dallas, TX, USA
Santa Cruz Biotechnologies Inc., Dallas, TX, USA
New England Biolabs GmbH, Frankfurt/Main, GER
BD Transduction Lab, Franklin Lakes, NJ, USA

Santa Cruz Biotechnologies Inc., Dallas, TX, USA

New England Biolabs GmbH, Frankfurt/Main, GER

New England Biolabs GmbH, Frankfurt/Main, GER

Antibodies – Immunofluorescence

Annexin A2 (rabbit polyclonal; 1:15)
 α -tubulin (rabbit polyclonal; 1:50)
Caveolin-1 (rabbit polyclonal ;1:400)
CD68 (rabbit polyclonal; 1:50)
Clathrin heavy chain (rabbit polyclonal; 1:100)
CD29 9EG7 (mouse monoclonal; 1:100)

New England Biolabs GmbH, Frankfurt/Main, GER
Santa Cruz Biotechnologies Inc., Dallas, TX, USA
New England Biolabs GmbH, Frankfurt/Main, GER
Proteintech Group Inc., Chicago, IL, USA
Bioss Inc., Woburn, MA, USA
BD Transduction Laboratories, Franklin Lakes, NJ

Tyr14 phosphorylated caveolin-1 (rabbit monoclonal; 1:50)	Santa Cruz Biotechnologies Inc., Dallas, TX, USA
NFκB p65 (mouse polyclonal; 1:50)	Santa Cruz Biotechnologies Inc., Dallas, TX, USA
PI3K p85α (rabbit polyclonal; 1:50)	Santa Cruz Biotechnologies Inc., Dallas, TX, USA
PIP2 Anti-phosphatidylinositol (mouse monoclonal 1:200)	Abcam, Cambridge, MA, USA
anti-rabbit-IgG-AF488 (goat polyclonal; 1:200)	Life Technologies GmbH, Darmstadt, GER
anti-mouse-IgG-AF488 (chicken polyclonal; 1:100)	Life Technologies GmbH, Darmstadt, GER
anti-rabbit-IgG-AF594 (goat polyclonal; 1:200)	Life Technologies GmbH, Darmstadt, GER

2.1.4 Consumable materials

Black 96-well plate	Greiner Bio-One GmbH, Kremsmünster, A
Cellometer Counting Chambers	Nexcelom Bioscience LLC, St. Laurence, MA, USA
Cell culture flasks: T ₂₅ , T ₇₅	Greiner Bio-One GmbH, Kremsmünster, A
Cell culture dish 4-well Nunc	Thermo Scientific Inc., Waltham, MA, USA
Cell culture dish 35 mm	Greiner Bio-One GmbH, Kremsmünster, A
Cell culture plates: 6-well, 12 well, 24-well	Greiner Bio-One GmbH, Kremsmünster, A
Cell scraper	Life Technologies GmbH, Darmstadt, GER
Criterion TM TGX Stain-Free TM Precast Gel	Bio-Rad Laboratories GmbH, Munich, GER
Cover slides (10 x 10 mm; 0.17mm thick)	Menzel GmbH, Braunschweig, GER
FACS Falcon 5 ml	BD Biosciences, Erembodegem, BE
Filter paper	Whatman International Ltd., Maidstone, UK
FlexiPERM®	Life Technologies GmbH, Darmstadt, GER
IBIDI μ-Dish (35 mm, high)	Ibidi LLC, Verona, WI, USA
Cryotube Cryo.S	Greiner Bio-One GmbH, Kremsmünster, A
Melanine 6 µm particles marked with FITC	Sigma-Aldrich Co. LLC., St. Louis, MO, USA
Object slide	Menzel GmbH, Braunschweig, GER
Optical adhesive film	Applied Biosystems, Darmstadt, GER
Optical 96-well reaction plate	Applied Biosystems, Darmstadt, GER

Pasteur pipettes	Plastibrand, BRAND, Wertheim, GER
Pipette tips: 10 µl, 100 µl, 1,000 µl, 5,000 µl	Greiner Bio-One GmbH, Kremsmünster, A
Pipettes serologic	Greiner Bio-One GmbH, Kremsmünster, A
PVDF membrane	Roche Diagnostics GmbH, Mannheim, GER
Tubes: 5 ml, 15 ml, 50 ml	Life Technologies GmbH, Darmstadt, GER
Safe-Lock-Tubes: 0.5 ml, 1.5 ml, 2.0 ml	Eppendorf AG, Hamburg, GER
SafeSeal tips: 10 µl, 20 µl, 200 µl, 1,000 µl	Biozym Scient. GmbH, Hessisch Oldendorf, GER

2.1.5 Laboratory instruments

Bio-Plex 200 array System	Bio-Rad Laboratories GmbH, Munich, GER
Cellometer®Mini	Nexcelom Bioscience LLC, St. Laurence, MA, USA
Centrifuge 5810R (10 - 50 ml tubes)	Eppendorf AG, Hamburg, GER
Centrifuge 5417R	Eppendorf AG, Hamburg, GER
Clean bench: Safeflow 1.2	Nunc™, Wiesbaden, GER
CO ₂ incubator series CB	BINDER GmbH, Tuttingen, GER
Confocal laser scanning microscope LSM780	Carl Zeiss AG, Oberkochen, GER
Criterion™ Cell	Bio-Rad Laboratories GmbH, Munich, GER
Critical point dryer K850	Emitech GmbH, Taunusstein, GER
FACSCalibur	BD Biosciences, Erembodegem, BE
Field emission scanning electron microscope Merlin VP	Carl Zeiss AG, Oberkochen, GER
ImageLab-ChemiDoc-MP	Bio-Rad Laboratories GmbH, Munich, GER
Heater MHR13	HCL, BioTech, Bovenden, GER
Magnetic separation block for 96-well plates	Merck KGAA, Darmstadt, GER
NanoDrop 1000	Thermo Scientific Inc., Waltham, MA, USA
Pipettes: 0.5-10 µl, 10-100 µl, 100-1,000 µl, 1,000-5,000 µl	Eppendorf AG, Hamburg, GER
Pipette helper (Accu®Jet pro)	BRAND GmbH & Co KG, Staufen, GER
Power Supply EPS 301	Amersham Pharmacia Biotech, Amersham, UK
PTC-150 MiniCycler™	Biozym Scientific GmbH, Oldendorf, GER
Real-Time PCR Applied Biosystem 7500	Applied Biosystems, Darmstadt, GER
Reflected-light microscope Axiovert 100	Carl Zeiss AG, Oberkochen, GER

Refrigerator	LIEBHERR, Ochsenhausen, GER
Rosys Anthos 2010	Anthos Mikrosysteme GmbH, Krefeld, GER
Scanning electron microscope DSM 910A	Carl Zeiss AG, Oberkochen, GER
Shaker: ST 5 CAT	NeoLab, Heidelberg, GER
Sputter Coater SCD 004	BAL-TEC, Macclesfield, UK
Suction system	INTEGRA Biosciences GmbH, Fertwaland, GER
Tecan Infinity 200	Tecan Group Ltd., Männedorf, CHF
Trans-Blot® Cell	Bio-Rad Laboratories GmbH, Munich, GER
Vortex mixer: REAX top	Heidolph Instruments GmbH, Kelheim, GER
Water bath: Type 1002	Gesellschaft Labortechnik mbH, Burgwedel, GER

2.2 Methods

2.2.1 Titanium surface preparation

Geometrically structured: For the cell-material interaction analysis, defined periodically micro-textured samples (size 1 cm²) with regular cubic pillar geometry having a dimension of 5x5x5 µm in width x length x height and 5 µm in spacing (P-5x5) were used throughout the experiments. In addition, micro-pillars with the dimensions 1x1x1 µm in width x length x height and 1 µm spacing (P-1x1x1); 2x2x5 µm and 2 µm spacing (P-2x2x5) as well as 3x3x5 µm and 3 µm spacing (P-3x3x5) were used. Unstructured, plane surfaces (Ref) were employed as controls. The samples were fabricated by deep reactive-ion etching (DRIE) of silicon wafers at the Center for Microtechnologies (University of Technology Chemnitz, Germany). For the DRIE process, the silicon wafers were concealed with a mask of silicon oxide (SiO₂) to cover the non-etching regions. Afterwards, a two-step dry etch process was applied at which etch and passivation steps alternated. For the etching process, the silicon wafers were treated in a plasma reactor with sulfur hexafluoride (SF₆) in high frequent plasma with argon. The chemical isotropic etch reaction and the physic anisotropic material removal occurred of the generated reactive gas, accompanied with the acceleration of the ions in an electric field. The etch reaction was stopped by initiating a gas mixture into the plasma reactor, which created a passivation layer on the sample surface that increased the anisotropy of the etching process. This two-step dry etch process was repeated until the desired topography depth was accomplished. Subsequently, the mask leftovers were removed and the samples were sputtered with 100 nm titanium. Before usage of the titanium arrays, they were treated for 10 min with 70 % ethanol and rinsed thrice with PBS. The samples were only used once and then discarded.

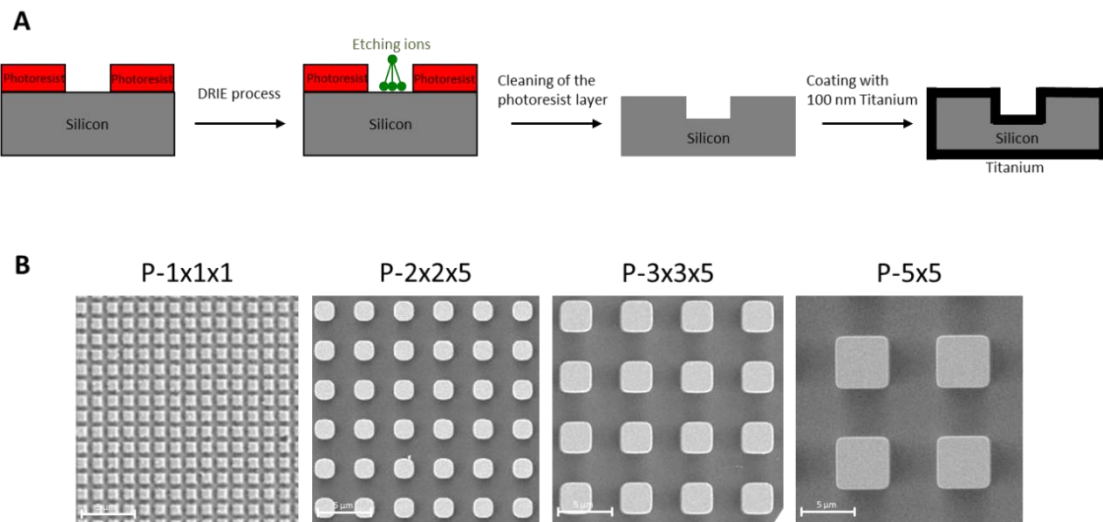


Figure 10: Geometrical micro-pillar topographies. **(A)** Schematic illustration of the deep reactive-ion etching (DRIE) process of silicon wafers printed with a photoresist layer (red) to determine the etching regions. After cleaning of the photoresist layer the micro-structured silicon wafer is sputtered with 100 nm titanium. **(B)** Scanning electron microscopy images of the used micro-pillar topographies, magnification 1,000x, bar 5 μ m, Merlin VP (Carl Zeiss).

Stochastically structured: As commercially available rough implant model surfaces, corundum blasted titanium disks and as controls polished titanium disks (diameter 30 mm, titanium with technical purity grade 2) from the company DOT GmbH (Rostock, GER) were purchased. Polishing was performed with SiC grinding paper (grit P4000) and corundum blasting with aluminum oxide particles 500-600 μ m in size at 6 bar. The surfaces revealed an average roughness values R_a of 0.19 μ m for the polished Ti and 6.07 μ m for the corundum blasted Ti [7;8]. Before usage the samples were ultrasonically cleaned for 5 min, sterilized with 70% ethanol for 10 min and washed thrice with PBS.

2.2.2 Surface functionalization with plasma polymerized allylamine (PPAAm)

The DRIE-fabricated Ti arrays were decontaminated and activated by pulsed oxygen plasma (500 W, 50 Pa, 100 sccm O₂/25 sccm Ar, 30 s effective) and coated by the plasma polymerization of the precursor allylamine using pulsed low pressure microwave plasma (2.45 GHz, 500 W, 50 Pa, 50 sccm allylamine/50 sccm Ar, 480 s effective) in a plasma reactor (V55G, Plasma Finish) of the Leibniz Institute of Plasma Science and Technology (INP) Greifswald (GER) [36].

2.2.3 Osteoblast cell lines and cell culture experiments

Cell types: The human osteoblast-like cell line MG-63 (American Type Culture Collection ATCC®, CRL-1427) was used throughout the experiments. The MG-63 osteosarcoma cell-line is established as model system for *in vitro* experiments of cell-material interactions because the cell-line conserved functional properties of primary osteoblasts, such as pattern of gene expression and adhesion, as well as signaling pathways [7;8;22]. Therefore, the MG-63 osteoblasts show similar sensitivity regarding topographical characteristics such as primary osteoblasts [77], having the advantage of continuously cell dividing and availability.

In addition, for the indicated investigations the human osteoblast-like cell lines SaOs-2 (ATCC, HTB-85) and U-2Os (ATCC, HTB-96), as well as human primary fetal osteoblasts (hFOB, ATCC, CRL11372) and human primary osteoblasts (hOB, PromoCell) were used. MG-63, SaOs-2 and U-2Os were grown in Dulbecco's modified eagle medium (DMEM, Life Technologies GmbH) with 10% fetal calf serum (FCS) (Biochrom FCS Superior, Merck KGaA) and 1% gentamycin (Ratiopharm GmbH) at 37 °C in a humidified atmosphere with 5% CO₂. hFOB were grown in Ham's F12 DMEM (Life Technologies GmbH) with 10% FCS (Biochrom FCS Superior, Merck) and hOB were cultured in osteoblast growth medium (PromoCell GmbH) at 37 °C in a humidified atmosphere with 5% CO₂.

Before use of the hOB, alkaline phosphatase production by the cells was verified, to ensure the cells are functional osteoblasts. Therefore, the cells were fixed with 4% paraformaldehyde for 10 min at RT, washed with Aqua dest. and then stained for 10 min with ALP staining solution. The resulted red colorization was observed under the reflected-light microscope Axiovert 100 (Carl Zeiss) and indicates ALP activity of functional osteoblasts.

Cell cultivation: Before thawing of the cryo-conserved cells (10⁶ cells in 1 ml) in a water bath with 37°C (2 min), 15 ml cell culture media was preincubated in a 75 cm² cell culture flask for 15 min in the incubator at 37°C and 5% CO₂. The thawed cells were then transferred into the prepared cell culture flask. 24 h later, a media change was performed to remove dead cells and the toxic dimethylsulfoxide (DMSO), which is part of the cryo-media. After 3 days, the cells formed a confluent monolayer at the cell culture flask bottom. At this point, the cells were ready to passage. For the passages as well as experiment seeding, the cells were rinsed with 5 ml PBS without Ca²⁺/Mg²⁺ (PAA Laboratories) and detached from the flask bottom by incubation with 2 ml 0.05% trypsin- 0.02% ethylenediaminetetraacetic acid (EDTA, PAA Laboratories) for 5 min in the incubator at 37°C. Trypsin is a protease which cleaves proteins after the amino acids arginine and lysine. As consequence, it lyses the adhesion proteins of the cells and achieves the cell detachment [78]. This process is called trypsinization.

The addition of the bivalent cation chelate complex builder EDTA enables stabilization of cell adhesion membrane proteins and the detached cells were resuspended in cell culture media. The FCS in the cell culture media contains protease inhibitors that hinder the trypsin-EDTA reaction. Determination of the cell number in the solution was done by filling 20 µl of the cell solution into the Cellometer Counting Chambers (Nexcelom Bioscience), read out and counted by the Cellometer™ (Nexcelom Bioscience).

According to the respective experimental setup, the cells were seeded onto the titanium samples and in a new cell culture flask. Only cell passages 5-25 were used for the experiments because higher passages inclined to inconstant cell growth. The cell growth and morphology was controlled with an inverse light microscope (Axiovert25, Carl Zeiss AG).

Cell seeding: In all experiments for the investigated cultivation times of 3, 24, and 48 h, 15,000 cells/cm² were seeded onto the samples placed in NUNC 4-well dishes (Thermo Fisher Scientific) or 6-well plates (Greiner Bio-One International GmbH). For the cultivation times of 72 and 96 h, 5,000 cells/cm² were seeded onto the samples and after 48 h a media change was made. For cultivation against gravity, the cells were seeded onto the Ti samples and after 15 min the samples were flipped around and placed on a spacer, so the cells hanging upside down from the pillars only secured by the adhesion to the pillars. Before use, the titanium samples were washed in 70% ethanol for 10 min and rinsed thrice in PBS.

Inhibition experiments: Filipin III (Sigma-Aldrich) is a macrolide pentene polyene, a class of substance that binds cholesterol and is commonly used as caveolae/lipid raft-inhibitor [79]. For caveolae inhibition purpose, vital, non-fixed MG-63 cells were incubated with 0.5 µg/ml Filipin III in DMEM for 15 min at 37 °C and 5 % CO₂ after 24 h cultivation on the Ti surfaces.

For phosphatidylinositol 3-kinase (PI3K) inhibition, the cells were treated with 10 µM LY294002 (Cell Signaling) after the seeding of the cells for the experiments.

Particle internalization: For internalization experiments, MG-63 cells were incubated with melamine particles 6 µm in size marked with FITC (Sigma Aldrich). For this purpose, cells were seeded on cover glasses and incubated for 1 h at 37 °C and 5% CO₂ to ensure adhesion. Afterwards, the cells were incubated with the 6 µm particles with a concentration of 10⁵/ml for 24 h (see **Fig. 11a**). Untreated cells grown on cover glass served as control. For mimicking the basal uptake, the micro-particles were fixed on the cover glass before cell seeding (see **Fig. 11b**). Therefore, the cover glass was coated with a 200 µg/ml rat tail collagen type I solution (BD Bioscience) for 1 h, after discarding the supernatant, the micro-particles (with a concentration of 10⁵, based on manufacturer's data sheet) were added and dried overnight under a clean bench.

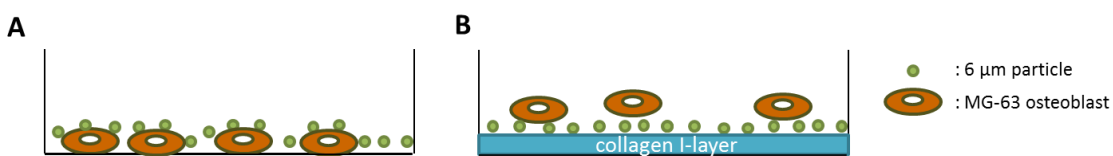


Figure 11: Schematic illustration of the 6 μm -sized particle internalization experiments. **(A)** Incubation of MG-63 cells seeded on a cover glass with micro-particles from the apical cell side. **(B)** Seeding of the MG-63 cells to micro-particles fixed on a collagen I-layer.

2.2.4 Real time-qPCR for mRNA expression analyses

Total RNA was isolated using a NucleoSpin®RNA II kit (Macherey-Nagel GmbH & Co KG), which includes the elimination of any genomic DNA by DNase (Macherey-Nagel GmbH & Co KG) treatment. The purity and quantity of the resulting RNA were determined via measurement of the absorbance at 280 nm and 260 nm with the Nano Drop 1000 (Thermo Scientific). 50 ng of total RNA was used for first strand cDNA synthesis using Superscript®II Reverse Transcriptase and Random Primers (Invitrogen AG). The real time quantitative polymerase chain reaction (Rt-qPCR) was performed using TaqMan® Universal PCR Master Mix and TaqMan® gene expression assays for actin-related 2/3 complex subunit 4 (ARPC4), alkaline phosphatase (ALP), caveolin-1 (Cav-1), cell division control protein 42 (CDC42), collagen type I (Col1), extracellular signal-regulated kinase 1/2 (ERK1/2), fibronectin (FN), glyceraldehyde-3-phosphate dehydrogenase (GAPDH), nuclear factor κ B (NF κ B), osteocalcin (OCN), phosphatidylinositol 3-kinase (PI3K), Ras homolog gene family member A (RhoA) and Rho-associated kinase 1 (ROCK1) (Life Technologies GmbH), all listed in the chapter **2 .1.3 Kits/Assays/Antibodies** under “*Kits*”. TaqMan® gene expression assays consist of a pair of unlabelled PCR primers and a TaqMan® probe with a fluorescent dye label (FAM™; fluorescein) on the 5' end as well as nonfluorescent quencher on the 3' end. The quencher molecule inhibits the fluorescence signal of the fluorophore as long as the fluorophore and the quencher are in proximity. The unlabelled primers are designed to anneal within a specific DNA region. The Taq polymerase (component of the TaqMan® Universal PCR Master Mix) extends the unlabelled primer and synthesizes the nascent strand. The 5' to 3' exonuclease activity of the Taq polymerase degrades the labelled probes, that has annealed to the template and this degradation relieves the quenching effect. The detected fluorescence is directly proportional to the fluorophore released and the amount of DNA template present in the PCR [80]. TaqMan® PCR assay for each target gene was performed in triplicates of 4 independent experiments. The PCR was performed with Real-Time PCR Applied Biosystem 7500 and the data were collected and analyzed by the 7500 System SDS Software (Applied Biosystems). Each expression was calculated relative to GAPDH (ΔCt) and then relative to the references ($\Delta\Delta \text{Ct}$).

2.2.5 Protein quantification

The quantifications of desired proteins were performed with two different methods, for once via western blot and secondly with the Bio-Plex®200 luminex bead multiplex analysis system (Bio-Rad Laboratories GmbH).

Preparation and concentration determination of the protein lysates

The BioPlex cell lysis kit (Bio-Rad Laboratories GmbH) was used for the cell lysis. Therefore, the MG-63 cells were washed three times with the kit provided wash buffer and then treated with ice-cold lysis buffer for 30 min, while shaking with 300 rpm on ice. Afterwards, the samples were rinsed with the lysis buffer to ensure a complete suspension of the cells, transferred into an Eppendorf reaction vessel and centrifuged for 10 min at 4 °C and 15,000 g. The supernatant contained the suspended proteins, conveyed into a new Eppendorf reaction vessel and were stored at -20 °C. Protein quantification was performed using the Bradford method in a 96-well micro-plate format. The Bradford method is a colorimetric spectroscopic measurement of the triphenylmethane dye Coomassie Brilliant-Blue, which features an absorption shift during protein binding [81]. Absorbance of the Bradford reagent (Bio-Rad Protein Assay, Bio-Rad Laboratories GmbH) was measured with the Rysos Anthos 2010 (Anthos Mikrosysteme GmbH) at $\lambda_{\text{ex}} = 595$ and $\lambda_{\text{em}} = 360$.

A BSA dilution row with concentrations ranging from 0 – 10 µg/ml served for the calculation of an absorbance-concentration plot. Secreted proteins were measured out of the cell culture media supernatant, which was collected after 24, 48 and 96 h cell culture time and stored at -20 °C.

Western-Blot and densitometric analysis

Immunoblots were performed from total lysates of MG-63 cells, which were cultivated on the Ti arrays for 3, 24 and 96 h. Total cellular protein was separated by SDS-PAGE (Bio-Rad Laboratories GmbH) and afterwards transblotted to PVDF membranes (Roche Diagnostics GmbH) via wet blot in a Trans-Blot® Cell (Bio-Rad Laboratories GmbH) for 1 h at 400 mA.[82;83]. Analyses were done for annexin A2 (AnxA2), bone sialo protein 2 (BSP-2), caveolin-1 (Cav-1), CD68, collagen Type I (Col1), extracellular signal-regulated kinase 1/2 (ERK 1/2), focal adhesion kinase (FAK), fibronectin (FN), nuclear factor κB (NFκB p65), phosphatidyl-3 kinase (PI3K p85α), Src kinase, Tyr14 phosphorylated caveolin-1 (pCav-1),

glyceraldehyde 3-phosphate dehydrogenase (GAPDH) with the listed antibodies in the chapter **2.1.3 Kits/Assays/Antibodies** under “*Antibodies-Western Blot*”. The membranes were incubated over night at 4°C with the appropriate primary antibody diluted in 5 % BSA in TBS-T, followed by 1 h incubation at RT with horseradish peroxidase (HRP)-conjugated secondary antibody diluted in 5 % skim milk in TBS-T (New England Biolabs GmbH), listed in the chapter **2.1.3 Kits/Assays/Antibodies** under “*Antibodies-Western Blot*”. Primary antibody binding was detected by using a fast chemiluminescent substrate for HRP (Femto Dura West Signal, Thermo Scientific). For each detected protein, 4 independent experiments were analyzed. Immunoblotting analyses were carried out with ImageLab-ChemiDoc-MP (Bio-Rad Laboratories GmbH) and the densitometric analysis with ImageJ (Wayne Rasband, National Institute of Health). GAPDH, as well as the gel stain free with total protein loading, were used as endogenous control.

Bio-Plex®200 luminex bead multiplex analysis

The Bio-Plex®200 system is a bead-based luminex xMAP™ technology for multiplex analysis. During the Bio-Plex assay an antibody binds to the target protein. This antibody is covalently bound to a paramagnetic micron-sized bead. These beads are filled with two fluorophores in various ratios and enable the differentiation of the emitted light into 100 distinct sections in the red channel. This red fluorescence is specific for the protein. Subsequently a second detection antibody binds to another epitope of the protein and is coupled with the fluorescent reporter (streptavidin-phycerythrin), which is specific for the quantification. The detection is performed via excitation of the fluorophores by two lasers with different wavelength in the flow cell in the Bio-Plex®200 system. Excitation of the beads at 635 nm with the first laser in the red channel identify the respective protein, excitation of the labeled reporter with the second laser at 523 nm let determine the quantity of the targeted protein, because the intensity of the emitted green light is proportional to the quantity of the targeted protein [84]. The investigated cellular proteins catalase (Cat), superoxide dismutase 1&2 (SOD1, SOD2), thioredoxin peroxidase (PRX2), the phosphorylated focal adhesion kinase (FAK) at Y397 (FAK(pY397)) and Y861 (FAK(pY861)), phosphorylated Src at Y419 (Src(pY419)) as well as the secreted proteins osteocalcin (OCN), osteopontin (OPN) and interleukin 6 (IL6) with their associated assays are listed in the chapter **2.1.3 Kits/Assays/Antibodies** under “*Luminex assays*”. For the luminex assay measurement, a 96 well plate was wetted with 200 µl washing buffer, supplied with each assay. The suspension of the magnetic beads coupled with the specific antibodies were sonicated for 30 sec, vortex for 1 min and then transferred to a mixing bottle. 25 µl of the bead mix was transferred to each well of the 96-well plate and mixed with 25 µl of the protein lysates for the cellular protein quantification or 25 µl of the cell culture supernatant for the quantification of secreted proteins, as well as 25 µl of standard and control samples, supplied by each

assay for the quantification of the specific protein concentration. The samples mixed with the magnetic beads were incubated over night at 4 °C shaking with 300 rpm. For the decantation of the well contents, the 96-well plate was put onto a hand-held magnetic separation block (Merck KGaA), which attracts the magnetic beads coupled with the antibodies bonded to the specific proteins desired to detect. The wells were washed three times with 200 µl washing buffer and incubated with 50 µl of a detection antibody solution that was supplied with each assay for 30 min at RT while shaking for 300 rpm. Afterward 50 µl of a Streptavidin-Phycoerythrin solution, also supplied with each assay, was added to each well and incubated for 30 min at RT while shaking for 300 rpm, followed by washing thrice with 200 µl washing buffer. For the detection run, 100 µl washing buffer was added to each well and the plate shook for 5 min at 300 rpm for the resuspension of the magnetic beads.

The protein quantification was collected with the Bio-Plex-System (Bio-Rad Laboratories GmbH) and the Bio-Plex Manager™ 4.1.1 software (Bio-Rad Laboratories GmbH), measured in Mean Fluorescence Intensity (MFI). The MFI values were normalized on the with the Bradford method measured protein lysate concentrations.

2.2.6 Protein localization via immunofluorescence staining

Osteoblastic cells were cultured on the Ti arrays (cell seeding of 15,000 cells for 3, 24, 48 h and 5,000 cells for 72, 96 h incubation time), washed three times with PBS and were then fixed with 4 % paraformaldehyde (10 min at RT) (Sigma-Aldrich). After washing thrice with PBS, the cells were permeabilized with 0.1 % Triton X-100 (10 min, RT) (Merck KGaA), washed again three times with PBS and blocked with 2 % bovine serum albumin (BSA) (Sigma-Aldrich) in PBS (30 min, RT).

Actin: For actin filament staining, the cells were incubated with phalloidin coupled with tetramethylrhodamine (TRITC) (5 µg/ml in PBS, Sigma-Aldrich) for 1 h at RT in the dark.

Immunolabeling: The immuno-fluorescent staining of the targets annexin A2, α-tubulin, caveolin-1, CD68, clathrin heavy chain, activated β1-integrin (CD29 9EG7), Tyr14 phosphorylated caveolin-1, NFκB p65, PI3K p85α and PIP2 (anti-phosphatidylinositoles) antibody labeling was performed with the antibodies listed in the chapter **2.1.3 Kits/Assays/ Antibodies** under “Antibodies - Immunofluorescence”. The primary antibodies (diluted in PBS) were used for the immunolabeling at RT for 1 h. Secondary antibodies are also listed in the chapter **2.1.3 Kits/Assays/ Antibodies** and were applied for 30 min at RT in the dark.

Nuclei: Nuclei were stained with a 1 µg/ml 4',6-diamidino-2-phenylindole (DAPI) solution (Sigma-Aldrich) for 15 min at RT. The DAPI dye intercalates into DNA double strands and enables their labeling in this way. Nucleus shape was quantified by calculating the circularity of each individual nucleus, described circularity = $4\pi A/P^2$, where A is the nucleus area and P is the nucleus perimeter. Circularity with the value of 1 reflects a perfectly round nucleus, whereas polygonal forms were displayed by a form factor < 1.0.

The samples were embedded with fluoroshield mounting media (Sigma-Aldrich) and the experiments were repeated 3 times.

2.2.7 Cholesterol quantification and staining

Filipin III is not only used as caveolae inhibitor, the interaction with cholesterol also alters the Filipin III fluorescence spectra allowing visualization of excitations at 340-380 nm and emission at 385-500 nm [79]. MG-63 cells were cultivated for 24 h on the Ti arrays. For the cholesterol quantification, the cells were washed with PBS, trypsinized and suspended in PBS with $\text{Ca}^{2+}/\text{Mg}^{2+}$ to stop the trypsinization reaction. A centrifugation at 400 xg for 5 min was performed. The cells were washed in PBS and fixated with 4 % paraformaldehyde (10 min, RT), again washed with PBS and incubated with 100 µg/ml Filipin III in PBS (30 min, RT). A centrifugation at 400 xg for 5 min was performed after every step. Fluorescence was measured in triplicates of 5 independent experiments in a black 96-well plate (Greiner Bio-One International GmbH) by Tecan Infinity 200 (Tecan Group Ltd.) with $\lambda_{\text{ex}} = 360 \text{ nm}$ and $\lambda_{\text{em}} = 480 \text{ nm}$. Filipin III solution without cells and cell solution without Filipin III were used as blanks during the calculation.

For the cholesterol staining, the cells on the Ti arrays were washed three times with PBS and were then fixed with 4 % paraformaldehyde (10 min at RT). After washing thrice with PBS, cholesterol staining was performed with 2.5 µg/ml Filipin III in PBS for 15 min at RT.

2.2.8 Cav-1 transfection

Small interfering RNA (siRNA) or silencing RNA is a class of RNA molecules, 20-25 base pairs in length. These RNA molecules interfere with the expressed mRNA of specific genes with complementary nucleotide sequence, leading to degradation of the mRNA and resulted in no protein translation [85].

In this thesis, siRNA against Cav-1, as well as control siRNA were obtained from Ambion (Life Technologies GmbH). For the transfection, 30,000 MG-63 cells were seeded in a 24-well plate and cultured overnight. Then the cells were transfected with 50 nM siRNA using MG-63 Transfection Reagent (Altogen Biosystems) according to the manufacturer's instructions. 48 h after the transfection, the cells were ready for further experiments. Once, they were treated for 24 h with 6 µm particles and secondly they were also trypsinized and seeded onto the Ti arrays for 24 h. The transfected cells were stained for the actin cytoskeleton via phalloidin-TRITC and Cav-1as already described above.

2.2.9 ATP and ADP measurement

MG-63 osteoblasts were cultured for 24 h on the Ti samples. Adenosine triphosphate (ATP) measurements were determined using the ATP colorimetric/fluorometric assay kit (Abcam, Cambridge, MA, USA) and adenosine diphosphate (ADP) with ADP colorimetric/fluorometric assay kit (Abcam). Measurements were performed using the fluorometric assay. Cells on the samples were washed with ice-cold PBS, trypsinized, washed twice with PBS and resuspended in 150 µl ATP- or ADP assay buffer. Past the second wash step, a 20 µl sample was taken for the cell counting with the Cellometer (Nexcelom Bioscience LLC). After a centrifugation at 4°C and 13,000 xg for 2 min, the supernatant was collected into a new Eppendorf reaction vessel. 50 µl of the collected supernatant and 50 µl of the ATP- or ADP master mix (composition listed in the chapter **2.1.2 Buffers/ Solutions**) were transferred into a black 96-well plate and incubated for 30 min at RT protected from light. Fluorescence was measured in triplicates in a black 96-well plate by Tecan Infinity 200 (6 independent experiments for the micro-pillared surfaces, 4 independent experiments for Ti-P and Ti-CB disks as well as for the particle-treated cells) with 5×10^4 cells for the Ti arrays (DRIE etched surfaces, Ref and P-5x5) and with 1.5×10^5 cells for the 6 µm particle treatment, as well as the polished (Ti-P) and corundum-blasted titanium (Ti-CB) disks for each triplicate. During the assay, no deproteinization step was performed, so the temporally used ATP bound by proteins was not measured, only the free ATP or ADP concentration in the cells.

2.2.10 Mitochondrial activity

The potential-sensitive fluorescence dye JC-1 (5,5',6,6'-tetrachloro-1,1',3,3'-tetraethylbenz-imidazolyl-carbocyanine iodide) (Life Technologies GmbH) was used to measure the mitochondrial activity [86].

The dye was dissolved to a stock concentration of 2.5 mg/ml in DMSO. MG-63 cells were cultivated for

24 h on the Ti arrays and then stained in a vital state with 10 µg/ml JC-1 in DMEM for 15 min at 37 °C in a humidified atmosphere with 5% CO₂. Afterwards the cells were rinsed twice with PBS and the fluorescence was immediately acquired with the inverted laser scanning microscope LSM 780 (Carl Zeiss AG) using a 20x (EC Plan-Neofluar) objective (Carl Zeiss AG). Therefore, the Ti arrays were placed into an IBIDI µ-Dish^{35 mm high} (IBIDI LCC) with the adherent cells towards the bottom of the dish containing 2 ml of PBS. Green fluorescence was observed through the bandpass of 493 - 578 nm and red fluorescence through 568 - 712 nm. Red/green fluorescence was measured with the ZEN 2011 (black version) software (Carl Zeiss AG) by collecting the individual single cell green and red fluorescence of 150 cells at each surface of 2 independent experiments.

2.2.11 Reactive oxygen species (ROS) determination

Intracellular ROS generation was assessed by using 2',7'-dichlorofluorescein diacetate (DCF-DA) (DCF-DA cellular ROS detection assay kit, Abcam). After washing with PBS, the cells were trypsinized and resuspended in PBS with Ca²⁺ /Mg²⁺ (PAA Laboratories). A centrifugation at 400 xg for 5 min was performed. The cells were washed again with PBS, followed by another centrifugation step. Subsequently, the cells were resuspended in a 20 µM DCF-DA solution and incubated for 30 min at 37 °C in the dark. As positive control, cells cultured at tissue culture polystyrene TCPS were treated with 50 µM tert-butyl hydrogen peroxide in the cell culture media for 1 h before staining. ROS in the cells cause oxidation of DCF-DA, yielding the fluorescent product 2',7'-dichlorofluorescein (DCF) [87]. The DCF fluorescence was measured in the flow cytometer FACSCalibur (BD Biosciences, excitation 488 nm). For data acquisition and analyses the software CellQuest Pro 4.0.1 (BD Biosciences) was used and results of 4 independent experiments were presented as arbitrary units (mean channel) of fluorescence intensity.

Mitochondrial ROS was quantified with the fluorescent dye MitoSOX™ Red (Thermo Fisher Scientific). MitoSOX™ Red is rapidly and selectively targeted to the mitochondria, where it is exclusively oxidized by superoxide and exhibits red fluorescence. MitoSOX™ Red was dissolved in DMSO to a 5mM stock solution. Working solution with the concentration of 5 µm MitoSOX™ Red was prepared in PBS containing Ca²⁺ and Mg²⁺. After washing the cells with PBS the MitoSOX™ Red working solution was added and incubated for 10 min at 37°C and 5 % CO₂. Subsequently, the cells were collected by trypsinization, washed and supplemented with PBS (with Ca²⁺/Mg²⁺). Measurements were performed with the flow cytometer FACSCalibur (BD Biosciences, excitation 488 nm). For data acquisition and analyses the software CellQuest Pro 4.0.1 (BD Biosciences) was used. Results of 4 independent experiments were presented as arbitrary units (mean channel) of FL-2 fluorescence intensity.

2.2.12 Live cell imaging

For the observation of actin in living cells, the green fluorescent protein (GFP)-actin baculovirus expression vector (CellLight™ Actin-GFP BacMam 2.0, Life Technologies) was transfected into MG-63 cells. The BacMam technology is based on double stranded DNA insect viruses (baculovirus) as vehicles to efficiently deliver and express genes in mammalian cells. The baculovirus has been modified by engineering of mammalian expression cassette for transgene expression in mammalian cells [88]. In this case, the DNA coded for actin coupled with GFP is contained in the BacMam particles, which were taken up by endocytosis, released for transcription and expression following migration to the nucleus. Therefore, 2 µl of BacMam 2.0 reagent per 10,000 cells were added in the cell culture media and incubated for 24 h at 37°C and 5% CO₂ to ensure the expression of actin coupled with GFP. Afterwards, the cells were trypsinized and seeded onto the Ti arrays for 15 min to ensure adhesion. Then the Ti arrays were placed into an IBIDI µ-Dish^{35 mm high} (IBIDI LCC) with the adherent cells towards the bottom of the dish, containing 2 ml of DMEM. The actin dynamics of the vital cells was visualized with the inverted confocal laser scanning microscope using a 20x (EC Plan-Neofluar) objective (Carl Zeiss AG) under incubation at 37°C and 5 % CO₂. Thus, actin dynamics were visualized with cultivation against gravity. Image acquisition was every 10 min for 7 h and converted to a video via the ZEN 2011 (black version) software.

2.2.13 Confocal laser scanning microscopy

Fluorescent image acquisitions of fixed and vital cells were performed by confocal laser scanning microscopy. The advantage of the confocal laser scanning microscopy towards conventional light microscopy is the option of displaying only one focus plane of the sample's reflected and emitted light. Generated light beyond the focus plane is suppressed by a variable pinhole [89].

This gives the opportunity to visualize sharp and high defined images of the investigated sample. A versatile mirror system enables optical sections in defined distances in the xy- and xz-dimensions and consequently with 3 dimensional (3D) z-stack generation. A focused laser beam scanned the sample point wise, which resulted in reduced scattered light from the neighboring regions, higher definition and contrast for the image in the focal plane. Light sensitive radiation detectors (Photomultiplier) recognize the generated fluorescence light intensities of the point wise measurements and convert them into electrical signals for reconstruction of the whole image. Image acquisition was done on an inverted confocal laser scanning microscope LSM 780 (Carl Zeiss AG).

The ZEISS oil immersion objective (C-Apochromat63) and the ZEN 2011 (black version) software (Carl Zeiss AG) were used for the image acquisition. All images were displayed as three dimensional (3D) z-stacks (13 stacks with an interval of 1 μm). Experiments were repeated at least three times. Z-stacking was used to generate a 3D representation to understand the overall cell structures not limited to one horizontal plain of the micro-topography, e.g. the top of the pillars. Thus, a false interpretation due to different observation levels (confocal principle) could be avoided.

For live cell imaging (see 2.2.12) cells were visualized using a 20x (EC Plan-Neofluar) objective (Carl Zeiss AG) under incubation at 37 °C and 5 % CO₂. Image acquisition was every 10 min for 7 h and converted to a video via the ZEN 2011 (black version) software.

2.2.14 Cell morphology analysis

Cell morphology of MG-63 osteoblast was examined by scanning electron microscopy. Therefore, the cells were washed with PBS three times and then fixed with 2.5 % glutardialdehyd (Merck KGaA) for 1 h at RT, dehydrated through a graded series of ethanol (30, 50, 75, 90 and 100 % for 5, 5, 15, 10 min and twice for 10 min, respectively), dried in a critical point dryer (K 850, EMITECH). The samples were sputtered with gold for 100 s (layer ca 20 nm) (SCD 004, BAL-TEC). Scanning electron microscopy (SEM) observations were performed with the scanning electron microscope DSM 960A (Carl Zeiss AG) and the field-emission scanning electron microscope MerlinVP microscope (Carl Zeiss AG) at the Electron Microscopy Center, University Medical Center Rostock.

2.2.15 Statistical analysis

Statistical analyses were carried out with GraphPad Prism5 software (GraphPad Software Inc.). Results are presented in box plots with medians, quartiles and an interquartile range (IQR) \pm 1.5 x IQR. Data analyses were performed using the Mann-Whitney U test. P-values < 0.05 were considered to indicate significant differences.

3. Results

3.1 Cell phenotype and cytoskeleton organization on micro-pillars

Actin is the essential element of the cytoskeleton, known to have a primal role in diverse cellular processes, controlling the functional and morphological behavior of cells. Changes in the cell morphology and the cell nucleus shape dependent on the growth of MG-63 osteoblasts on the micro-pillared topography (dimension 5x5x5 µm, P-5x5) are shown in **Fig. 12**. Cell morphology studies were performed with scanning electron microscopy (SEM). The MG-63 osteoblasts exhibited an elongated phenotype on the pillar structures, also observed by Staehlke and Matschegewski et al. [10;90].

The cells spread out on the top of the pillars and only the filopodia reached out to the bottom of the topography. This was opposite to the planar reference samples (Ref), where the MG-63 cells showed a randomly oriented, flattened phenotype and attachment with the entire cell body to the surface.

MG-63 osteoblasts strongly adapt to the micro-pillar topography and fluorescent staining of the nucleus should show if the deformation also extends to the interior of the cell. Microscopic analysis of the dyed nuclei revealed a nucleus deformation, when growing on the micro-pillars (**Fig. 12b**). The nucleus embedded the pillars, leading to a decline of nucleus circularity, indicating a less rounded shape, because of the deformation by the micro-pillar topography.

To investigate whether the actin polymerization machinery is altered by the micro-pillars, gene expression analysis of genes involved in the actin polymerization were carried out. Therefore, the actin related protein 2/3 (Arp 2/3) complex (ARPC4), the cell devision control protein 42 (CDC42), Ras homolog family member A (RhoA) and Rho-associated protein kinase (ROCK1) were analyzed. It has been seen, that the gene expression of the proteins responsible for actin filament or network formation are not influenced by the micro-pillared topography (**Fig. 13**).

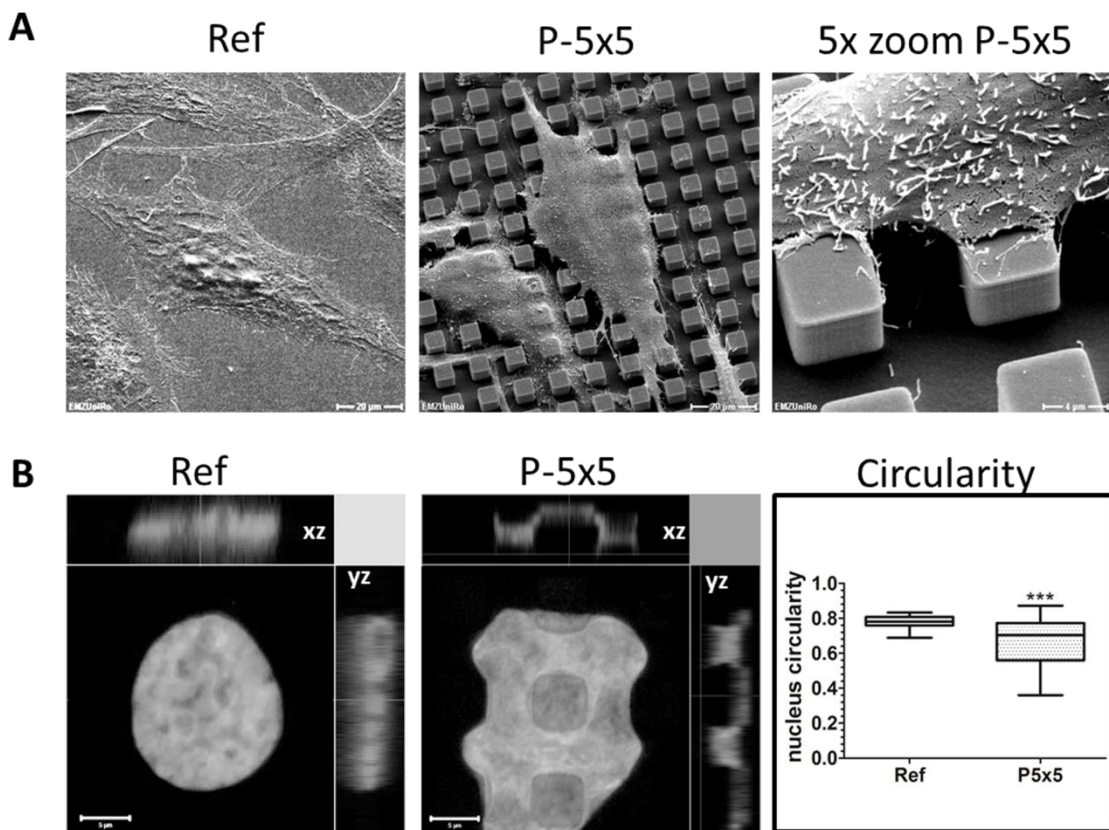


Figure 12: Morphology of MG-63 cells on the micro-pillared topography (P-5x5) compared to the planar reference after 24 h. **(A)** Scanning electron microscopy (SEM) images, (left and middle: 1,000x magnification, bar 20 µm; right: 5,000x magnification, bar 4 µm, P-5x5 30° twisted, DSM910 (Carl Zeiss)). **(B)** DAPI nuclei staining with nucleus circularity of cells, ($n = 55$ of 2 independent experiments, Mann-Whitney U test, $***: P < 0.001$). After 24 h the cells lied on top of the micro-pillars and displayed nuclei embedding the micro-pillars, thus the nucleus became more elongated.

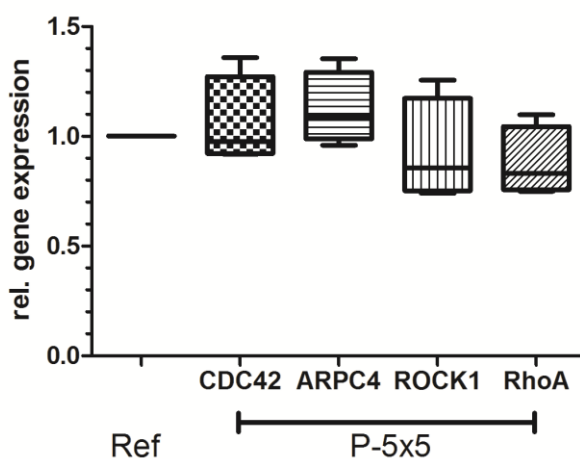


Figure 13: Relative gene expression of the actin polymerization proteins cell devision control protein 42 (CDC42), actin related protein 2/3 complex (ARPC4), Ras homolog family member A (RhoA) and Rho-associated kinase (ROCK1) in MG-63 osteoblasts on 5x5 µm micro-pillars (P-5x5) compared to the planar reference (Ref) after 24 h, ($n = 4$, Ref values normalized on 1, Mann-Whitney U test). The micro-pillar topography did not alter gene expression of actin polymerization proteins.

Confocal microscopy with three dimensional (3D) z-stack generation was applied to visualize the short compact actin filaments on the pillar plateaus, as well as the actin formation in between the pillars. Z-stacking was used to generate a 3D representation to understand the overall cell structures not limited to one horizontal plain of the micro-topography. Therefore, all immunofluorescence images in this thesis, with exception of the xz- and yz-plane images, were displayed as 3D z-stacks.

The micro-pillars drastically altered the actin cytoskeleton organization of MG-63 cells (**Fig. 14**), resulting in clustered, short filaments on the pillar tops, as already shown by our group in studies of Matschegewski and Staehlke et al. [9;10;90]. The altered actin cytoskeleton led to the question, if the other components of the cytoskeleton are as well rearranged? Therefore, the α -tubulin organization in MG-63 cells on the micro-pillared textures was investigated via immunofluorescence staining, but showed no effect on the tubulin polymerization, whereas the microtubule orientate themselves along the micro-pillared topography (**Fig. 14**).

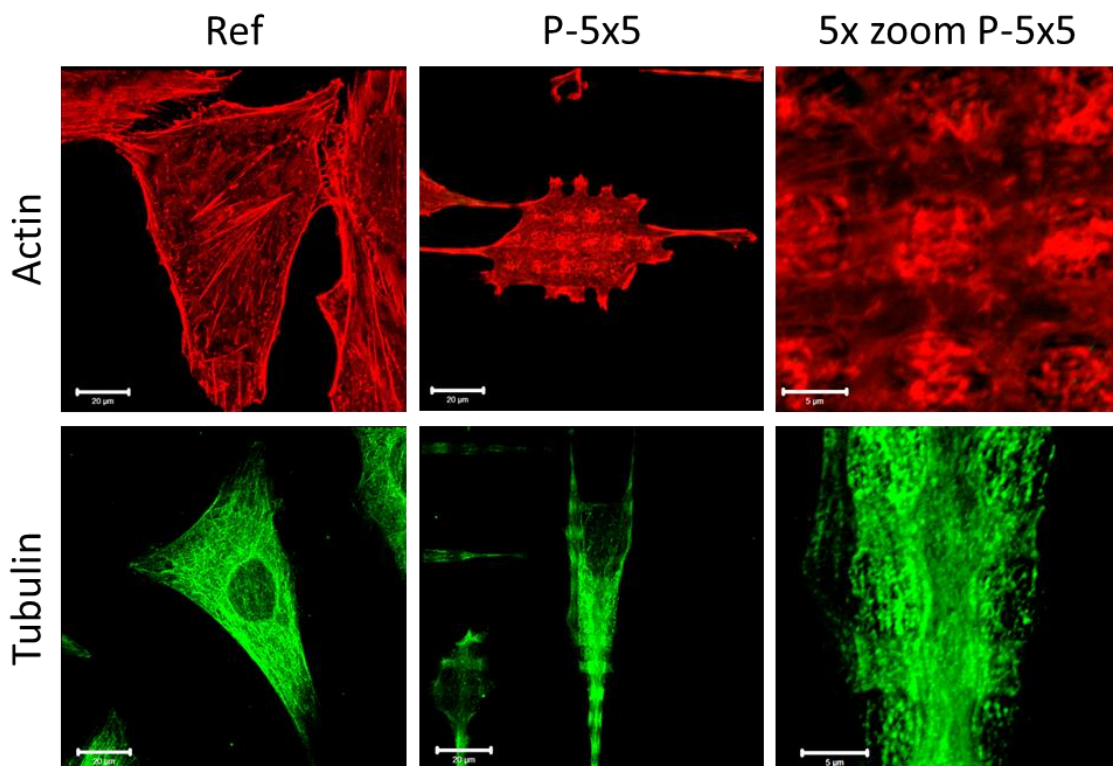


Figure 14: Immunofluorescence staining of the actin cytoskeleton (red) and α -tubulin (green) as component of the microtubuli in MG-63 osteoblasts grown for 24 h on micro-pillars (P-5x5) and on planar reference (Ref), (left and middle bar 20 μ m, right 5 μ m). After 24 h the cells displayed short clustered actin filaments on the pillar plateaus, whereas the micro-pillared topography led to no drastically changes in in the tubulin polymerization but to an orientation of the microtubules along the topography.

3.2 Osteoblast-specific functions on the micro-pillars

Osteoblasts are specialized cells and their function, as bone-forming cells, implicates their production of the inorganic as well as organic bone matrix. For the initial cell-topography interaction analysis after 24 h cultivation, mRNA expression was determined via Rt-qPCR. The mRNA expression analyses of the osteoblast marker proteins and organic bone matrix components alkaline phosphatase (ALP), collagen type I (Col1), fibronectin (FN) and osteocalcin (OCN) displayed a significant reduction after 24 h on the micro-pillars (**Fig. 15**). Gene expression changes are adapted fast by cells, whereas protein production changes, especially by secreted proteins such as BSP-2, Col1, FN, OCN and osteopontin (OPN) are more time sophisticated. Protein expression investigations can be used for medium-long term studies, such as in this thesis investigated after 96 h cultivation time. The protein secretion of OCN and OPN (**Fig. 16a**) as well as expression of Col1 and FN were significantly reduced, and tendentially for BSP-2, after 96 h cultivation of MG-63 osteoblasts on the micro-pillars (**Fig. 16b**). Consequently, the initial decrease in osteoblast-specific function was retained during medium-long term observations after 96 h cultivation time.

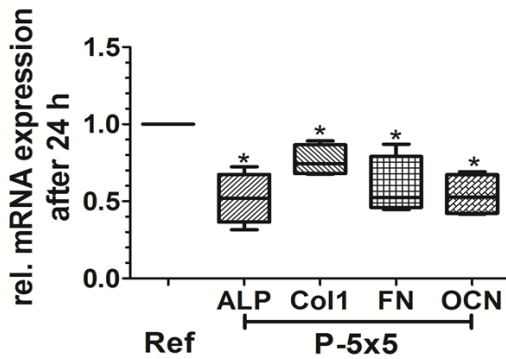


Figure 15: Relative mRNA expression of the osteoblast function markers alkaline phosphatase (ALP), collagen type I (Col1), fibronectin (FN), osteocalcin (OCN) and osteopontin (OPN) in MG-63 cells grown on micro-pillared topography (P-5x5) and planar reference (Ref) for 24 h measured by Rt-qPCR, (Ref values normalized on 1, n = 4, Mann-Whitney U test, *: P < 0.05). Gene expression of osteoblast marker was disturbed on micro-pillared topography after 24 h.

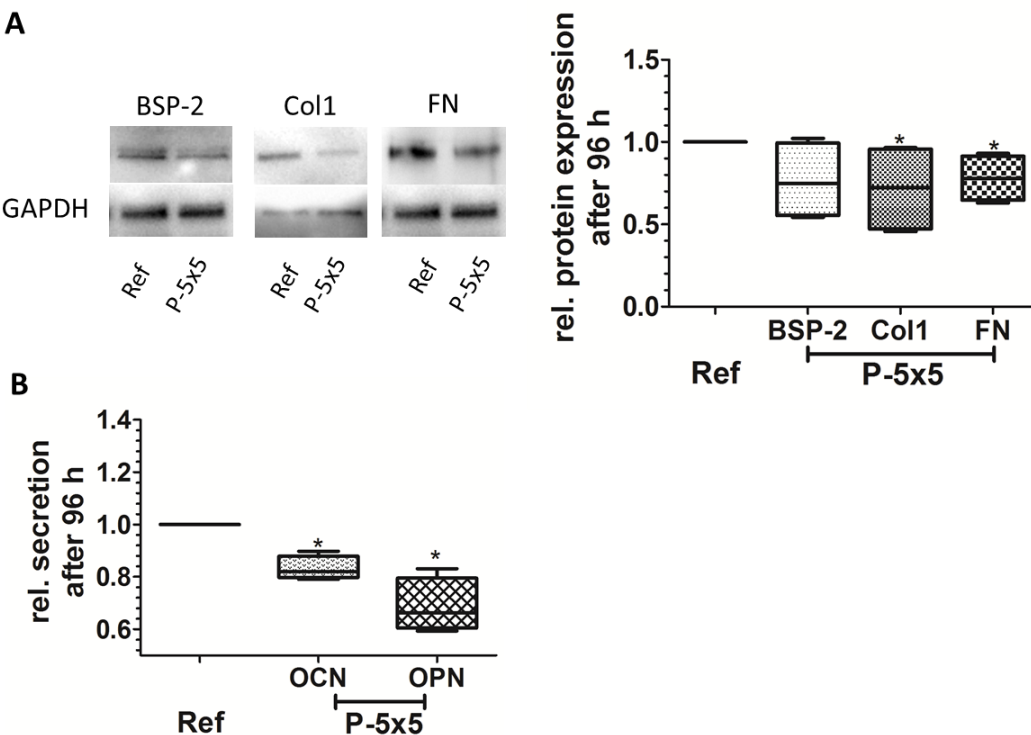


Figure 16: Quantification of the osteoblast function markers bone sialo protein-2 (BSP-2), collagen type I (Col1), fibronectin (FN), osteocalcin (OCN) and osteopontin (OPN) in MG-63 cells grown on micro-pillared topography (P-5x5) and planar reference (Ref) for 96 h. **(A)** Relative protein expression of BSP-2, Col1 and FN after 96 h cell culture, measured by western blot, left representative western blots, right densitometric analyses, ($n = 4$, Mann-Whitney U test, *: $P < 0.05$). **(B)** Relative protein secretion of OCN and OPN after 96 h cultivation time measured by luminex assay, ($n = 4$, Mann-Whitney U test, *: $P < 0.05$). Osteoblast marker protein expression and secretion was impaired on micro-pillared topography after 96 h.

3.3 Caveolae-mediated micro-pillar phagocytosis

The observed topography-induced actin cytoskeleton reorganization is also characteristic for phagocytic processes and resulted in the hypothesis of an attempted micro-pillar phagocytosis by the MG-63 osteoblasts. Clathrin-mediated phagocytosis played no role in the micro-pillar phagocytosis because the clathrin localization showed no alterations in osteoblasts grown on the micro-pillars (**Fig. 17**). On the planar reference clathrin-coated vesicles were formed (highlighted in the 10x zoom in **Fig. 17**) whereas no such vesicles were observed in the regions of the micro-pillars.

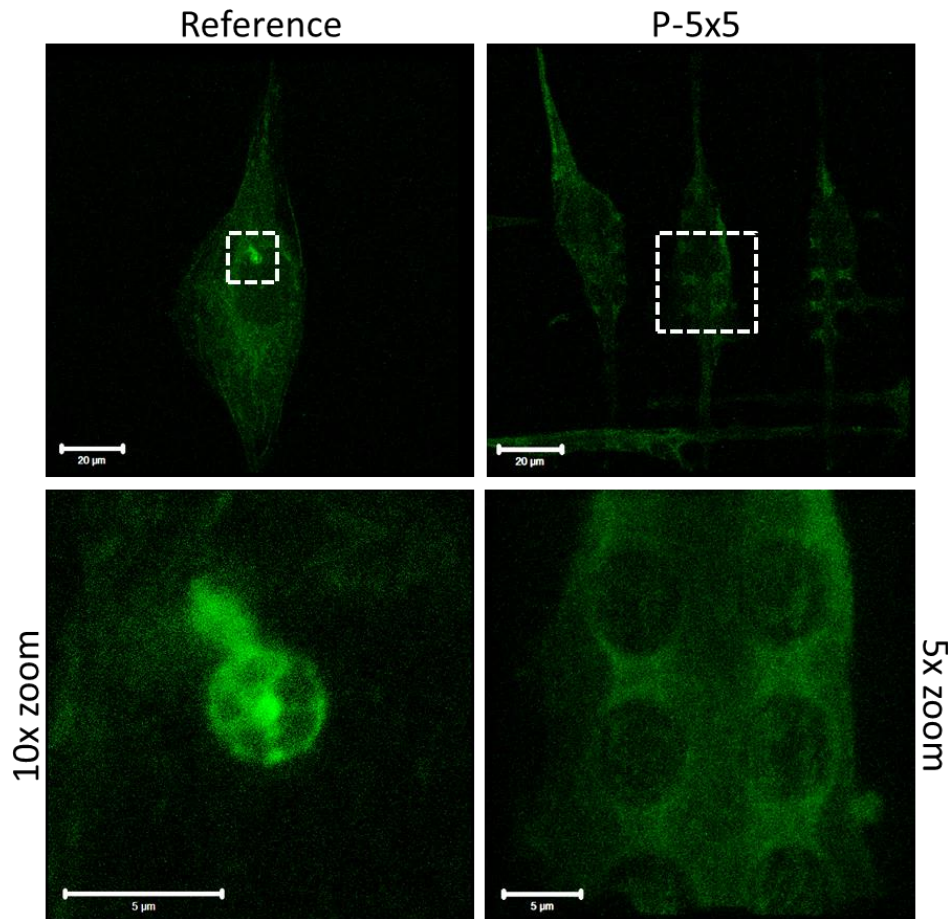


Figure 17: Immunofluorescence images of clathrin in MG-63 osteoblasts after 24 h on micro-pillared topography (P-5x5) and planar reference (Ref), (zoom regions indicated by dashed, white lines, bars 20 μm and for the zooms 5 μm). No clathrin-coated vesicle formation was found at the micro-pillared topography.

For the determination of the existence of caveolae, the two major caveolae components caveolin-1 (Cav-1) and cholesterol were localized by immunofluorescence labeling or by interaction with the fluorophore Filipin III. Cav-1 and also cholesterol displayed a dot-like localization on the micro-pillar plateaus after 24 h of cultivation (**Fig. 18a + b**, **Fig. 19**). The dot-like locations of Cav-1 and cholesterol imply the local existence of caveolae/lipid rafts on the pillar plateaus, which was not seen on the planar surfaces. To prove the existence of caveolae formation on the micro-pillar plateaus, cells were treated with the caveolae/lipid raft inhibitor Filipin III [63] (which stains cholesterol, but also acts as an inhibitor; in the latter case the vital cells were incubated with Filipin III before fixation and staining). The dot-like cholesterol formation on top of the micro-pillars started to disappear after inhibitor treatment, which was accompanied by the disruption of the caveolae/lipid rafts (**Fig. 18c**).

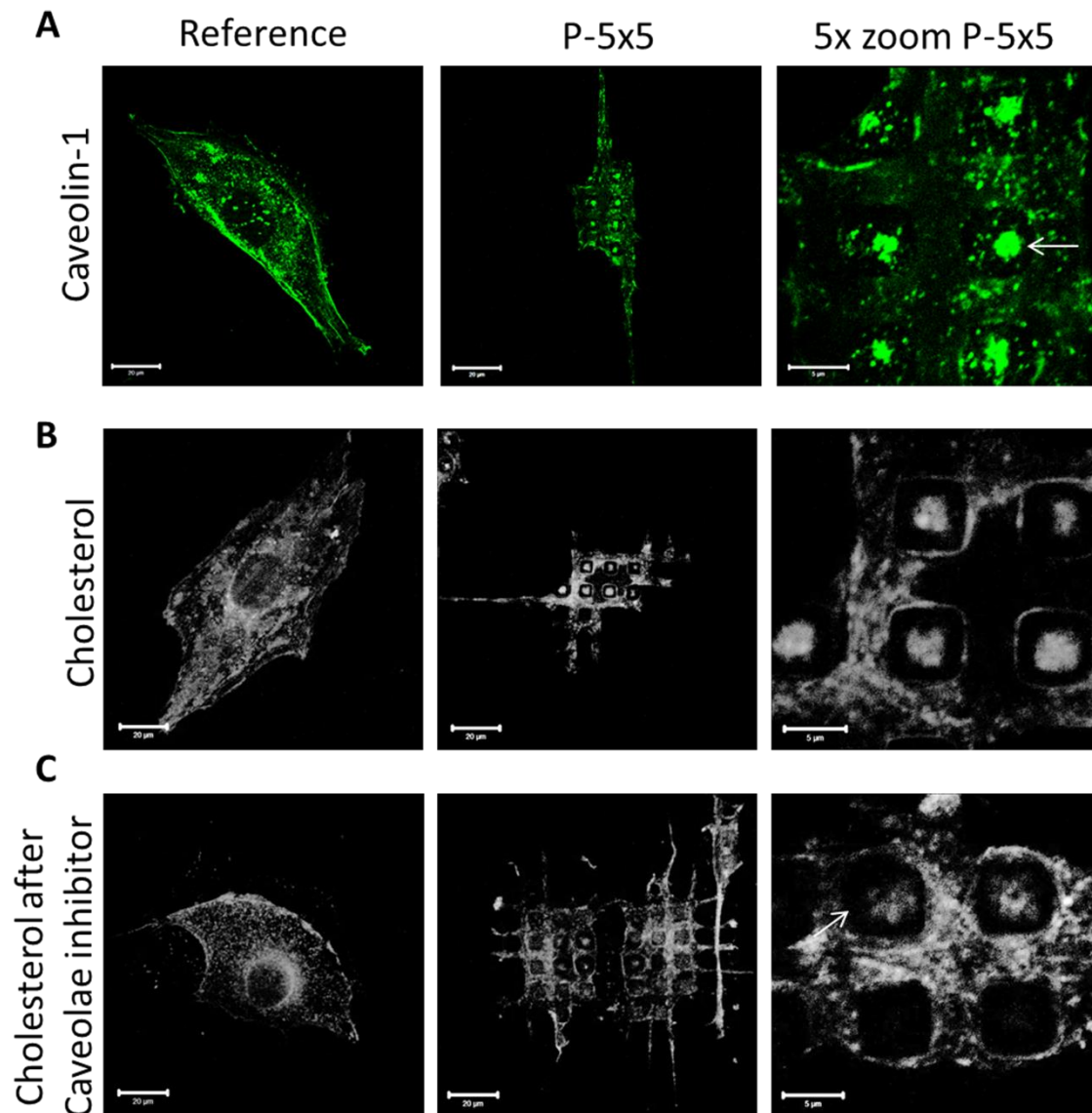


Figure 18: Immunofluorescence images of MG-63 osteoblasts after 24 h on micro-pillared topography (P-5x5) and planar reference (Ref). **(A)** Caveolin-1 (Cav-1, green). **(B)** Cholesterol. **(C)** Cholesterol after pretreatment with Filipin III inducing raft/caveolae inhibition (left and middle bar 20 μ m, right 5 μ m). *The caveolae components Cav-1 and cholesterol were dot-like clustered on the micro-pillar plateaus after 24 h indicating cellular processes found in phagocytosis.*

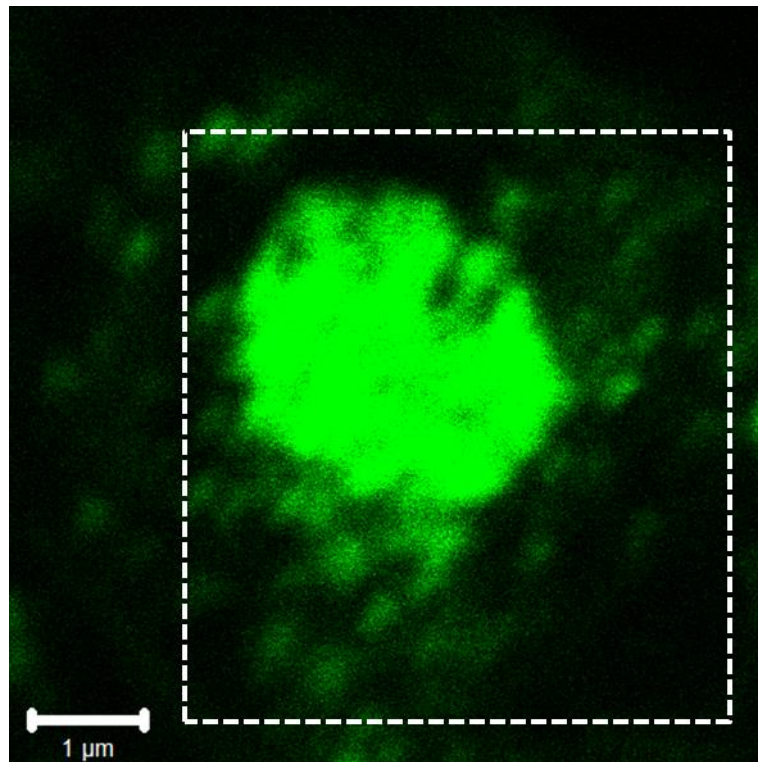


Figure 19: High magnification confocal image of a caveolin-1 cluster on top of one $5 \times 5 \mu\text{m}$ micro-pillar plateau (marked with white dashed lines) in MG-63 osteoblasts after 24 h, (25x zoom, bar $1 \mu\text{m}$).

The dot-like Cav-1 and cholesterol enrichments on top of the pillars revealed caveolae formation. MG-63 osteoblasts are an acknowledged osteoblast cell line derived from osteosarcoma. Hence, the origin of this cell line is a bone tumor; as a result the MG-63 cells are tumor cells. For excluding the fact that caveolae formation on the pillar plateaus is exclusively observed in the MG-63 osteoblasts, the human osteoblast cell lines SaOs-2 and U-2Os, as well as primary human osteoblasts and primary fetal osteoblasts were also investigated for caveolae formation (**Fig. 20**). Both primary osteoblastic cell types, as well as the two osteoblastic cell lines exhibited caveolae formation after 24 h cultivation on the micro-pillared topography and showed that the caveolae formation is a common osteoblast-specific reaction induced by the topography.

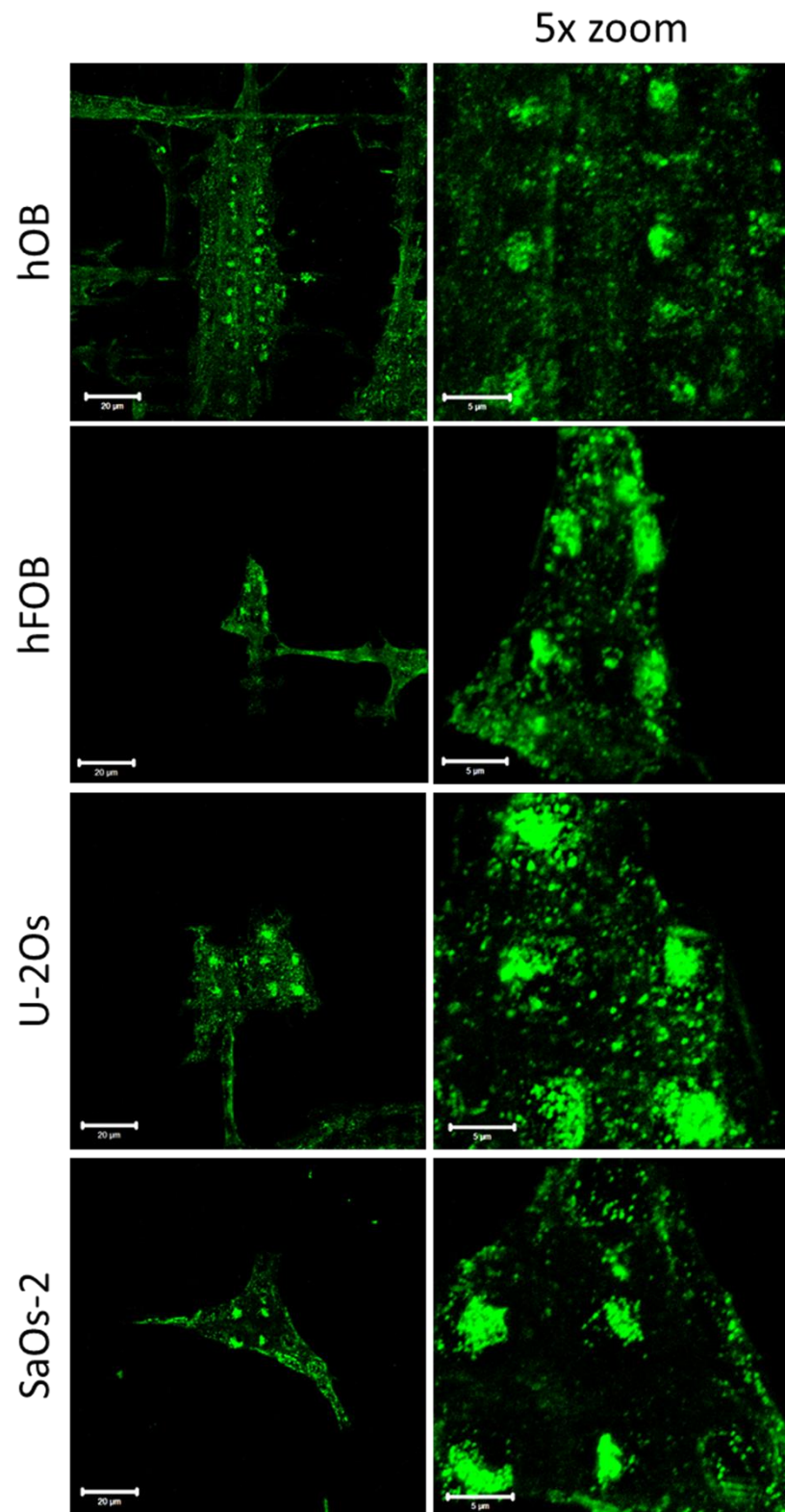


Figure 20: Immunofluorescence images of caveolin-1 (Cav-1) of human primary osteoblasts (hOB), human fetal osteoblasts (hFOB), U-2Os and SaOs-2 osteoblast-like cells on the micro-pillars (P-5x5), (bar left column = 20 μ m and right column = 5 μ m). Dot-like Cav-1 clusters were formed in different osteoblastic cell types indicating similar phagocytic approaches of the cell lines.

Cav-1 mRNA expression was significantly elevated (**Fig. 21a**) after 24 h cultivation of the MG-63 osteoblasts on the micro-pillars. Protein expression analysis of Cav-1 by western blot revealed no changes for MG-63 cells grown on the micro-pillared topography (**Fig. 21b**). Tyrosine (Y) 14 of Cav-1 receives regulated phosphorylation (pCav-1) by Src kinases and it is involved in modulation of the focal adhesion sites dynamics to increased focal adhesions turnover. pCav-1 protein amount was augmented after 24 h cultivation of the MG-63 osteoblasts on the micro-pillars, displaying an increased phosphorylation state of Cav-1 (**Fig. 21b**). The via immunofluorescence determined localization of pCav-1 was enhanced at the pillar edges and pillar walls, indicating cell mobility at these regions, whereas it was regularly distributed on the reference (**Fig. 21c**).

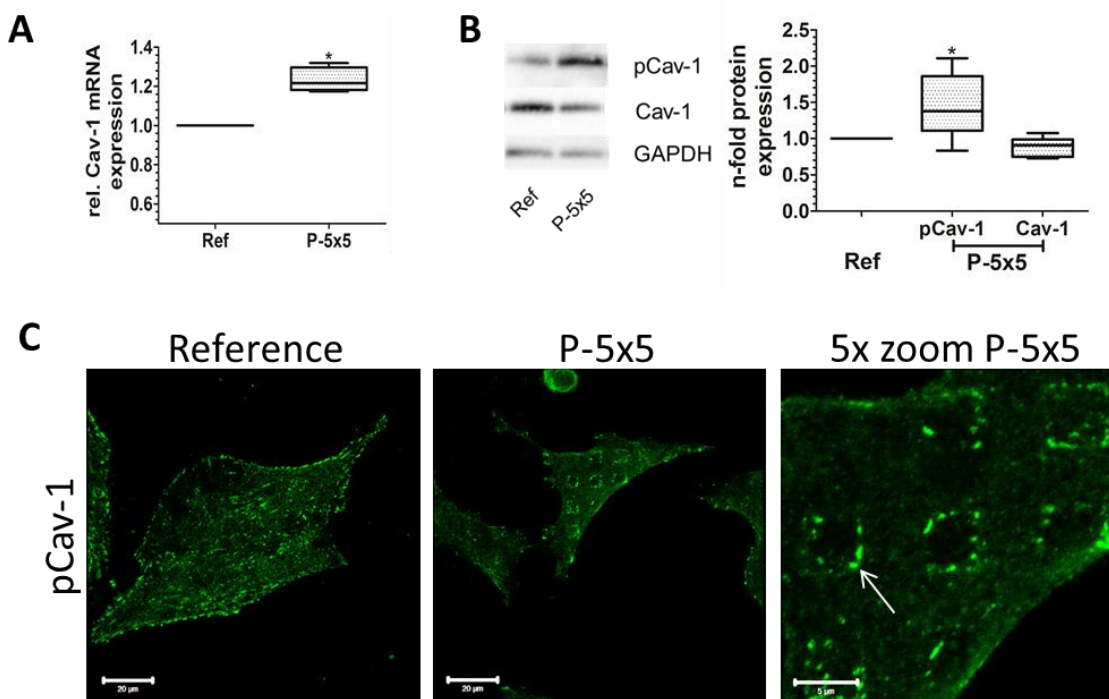


Figure 21: Caveolin-1 (Cav-1) analysis of MG-63 osteoblasts grown for 24 h on micro-pillared topography (P-5x5) and planar reference (Ref). **(A)** Relative Cav-1 mRNA expression via Rt-qPCR, (Ref values normalized on 1, n = 4, Mann-Whitney U test, *: P < 0.05). **(B)** Relative protein expression of Cav-1 and phosphorylated caveolin-1 (pCav-1), measured by western blot, left representative western blots and right densitometric analyses, (Ref values normalized on 1, for pCav-1 n = 6 and for Cav-1 n = 4, Mann-Whitney U test, *: P < 0.05). **(C)** Immunofluorescence images of pCav-1, (left and middle bar 20 µm, right 5 µm). *Micro-pillar topography enhanced Cav-1 gene expression and protein phosphorylation. Phosphorylated caveolin-1 is located at the micro-pillar edges after 24 h (arrow).*

Relative quantification of the second major caveolae component cholesterol by fluorescence measurements of Filipin III, demonstrated a decline of cholesterol in MG-63 osteoblasts cultivated on the micro-pillared topography after 24 h (**Fig. 22**).

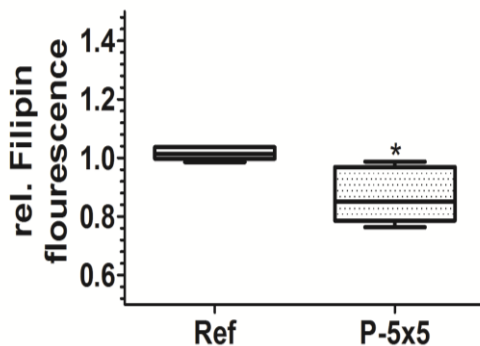


Figure 22: Relative cholesterol quantification by measurement of Filipin III fluorescence in MG-63 cells after 24 h on micro-pillared topography (P-5x5) and planar reference (Ref), (mean value of Ref normalized on 1, n = 5, Mann-Whitney U test, *: P < 0.05). Cholesterol content was decreased in cells on the micro-pillars after 24 h.

After 96 h cultivation, MG-63 osteoblasts on the micro-pillared topography revealed a significant increase in Cav-1 protein amount (**Fig. 23**). The caveolae assembly and actin organization on the pillar plateaus was consistent over 96 h and was also formed during cultivation against gravity. After 72 h cultivation, the actin cytoskeleton started to engulf the pillar walls. The dot-like Cav-1 clusters moved to the pillar edges hinting at phagocytosis of the micro-pillars by the cells, because of the actin cytoskeleton formation and the Cav-1 coat around the micro-pillars (**Fig. 24**).

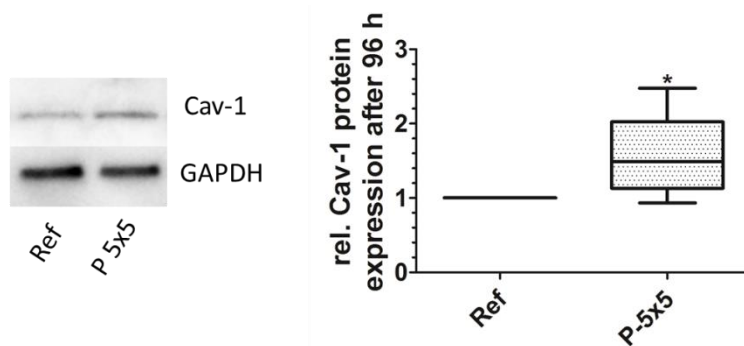


Figure 23: Relative protein expression of caveolin-1 (Cav-1) after 96 h cultivation of MG-63 osteoblasts on micro-pillared topography (P-5x5) and planar reference (Ref), left representative western blots and right densitometric analyses, (Ref values normalized on 1, n = 4, Mann-Whitney U test, *: P < 0.05). Cav-1 protein amount was increased after 96 h on the micro-pillars.

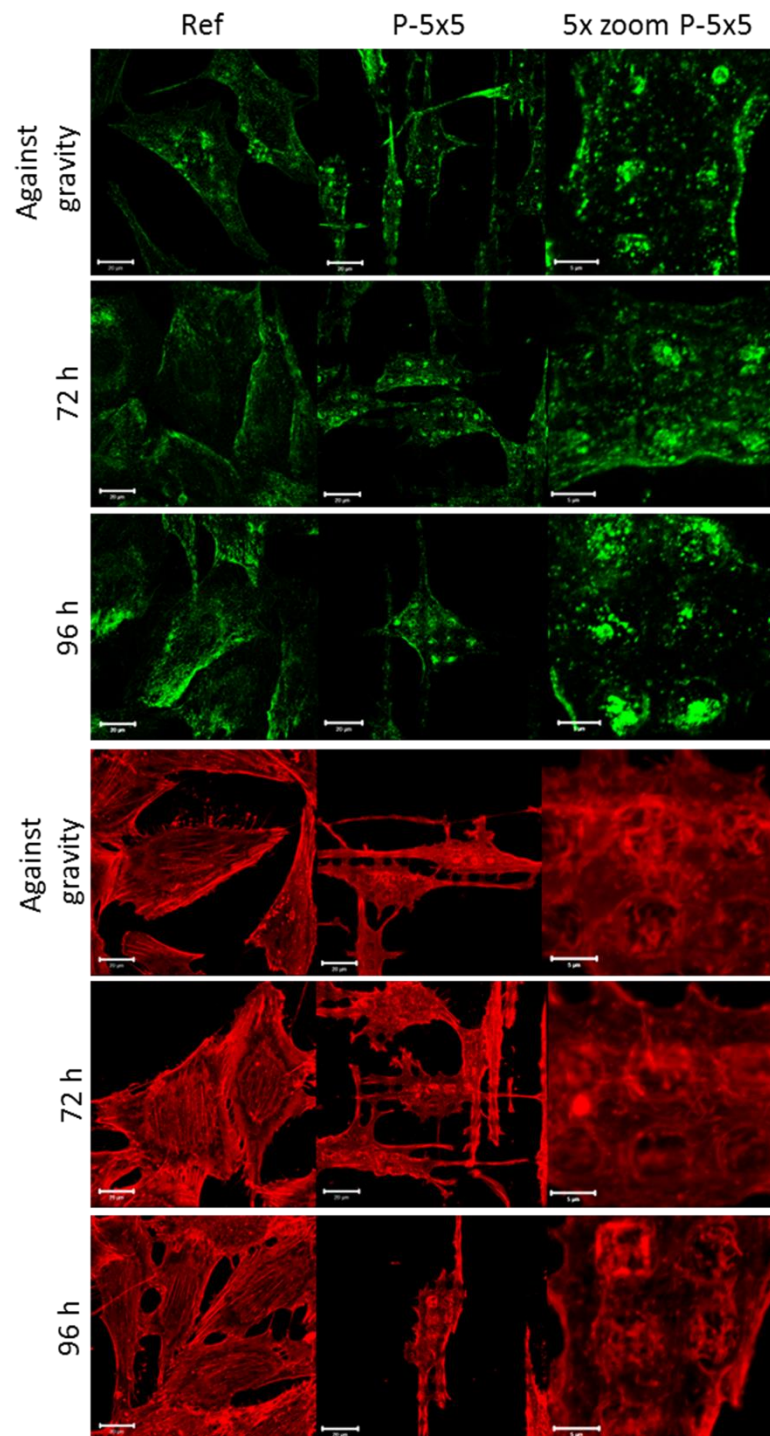


Figure 24: Immunofluorescence images of caveolin-1 (Cav-1, green) and the actin cytoskeleton (red) in MG-63 cells on micro-pillar topography (P-5x5) and planar reference (Ref) after cultivation against the gravity for 24 h (first row), or otherwise normal cell culture for 72 h (second row) and 96 h (third row), (bars 20 μ m, but for 5x zoom bars 5 μ m). *Cav-1 and the actin cytoskeleton shifted to the pillar edges and walls up to 96 h cultivation time and the clusters at the pillars are independent of the gravity.*

Scanning electron microscopy (SEM) images after 72 and 96 h of cultivation time revealed MG-63 cells reaching to the bottom of the micro-pillared topography, hence embedding the micro-pillars (**Fig. 25**). Live cell imaging of MG-63 osteoblasts on the micro-pillared topography showed that the cells are actively testing the underlying topography with their filopodia during the first hours of adhesion (**Fig. 26**). The cells also moved and started to test the underlying structure again, before they settle. Thus, the MG-63 cells scanned the underlying topography, before they started to internalize the micro-pillars.

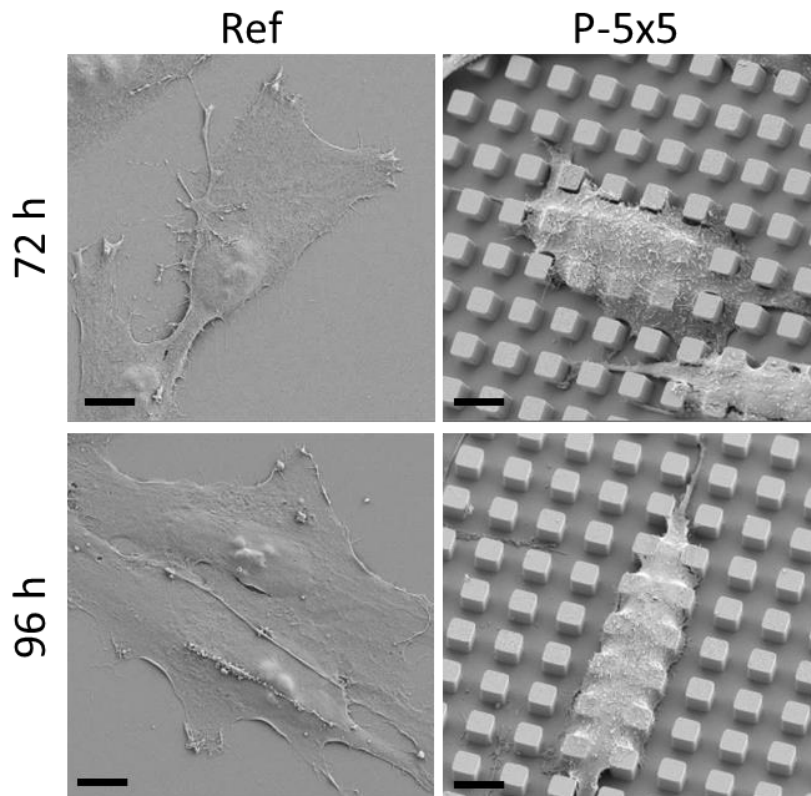


Figure 25: Morphology of MG-63 cells after 72 and 96 h on micro-pillar topography (P-5x5) and planar reference (Ref). Scanning electron microscopy (SEM) images with 1,000x magnification, (bars 10 µm, and 30° twisted for P-5x5, Merlin VP (Carl Zeiss)). After 72 h the cells embedded the micro-pillars and reached the topography bottom with their cell margins and the cell body in the whole or in part.

The used micro-pillared topography with pillar dimensions of 5 µm in pillar length, width, height and spacing represent big structures for the internalization. Variation of the pillar sizes to smaller dimensions (length x width x height x spacing: 1x1x1x1 µm; 2x2x5x2 µm; 3x3x5x3 µm) showed as well a dot-like Cav-1 clustering on the pillars but also around them after 24 h of cultivation in MG-63 osteoblast-like cells (**Fig. 27**). For this smaller pillar sizes, Cav-1 was localized around the pillars already after 24 h, whereas at the bigger P-5x5, Cav-1 was found located around the pillar first after 72 h.

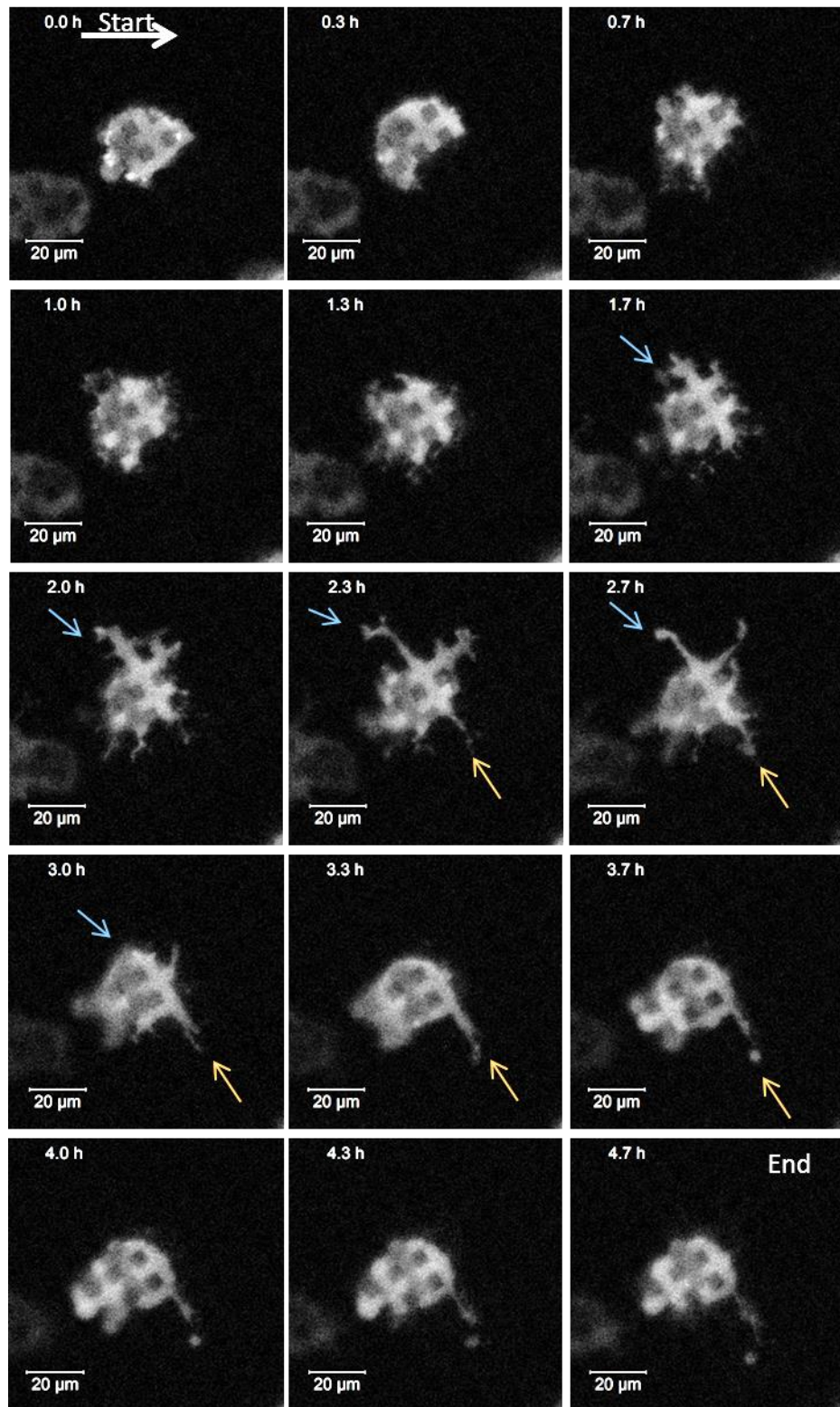


Figure 26: Immunofluorescence images of MG-63 osteoblasts expressing actin coupled with the green fluorescent protein (GFP, colored in grey) during their first 5 h on the micro-pillared topography, (starting above first row left and ending down forth row right). *The cells were testing the micro-topography with their filopodia (blue and yellow arrows).*

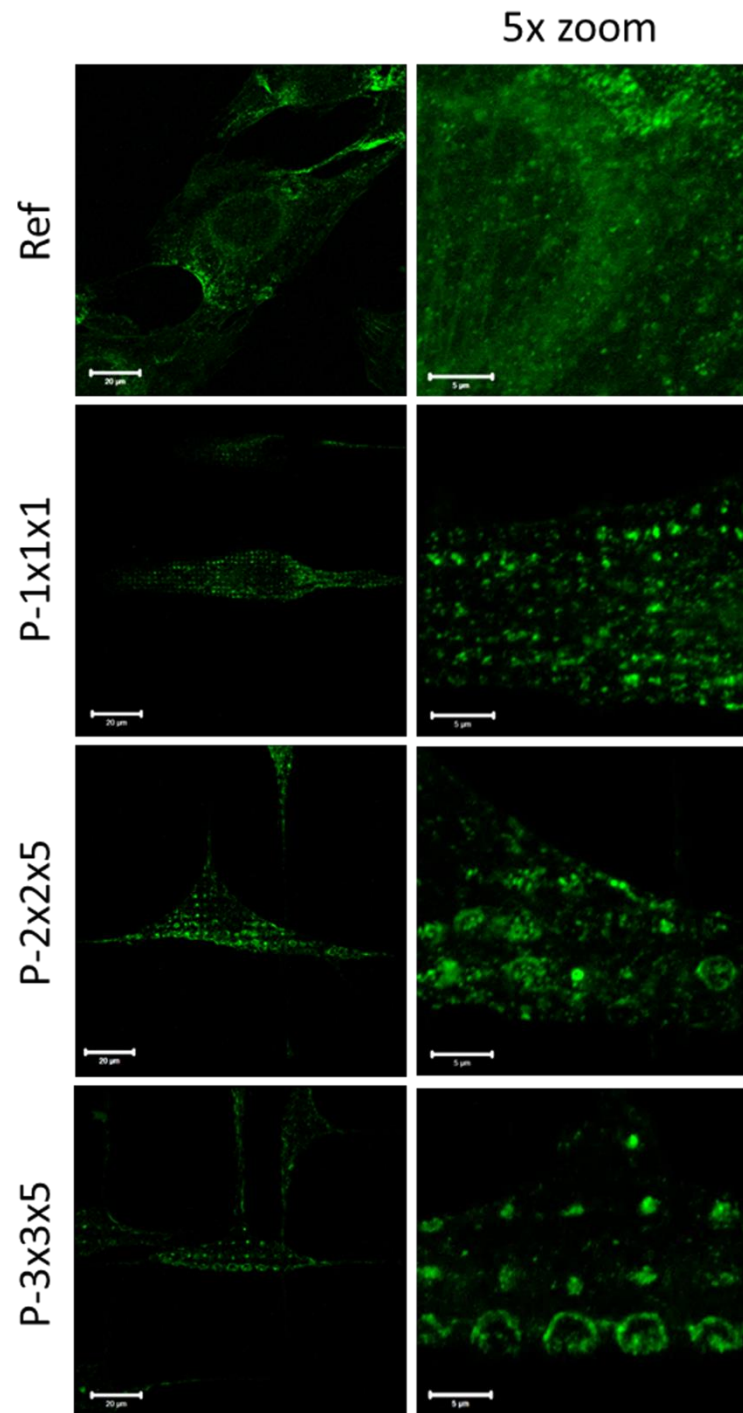


Figure 27: Immunofluorescence images of caveolin-1 (Cav-1) in MG-63 osteoblast after 24 h on topographies with micro-pillars (P) having the dimensions of width x length x height in μm : P-1x1x1 with 1 μm spacing, P-2x2x5 with 2 μm spacing, P-3x3x5 with 3 μm spacing compared to the planar reference (Ref), (bars: 20 μm , for 5x zoom 5 μm). Cav-1 clusters were also seen on and around smaller micro-pillar sizes.

3.4 Micro-particle uptake by human MG-63 osteoblasts

Caveolae/lipid rafts are associated with the phagocytosis of micron-sized titanium particles [91]. Based on the hypothesis, that MG-63 cells attempt to phagocytize the fixed micro-pillars of the P-5x5 topography, we wanted to clarify if they are also able to internalize particles in size of the used micro-pillars. So then, treatment of the MG-63 cells with 6 µm particles in the concentration of 10^5 particles/ml served as control experiment. Cell morphology analysis and internalization verification were performed via SEM and fluorescent actin cytoskeleton staining. Immunofluorescence staining of Cav-1 as major caveolae component, should verify if the particle phagocytosis is caveolae-mediated.

The immunofluorescence and SEM images showed that the MG-63 cells internalize particles 6 µm in size after 24 h of cultivation (**Fig. 28**). **Fig. 28a** revealed a complete engulfment of the 6 µm particles with the actin cytoskeleton by the MG-63 osteoblasts. For verification of the internalization, the immunofluorescence of the xz- and yz- axis, as well as 3D z-stack pictures were listed. Not only the actin cytoskeleton but also Cav-1 surrounded the whole particle. There was a Cav-1 coat formed around the internalized particle, which led to the assumption of a caveolae/lipid raft-mediated internalization process for the 6 µm particles. The experiments demonstrated an uptake of several 6 µm particles by the osteoblast-like cells, but after internalization, all particles were concentrated and not freely distributed inside the cells (**Fig. 28b**).

For mimicking only a basal phagocytosis of the micro-particles, the particles were fixed on a cover glass by a collagen I-layer. The **Fig. 29** illustrates the fixed position of the micro-particles, because after intense rinsing before cell seeding and during the immunofluorescence staining protocol, fixed particles are still found on the cover glass. Now, the cells should only have contact to the micro-particles via their basal side analog to the micro-pillar topography. For the fixed micro-particles, the cells exhibited the same actin cytoskeleton pattern as was observed after cell cultivation onto unbound micro-particles and treatment after adhesion. As a result, incubation of the MG-63 osteoblasts with micro-particles either from their apical or their basal side both led to phagocytosis of the particles.

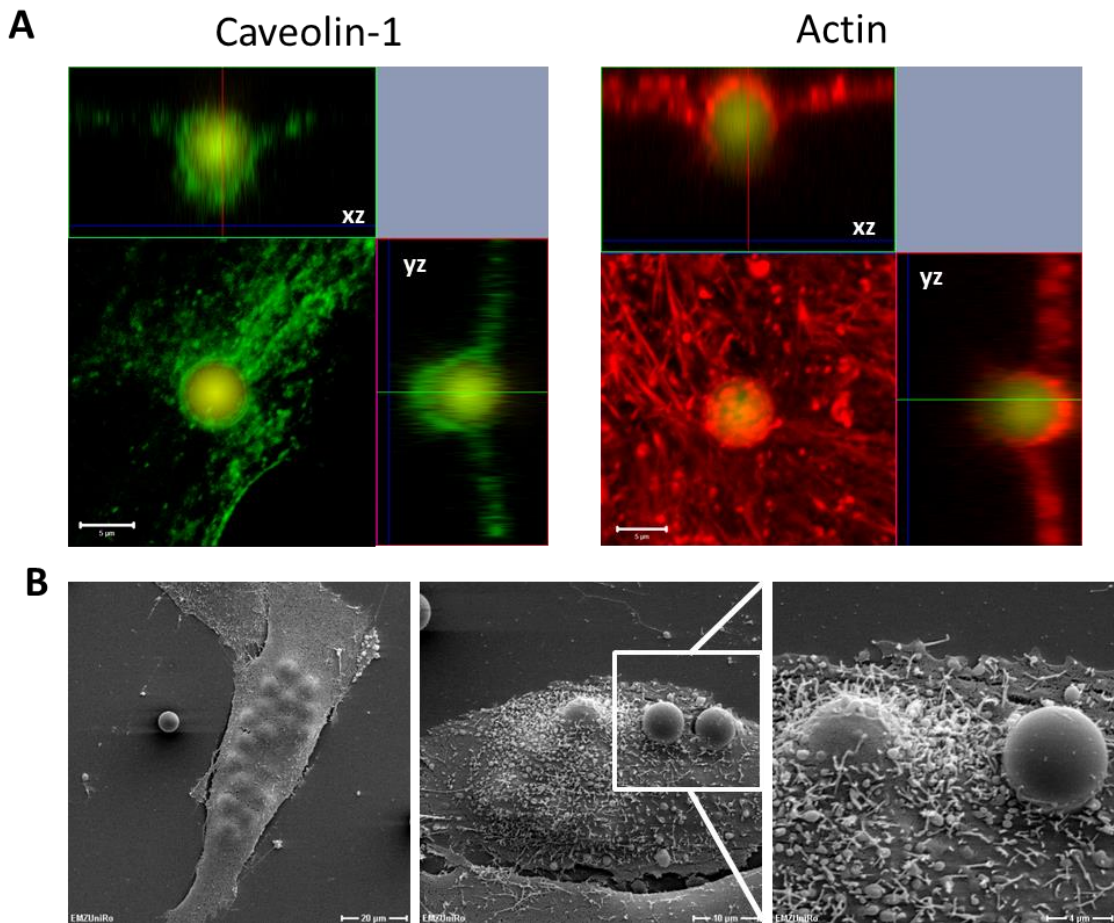


Figure 28: MG-63 osteoblasts after treatment with 6 μm FITC-labelled particles for 24 h. **(A)** Immunofluorescence images of left: caveolin-1 (Cav-1, green) and right: actin cytoskeleton (red) with xz- and yz-planes, (false color illustration of Cav-1 (green) and 6 μm particles (yellow), bars 5 μm). **(B)** Scanning electron microscopy (SEM) images, (left: 1,000x magnification and bar 20 μm , middle: 2,000x magnification and bar 10 μm , right: 5,000x magnification and bar 4 μm , DSM910 (Carl Zeiss)). *Cav-1 accumulation and clustered actin filaments were found around internalized micro-particles.*

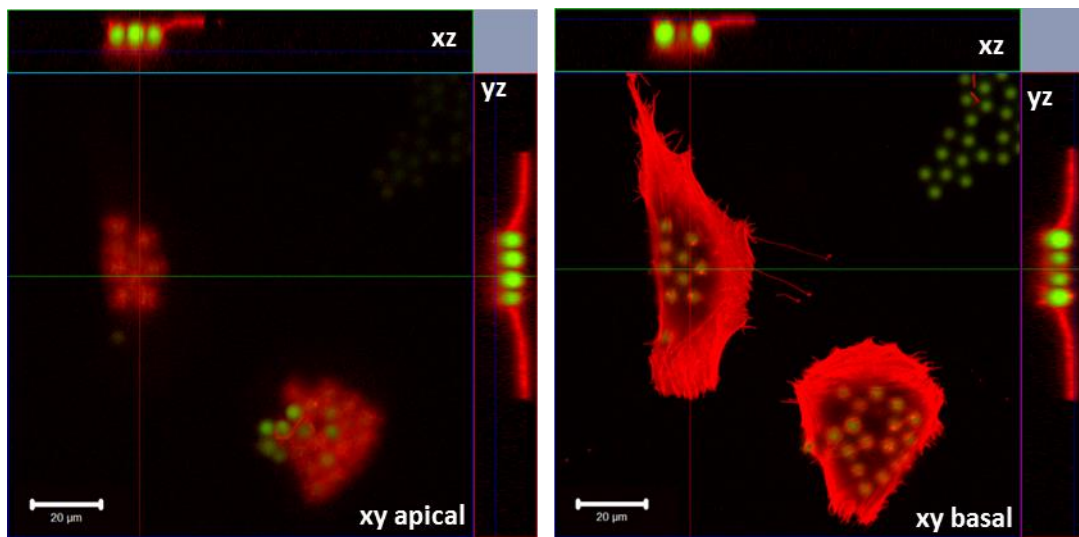


Figure 29: Immunofluorescence images of the actin cytoskeleton (red) in MG-63 cells grown on surface-fixed micro-particles (see schema in **Fig. 10**) 6 μm in size (FITC, green) for 24 h, confocal xy images of the apical cell side (left) and the basal cell side (right), (bars 20 μm). *Cells took up surface-fixed micro-particles via their basal side.*

Cav-1 plays a relevant role in the formation and stabilization of caveolae, consequently also in the caveolae-mediated phagocytosis. Depletion of Cav-1 via short interfering RNA (siRNA) should demonstrate whether Cav-1 is essential for the topography-induced actin reorganization, caused by the triggered phagocytosis. The siRNA is complementary to the target mRNA and when the siRNA is introduced into the cells cytoplasma, it binds to the target mRNA and forms double-stranded RNA. These double-stranded RNAs cannot be translated into a protein and get degraded. Silencing genes through mRNA degradation is called RNA interference [92].

siRNA-mediated knockdown of Cav-1 revealed a reduced particle phagocytosis by MG-63 cells, but no complete inhibition of the phagocytosis (**Fig. 30**), consistent with the literature [46;93]. The actin cytoskeleton after Cav-1 depletion was arranged in short filaments around non-internalized particles, which were washed away during the preparation. The cells attempted to phagocytize these particles as well, but they were not able to finish the process after the Cav-1 attenuation during 24 h incubation with the 6 μm particles. The MG-63 osteoblasts with siRNA mediated Cav-1 knockdown grown on the micro-pillars indicated the same rearrangement of the actin cytoskeleton as seen in control cells without Cav-1 attenuation (**Fig. 31**).

For the verification of the Cav-1 knockdown, the cells were analyzed for Cav-1 expression via western blot and Cav-1 immunofluorescence staining. A representative western blot is shown in **Fig. 32**. A totally Cav-1 knockdown could not be achieved.

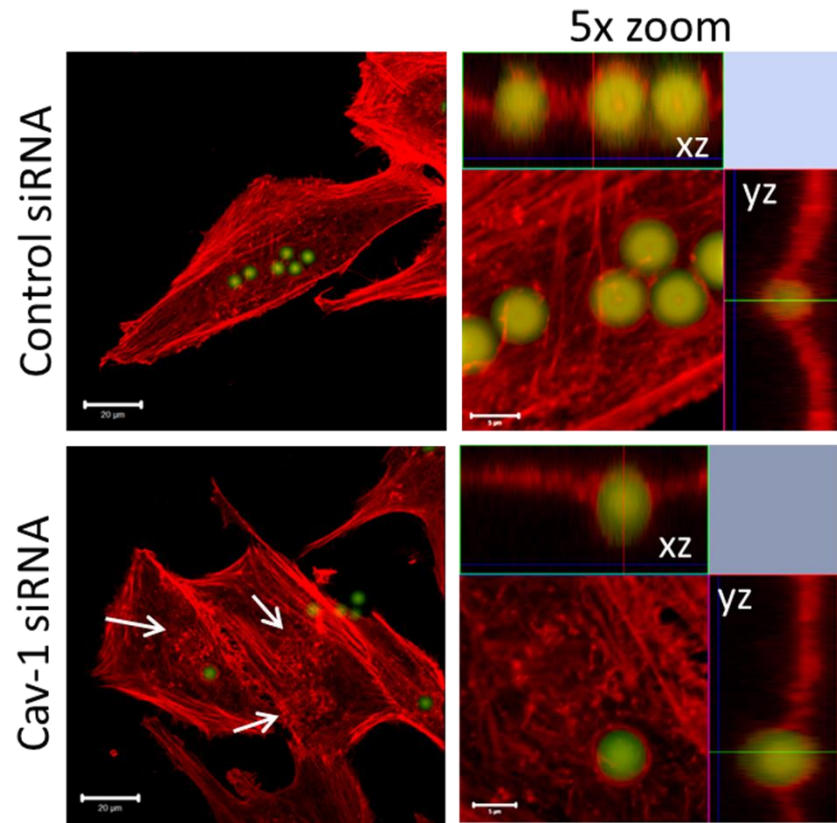


Figure 30: Immunofluorescence images of the actin cytoskeleton after caveolin-1 (Cav-1) siRNA-mediated knock-down in MG-63 osteoblasts after 24 h incubation with micro-particles (green), (left: bar 20 μ m and right: 5 μ m). Arrows indicate at the actin filaments formed at sides of non-internalized particles. *After Cav-1 attenuation the cells showed a reduced micro-particle phagocytosis.*

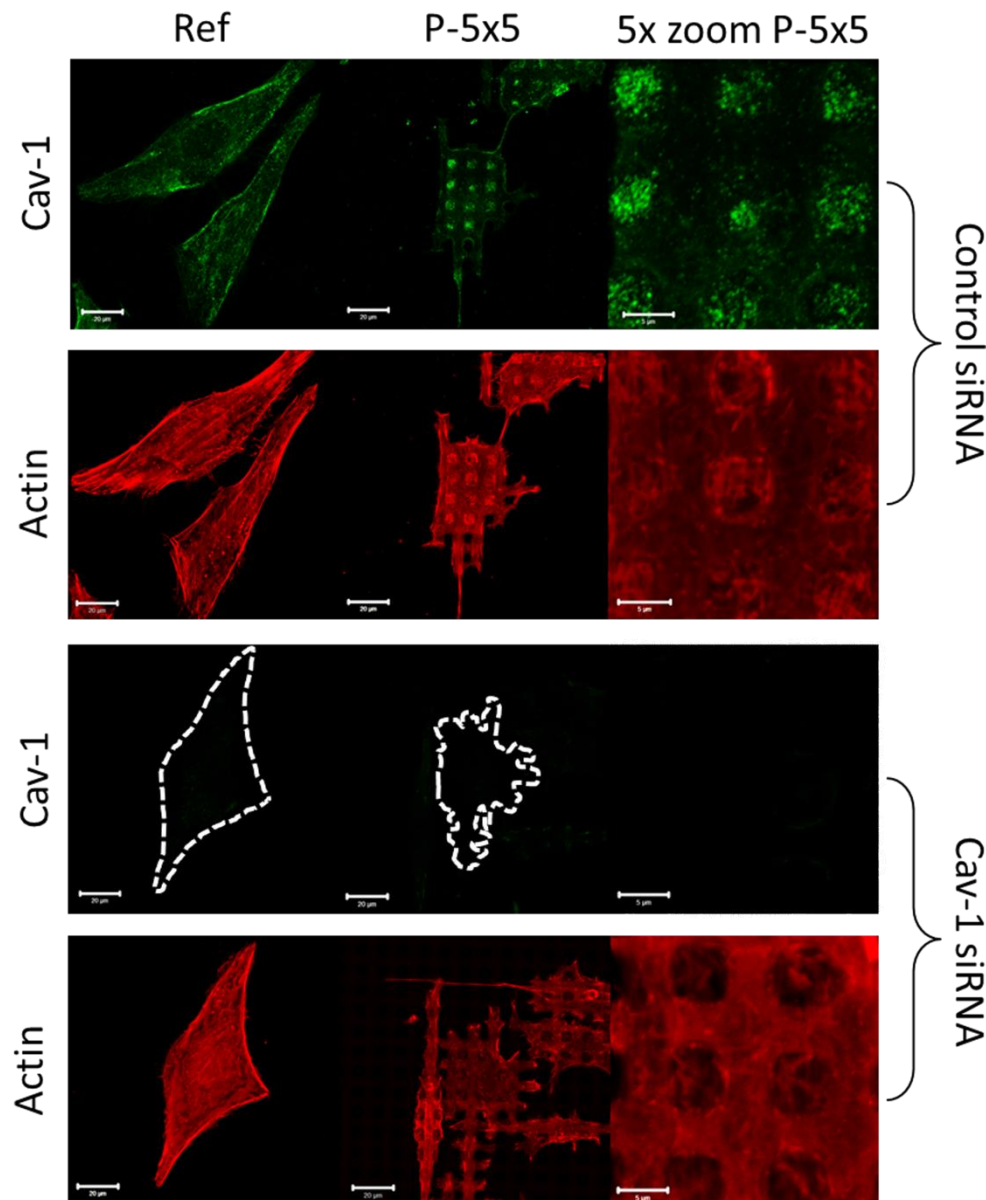


Figure 31: Immunofluorescence images of caveolin-1 (Cav-1, green) and the actin cytoskeleton (red) after Cav-1 siRNA-mediated knock-down in MG-63 osteoblasts, (bar: 20 μ m and for 5x zoom 5 μ m). Actin reorganization was unaltered after Cav-1 depletion.

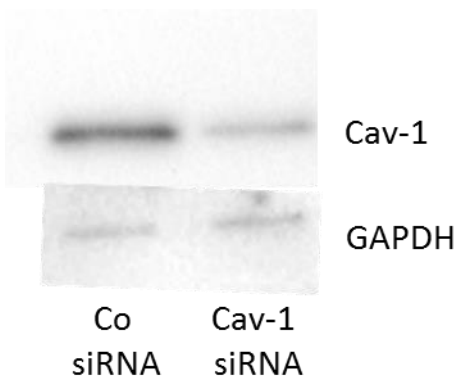


Figure 32: Representative western blots for caveolin-1 (Cav-1) protein expression after siRNA-treatment of MG-63 osteoblasts. After Cav-1 siRNA treatment, Cav-1 protein expression was attenuated.

3.5 Phagocytosis – ATP and ROS

Phagocytosis is known to be a high energy-consuming process, therefore the amounts of adenosine triphosphate (ATP) and adenosine diphosphate (ADP) was analyzed via a fluorometric assay of cells grown on the micro-pillars, as well as stimulated with 6 µm particles as phagocytosis-trigger. The micro-pillared topography and also the treatment with the micro-particles showed significant decreases in the cells intracellular ATP concentrations, but no changes in the ADP levels compared to untreated cells or cells on the planar surface (Ref) (**Fig. 33a + b**). During the assay, no deproteinization step was performed, hence only the free ATP could be detected and not the protein-bounded, metabolized ATP. Accordingly, while growing on the micro-pillar topography, the osteoblasts were metabolizing more ATP compared with cells growing on the planar surface. The same effect was visible after treatment with the 6 µm particles as phagocytosis trigger.

The cells' process of converting energy into ATP causes the greatest amount of reactive oxygen species (ROS) production [65], therefore the generated ROS were quantified by a fluorometric FACS analysis. For this reason, two ROS quantifications were performed. Firstly, with DCFDA cellular reactive oxygen species detection assay kit to detect ROS heterogeneity (mitochondrial and cytosolic ROS) and secondly with MitoSOX™ to measure especially in mitochondria produced superoxide. MG-63 osteoblasts cultured on micro-pillared surfaces exhibited elevated ROS levels compared to the cells on the unstructured samples (**Fig. 33c**). This was obviously observable for the whole ROS heterogeneity, detected by DCF fluorescence, but only by trend for the exclusively in mitochondria produced and located superoxide, measured by MitoSOX™.

Antioxidative enzymes, e.g. catalase, superoxide dismutase or peroxidases, eliminate ROS by catalyzing reactions that neutralize the ROS. The protein expression of these ROS-scavenging enzymes were quantified via luminex assay and showed significant increased protein expression for catalase (CAT), tendential raise for thioredoxin peroxidase (PRX2) and superoxide dismutase 2 (SOD2) but no change for SOD1 in MG-63 cells grown for 24 h on the micro-pillars (**Fig. 33e**).

In addition, MG-63 osteoblast grown on the micro-pillars for 24 h showed an increased mitochondrial activity (**Fig. 34**) reflecting the higher ATP metabolism rate and the higher ROS production.

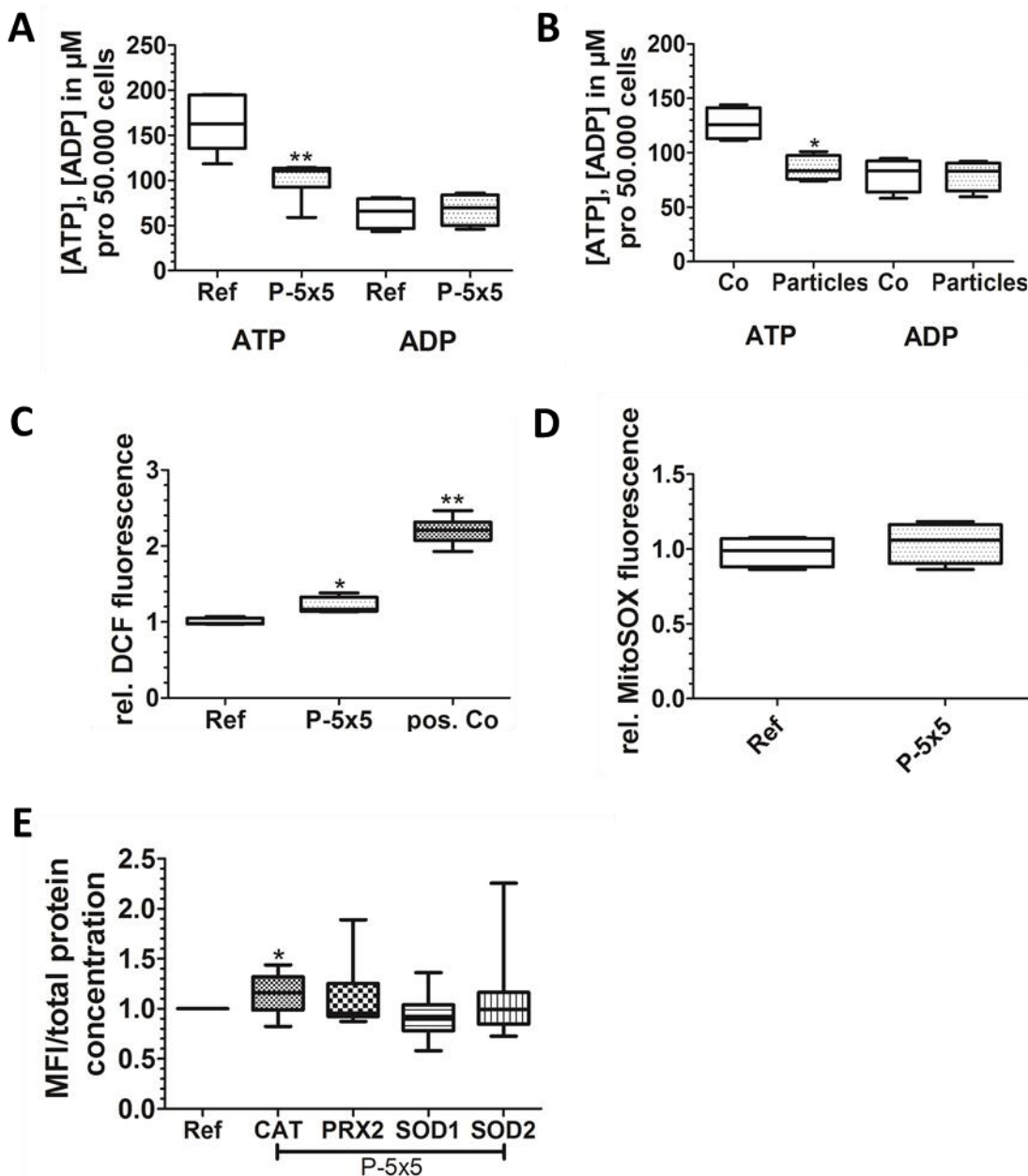


Figure 33: Energy metabolism analysis of MG-63 osteoblasts grown for 24 h on micro-pillared topography (P-5x5) and planar reference (Ref), as well as cells treated with 6 μm particles. **(A)** Cellular adenosine triphosphate (ATP) and adenosine diphosphate (ADP) quantification after cell growth on the pillar surfaces, ($n = 4$, Mann-Whitney U test, *: $P < 0.05$). **(B)** Cellular ATP and ADP quantification after micro-particle treatment, ($n = 4$, Mann-Whitney U test, *: $P < 0.05$). **(C)** Reactive oxygen species (ROS) determination via measurement of 2',7'-dichlorofluorescin fluorescence (DCF), (treatment with 50 μM tert-butyl hydrogen peroxide served as positive control, mean value of Ref normalized on 1, $n = 4$, Mann-Whitney U test, *: $P < 0.05$, **: $P < 0.01$). **(D)** Mitochondrial ROS determination by measurement of MitoSOX™ red fluorescence via flow cytometry, (mean value of Ref normalized on 1, $n = 4$). **(E)** Quantification of ROS-scavenging enzymes catalase (Cat), thioredoxin peroxidase (PRX2), superoxide dismutase (SOD) 1 and 2 via luminex assay, (Ref values normalized on 1, $n = 8$, Mann-Whitney U test, *: $P < 0.05$, MFI: mean fluorescence intensity). Micro-pillar topography and micro-particle treatment both led to decreased intracellular ATP amount. Micro-pillars also induced higher cytosolic ROS generation and expression of the ROS-scavenging enzyme catalase.

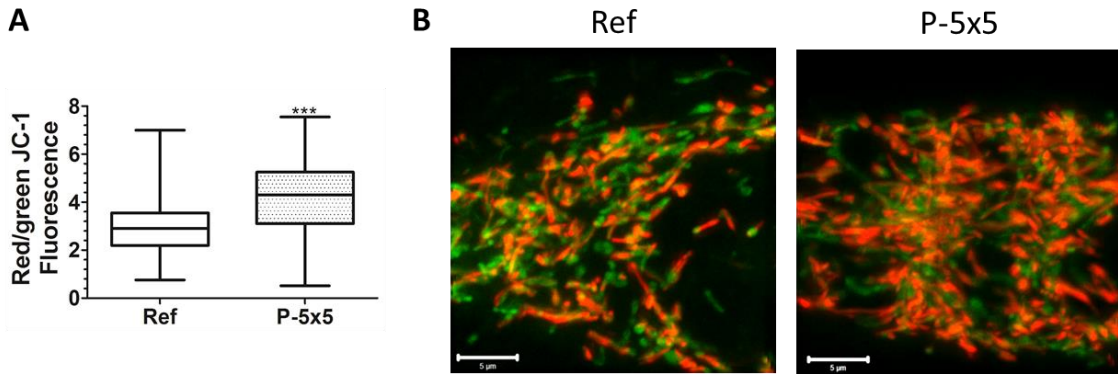


Figure 34: Mitochondrial activity of MG-63 osteoblasts cultured for 24 h on micro-pillared topography (P-5x5) and planar reference (Ref). **(A)** Red/green fluorescence single cell analysis of the mitochondrial potential membrane dye JC-1 in 2 independent experiments with 150 cells respectively, (Mann-Whitney U test, ***: $P < 0.001$). **(B)** Immunofluorescence images of the mitochondria dyed with the mitochondrial potential membrane dye JC-1 (bar 5 μm). The mitochondrial membrane switch to higher mitochondrial activity for the cells on the micro-pillar topography is indicated by the color shift from green to red.

SEM images revealed that at the time point of 96 h, the micro-pillars were fully engulfed by the osteoblast-like cells and the attempted phagocytosis might be finished. After 96 h cultivation time, the MG-63 osteoblasts showed no significant changes in the cellular ATP amount (**Fig. 35a**) and ROS generation (**Fig. 35b**), indicating that after 96 h culture time the micro-pillared topography caused no augmented energy requirements and the therefore resulting ROS generation.

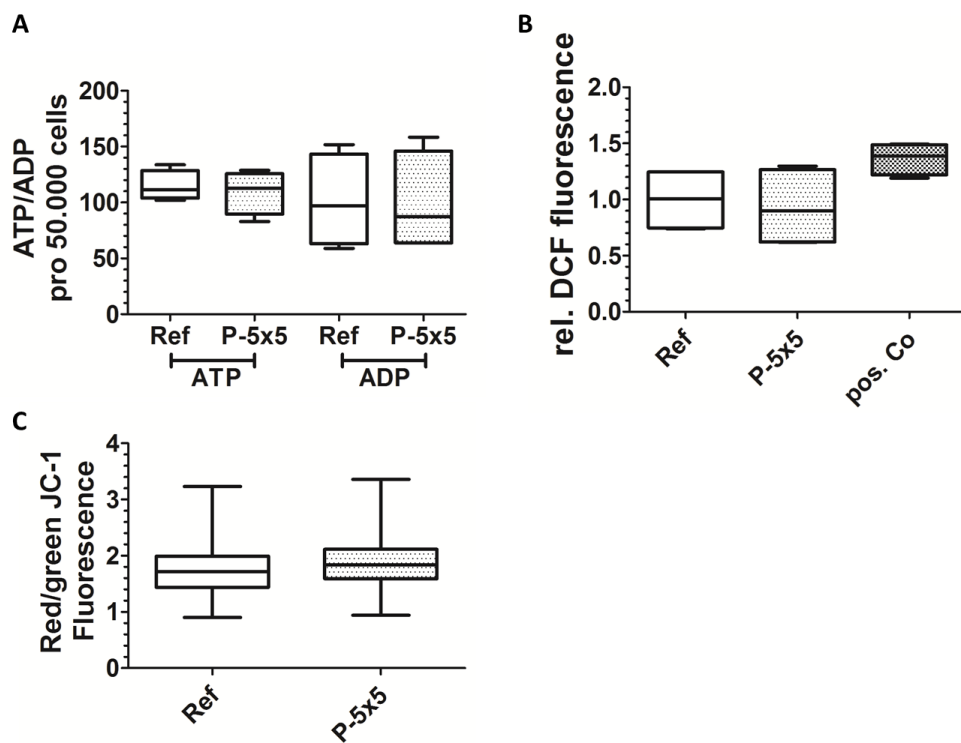


Figure 35: Energy metabolism of MG-63 osteoblasts grown for 96 h on micro-pillared topography (P-5x5) and planar reference (Ref). **(A)** Intracellular adenosine triphosphate (ATP) and adenosine diphosphate (ADP) quantification, ($n = 4$). **(B)** Reactive oxygen species (ROS) determination via measurement of 2',7'-dichlorofluorescin fluorescence (DCF), (treatment with 50 μ M tert-butyl hydrogen peroxide served as positive control, mean value of Ref normalized on 1, $n = 4$). **(C)** Mitochondrial activity analysis by calculation of the single cell red/green fluorescence ratio of the mitochondrial potential membrane dye JC-1, ($n = 3$ with 150 cells, Mann-Whitney U test). After 96 h, ATP amount, ROS production and mitochondrial activity were unaltered dependent on the underlying topography.

3.6 Endocytic and raft proteins, $\beta 1$ -integrin and integrin-associated signaling proteins

Endocytic and raft proteins: CD68, a lysosome-associated membrane glycoproteins (LAMP) family member, was localized in regions of endocytic activity (**Fig. 36**), visualized by an accumulation of CD68 around phagocytized 6 μ m particles by MG-63 cells. Immunofluorescence staining showed an enrichment of CD68 also on the pillar plateaus of the micro-structured surface (**Fig. 37a**) after 24 h. CD68 protein expression analysis (**Fig. 37b**) showed a tendential decrease in the amount of CD68 protein in cells grown on the micro-pillared surfaces.

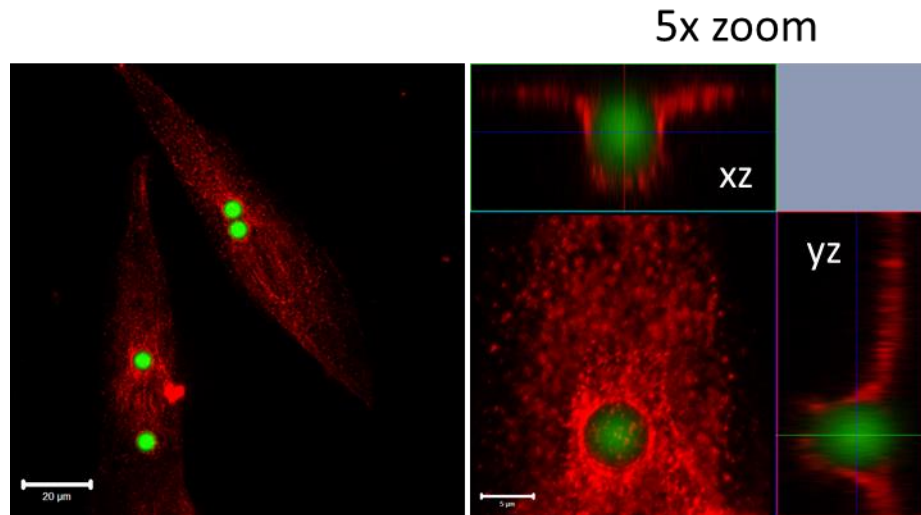


Figure 36: Immunofluorescence images of CD68 (red) in MG-63 osteoblasts treated with 6 μm particles (green), (left: bar 20 μm and right 5 μm). CD68 was accumulated around internalized micro-particles.

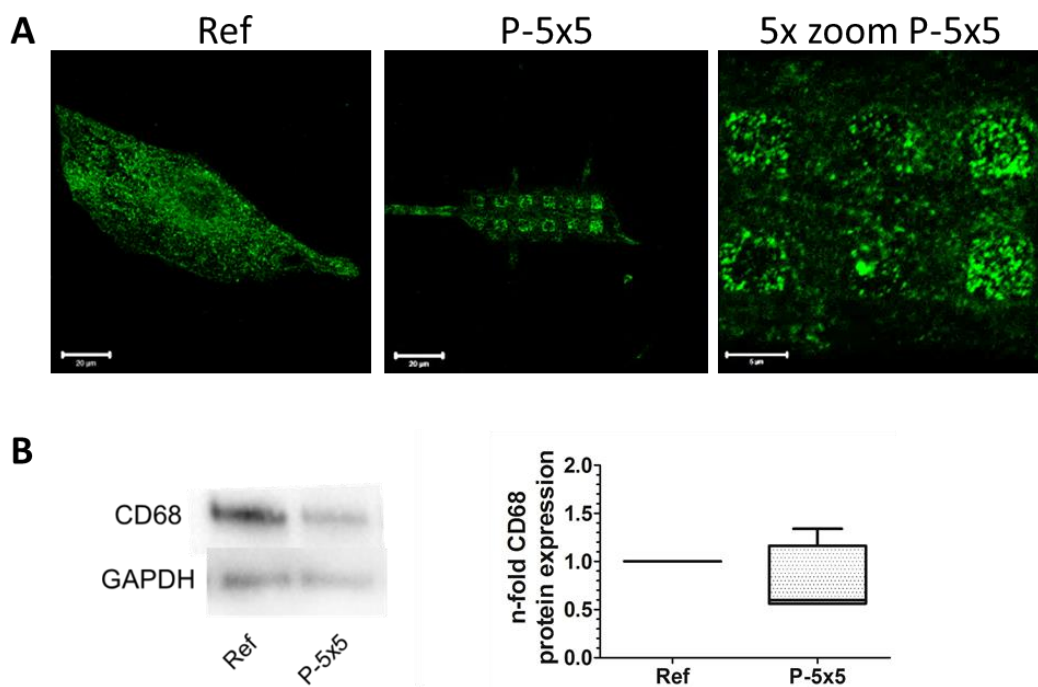


Figure 37: CD68 analysis in MG-63 osteoblasts grown on micro-pillared topography (P-5x5) vs. planar reference (Ref). **(A)** Immunofluorescence images of CD68 (green), (left and middle bar 20 μm and right 5 μm). **(B)** CD68 representative western blots and densitometric analysis, (Ref values normalized on 1, n = 4, Mann-Whitney U test). Micro-pillar topography led to clusters at the pillar plateaus but in general to tendential decreased CD68 protein amount in MG-63 osteoblasts after 24 h.

Annexin A2 (AnxA2) is reported to stabilize caveolae, but also to bind and recruit the actin cytoskeleton to the micro-domains [57]. Western blot experiments revealed significantly elevated AnxA2 protein amounts in the osteoblasts on the micro-structured surfaces after 24 h of cultivation (**Fig. 38a**). In contrast, immunofluorescence labelling displayed an accumulation in cells after 3 h only on the pillar plateaus, but no changes after 24 h in cells on the pillars compared to those on planar references (**Fig. 38b**).

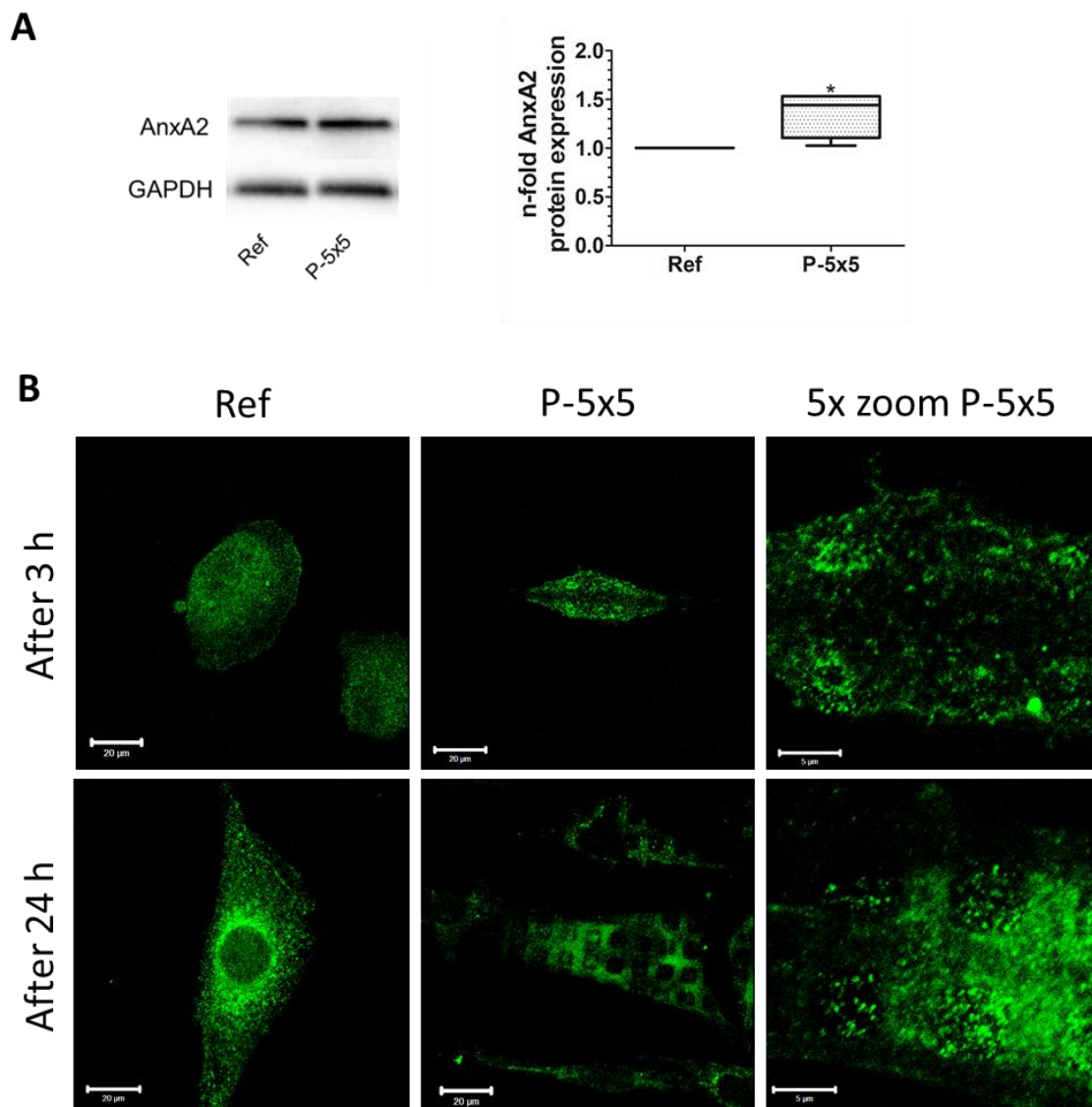


Figure 38: Annexin A2 (AnxA2) analysis in MG-63 osteoblasts cultured on micro-pillared topography (P-5x5) and planar reference (Ref). **(A)** AnxA2 representative western blots and densitometric analysis after 24 h cultivation, (Ref values normalized on 1, n = 4, Mann-Whitney U test, *: P< 0.05). **(B)** Immunofluorescence images of AnxA2 (green) after 3 h (first row) and 24 h (second row) cultivation, (bars left and middle 20 μ m and for 5x zoom 5 μ m). After 3 h, AnxA2 was located at the micro-pillar plateaus and displayed an increased protein amount after 24 h.

Integrins: Activated $\beta 1$ -integrin immunolabelling indicated clusters of activated $\beta 1$ -integrin on top of the pillars (**Fig. 39**) instead of regularly distribution, such as observed on the unfeatured planar reference.

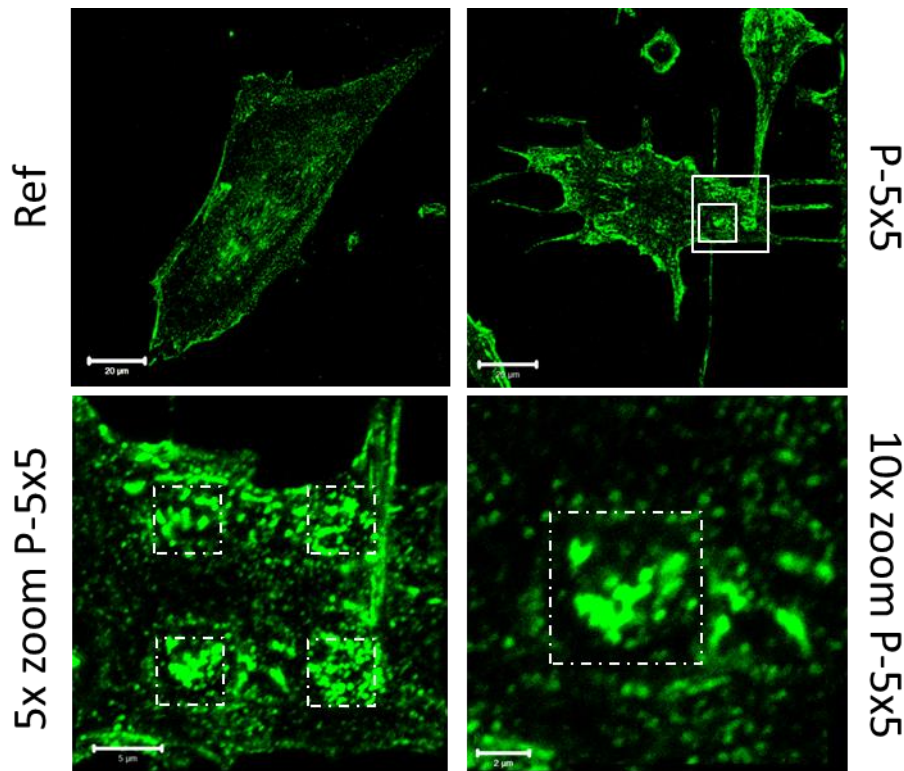


Figure 39: Immunofluorescence images of activated $\beta 1$ -integrin (CD29 9EG7) in MG-63 osteoblasts grown on micro-pillared topography (P-5x5) and on planar reference (Ref). Zoom region indicated by a white square and pillar plateaus dimension illustrated with dashed lines at 5x and 10x zoom, (bars 20 μm , for 5x zoom 5 μm , for 10x zoom 2 μm). Activated $\beta 1$ -integrin was found as clusters on the micro-pillar plateaus.

FAK is a non-receptor tyrosine kinase interacting with integrins at focal adhesion sides. This interaction activates FAK by leading to its autophosphorylation of Y397, which provides binding sites for Src kinase and other signaling molecules. Determination of the total protein amount of FAK (**Fig. 40a**) and Src kinase (**Fig. 40b**) by western blotting revealed no alternation in FAK but a tendential decrease of Src kinase protein amount on the micro-pillars after 24 h of MG-63 osteoblast cultivation. Analysis of the phosphorylated states of the proteins showed a significant reduction of the FAK phosphorylation at its Y397 (FAK(pY397)). For the Src kinase a significant remission in phosphorylated Y419 (Src(pY419)) was observed as well.

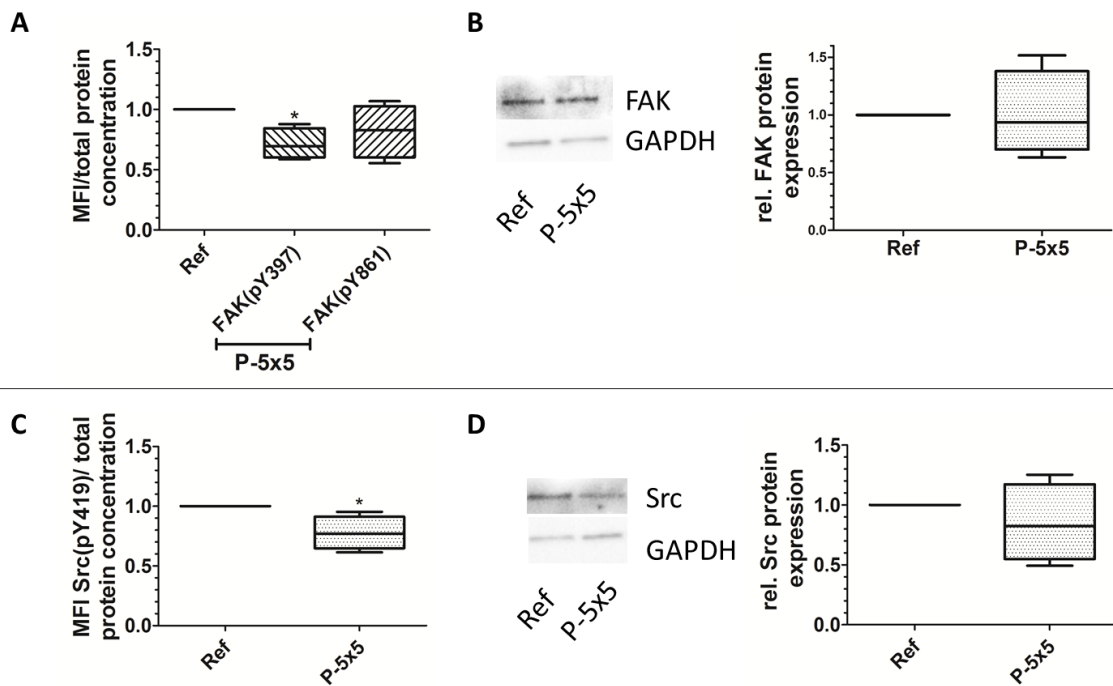


Figure 40: Focal adhesion kinase (FAK) and Src kinase (Src) phosphorylation in MG-63 osteoblasts after 24 h cultivation on micro-pillared topography (P-5x5) and planar reference (Ref). **(A)** Quantification of phosphorylated FAK at Y397 and Y861 via luminex assay. **(B)** Total protein expression of FAK via western blot with representative western blots and densitometric analyses, (Ref values normalized on 1, n = 4, Mann-Whitney U test, *: P < 0.05). **(C)** Quantification of phosphorylated Src kinase at Y419 via luminex assay. **(D)** Total protein expression of Src kinase via western blot with representative blots and densitometric analyses, (Ref values normalized on 1, n = 4, Mann-Whitney U test, *: P < 0.05). *Micro-pillar topography did not alter FAK and Src protein amount but reduced FAK phosphorylation at Y397 and Src phosphorylation at Y419.*

3.7 Attempted phagocytosis – Signaling molecules

The regulation of the phagocytic process involves complex signaling pathways. Therefore, the gene expression analysis by Rt-qPCR of the following signal kinases was performed: extracellular signal-regulated kinase (ERK1/2), phosphatidylinositol 3-kinase (PI3K) and the transcription factor nuclear factor κ B (NF κ B). mRNA expression studies showed no alteration of the ERK1/2 and NF κ B gene expression in MG-63 osteoblasts growing on micro-pillars after 3 and 24 h (**Fig. 41a**). This was confirmed by protein quantification via western blot for the 24 h cultivation time (**Fig. 41b**). PI3K gene expression was tendentially enhanced after initial 3 h cultivation period, but significantly decreased after 24 h cell cultivation on the micro-pillars. PI3K protein expression indicates only a slight tendency towards a reduced amount of PI3K protein after 24 h. Immunofluorescence staining revealed no altered localization of PI3K in osteoblasts on the micro-pillars (**Fig. 42**).

Whereas, immunofluorescence staining of the phosphatidylinositol lipids, including phosphatidylinositol-4-phosphate, phosphatidylinositol-4,5-bisphosphate (PI(4,5)P₂) and phosphatidylinositol-3,4,5-trisphosphate (PI(3,4,5)P₃), displayed a changed localization in the cell membrane of MG-63 osteoblasts towards more located on top and around the micro-pillars grown for 24 h (**Fig. 43**).

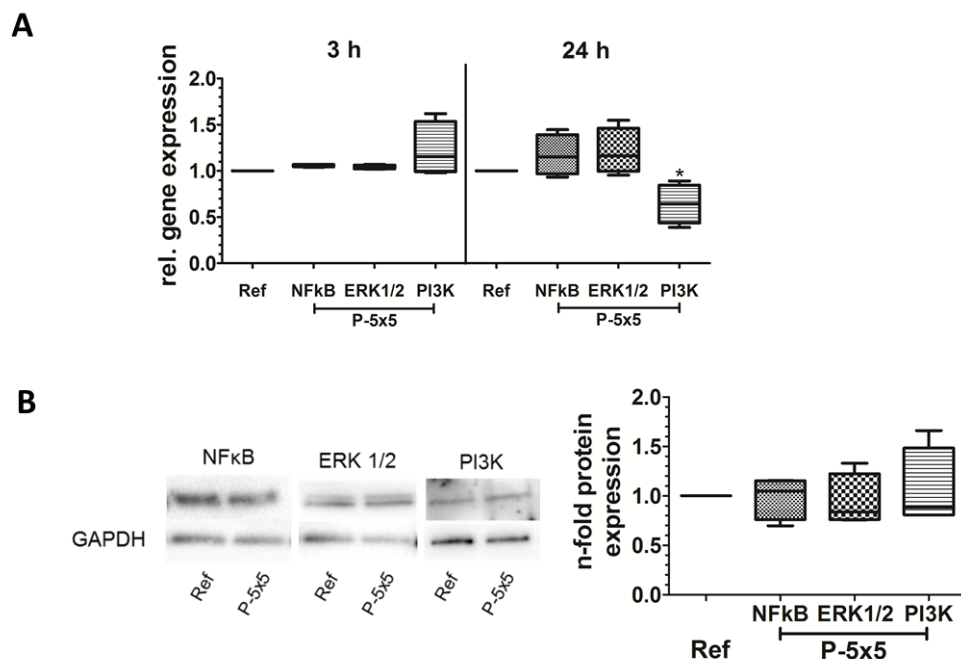


Figure 41: Investigation of the signaling proteins nuclear factor κB (NFκB), extracellular signal-regulated kinase 1/2 (ERK1/2) and phosphatidylinositol 3-kinase (PI3K) on micro-pillared topographies (P-5x5) and planar reference (Ref). **(A)** Relative gene expression (mRNA) after 3 and 24 h cell cultivation, (Ref values normalized on 1, n = 4, Mann-Whitney U test, *: P < 0.05). **(B)** Protein expression determination after 24 h via western blot with representative western blots and densitometric analyses, (Ref values normalized on 1, n = 4, Mann-Whitney U test). Gene and protein expression of the signaling proteins were unaltered by the topography, except for the decreased PI3K gene expression after 24 h.

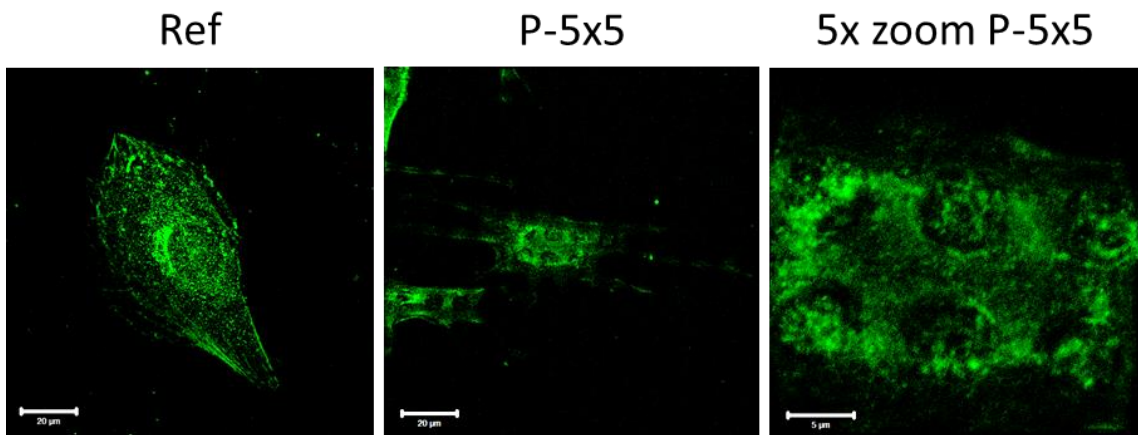


Figure 42: Immunofluorescence images of phosphatidylinositol 3-kinase (PI3K, green) in MG-63 osteoblasts grown for 24 h on micro-pillared topography (P-5x5) and planar reference (Ref), (left and middle bar 20 μm and right 5 μm for the 5x zoom). PI3K localization was unchanged dependent on the micro-topography.

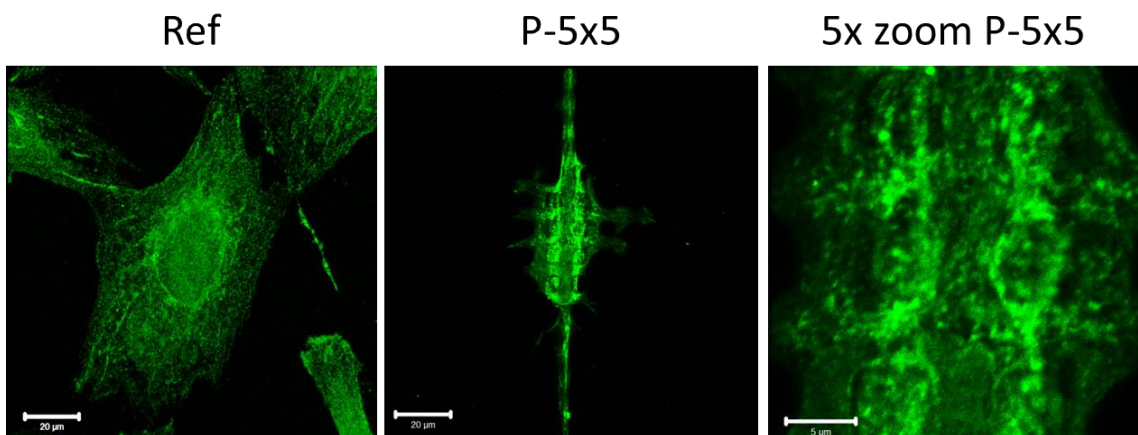


Figure 43: Immunofluorescence staining of the phosphatidylinositols phosphatidylinositol-4-phosphate, phosphatidylinositol-4,5-bisphosphate (PI(4,5)P₂) and phosphatidylinositol-3,4,5-trisphosphate (PI(3,4,5)P₃) with PIP2 anti-phosphoinositol antibody in MG-63 osteoblasts grown for 24 h on micro-pillared topography (P-5x5) and planar reference (Ref), (bars 20 μm and for 5x zoom 5 μm). Micro-pillar topography led to increased phosphatidylinositol localization around the micro-pillars.

Treatment with the PI3K inhibitor LY294002 revealed an impaired phagocytosis of the 6 μm particles (**Fig. 44**) and drastically reduced cell spreading (**Fig. 45**), consistent with the literature for macrophages [94]. Cell area measurements revealed a 3-fold reduction after particle and LY294002 treatment, whereas the LY294002 treatment alone without particles had no effect on the cell area after 24 h cultivation. However, the PI3K inhibition did not affect the typically clustered caveolae formation or the actin organization as short filaments, both concentrated on the pillar plateaus (**Fig. 46**).

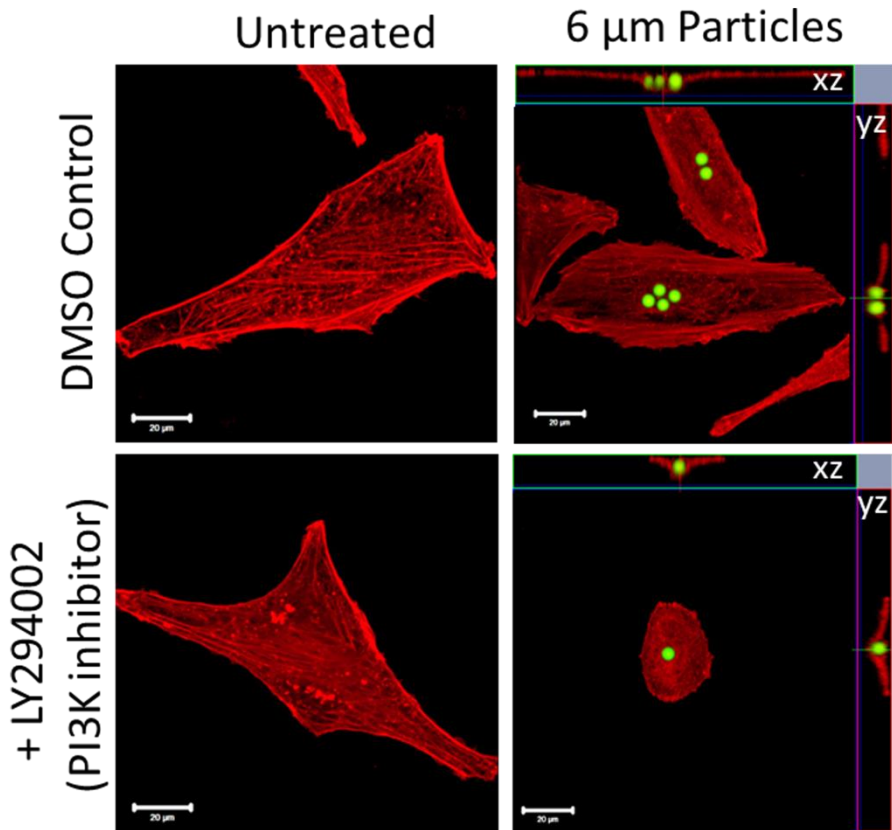


Figure 44: Immunofluorescence images of MG-63 osteoblasts after phosphatidylinositol 3-kinase (PI3K) inhibition with LY294002 (10 μ M) for 24 h. Actin cytoskeleton (red) and 6 μ m particles (green), (bars 20 μ m). PI3K inhibition diminishes micro-particle phagocytosis.

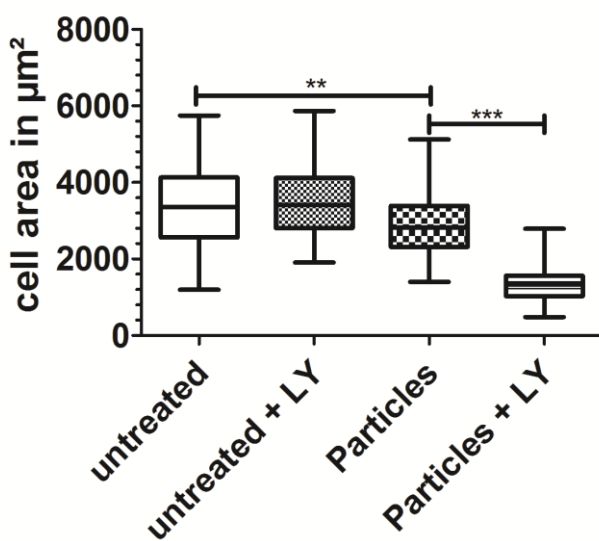


Figure 45: Cell area determination of MG-63 osteoblasts after 24 h cultivation with phosphatidylinositol 3-kinase (PI3K) inhibition via LY294002 (10 μ M) in combination with 6 μ m particle exposure. Untreated: no PI3K inhibition and no particle treatment; Untreated + LY: PI3K inhibition and no particle treatment; Particles: no PI3K inhibition but particle treatment; Particles + LY: PI3K inhibition and particle treatment, ($n = 2$ with 75 single cell measurements; Mann-Whitney U test; **: $P < 0.01$; ***: $P < 0.001$). PI3K inhibition and treatment with micro-particles to trigger phagocytosis reduced cell area of the osteoblastic cells.

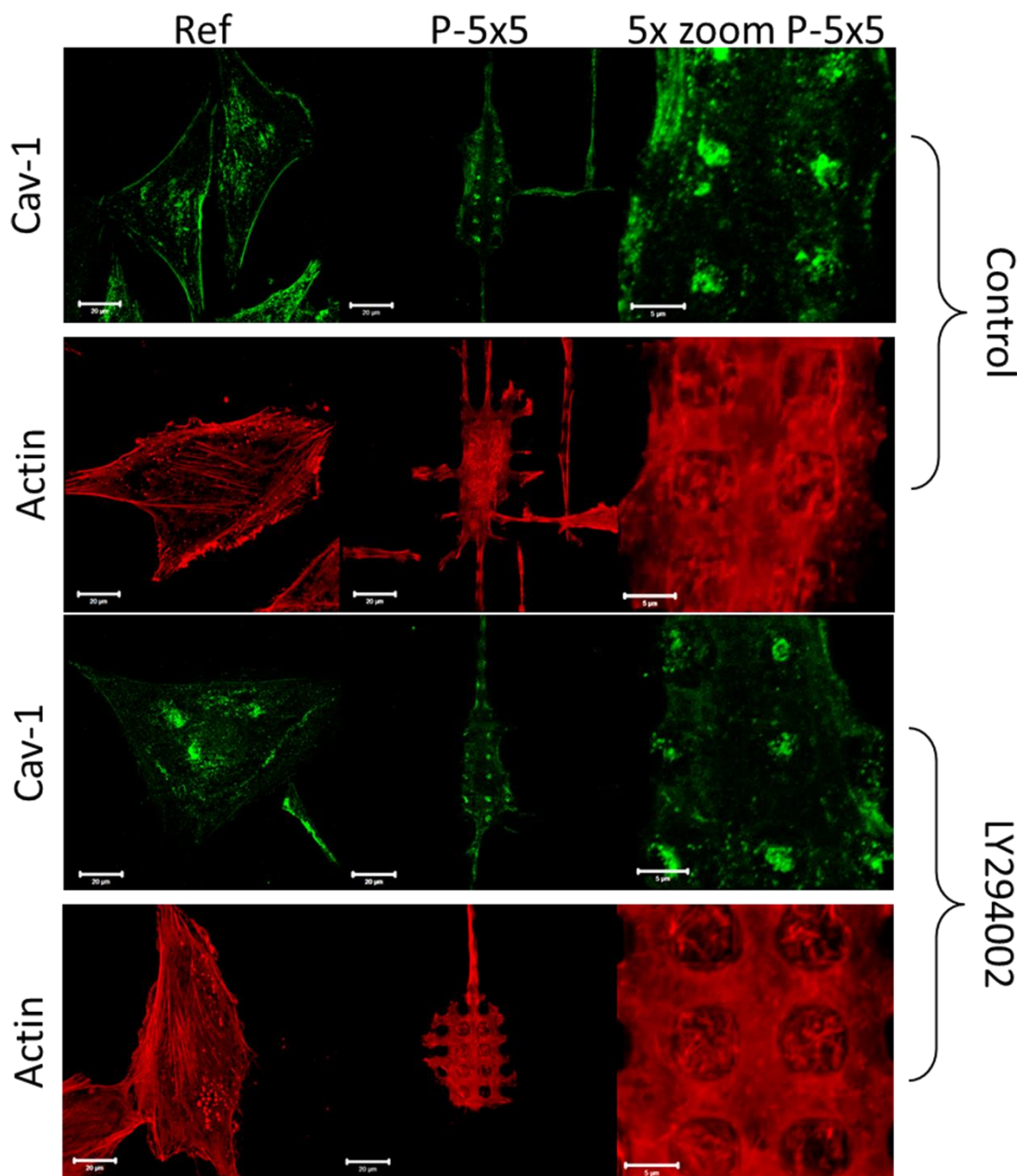


Figure 46: Immunofluorescence images of caveolin-1 (Cav-1, green) and the actin cytoskeleton (red) in MG-63 osteoblasts after phosphatidylinositol 3-kinase (PI3K) inhibition with LY294002 (10 μ M) for 24 h on micro-pillar topography (P-5x5) and planar reference (Ref), (bars 20 μ m and for 5x zoom 5 μ m). Cav-1 clustering and actin reorganization were unaltered after PI3K inhibition.

3.8 Inflammation response of MG-63 osteoblast towards the micro-pillared textures

Osteoblasts produce cytokines to regulate inflammation, which includes secretion of interleukins (IL), especially interleukin-6 (IL-6) [47]. The phagocytosis of implant wear particles was reported to stimulate the expression of pro-inflammatory factors, such as IL-6 and the inflammatory-related transcription factor NF κ B [48]. Therefore, the IL-6, as well as NF κ B expression were analyzed in MG-63 osteoblasts grown on the micro-pillars, as well as cells treated with the 6 μ m particles as positive control. IL-6 was determined out of the cell culture supernatant, so the secreted amount of IL-6, and measured via magnetic luminex assay. NF κ B protein amount was ascertained by western blot. Treatment of the MG-63 osteoblasts with 6 μ m particles led to increased NF κ B protein expression and IL-6 secretion. (Fig. 47)

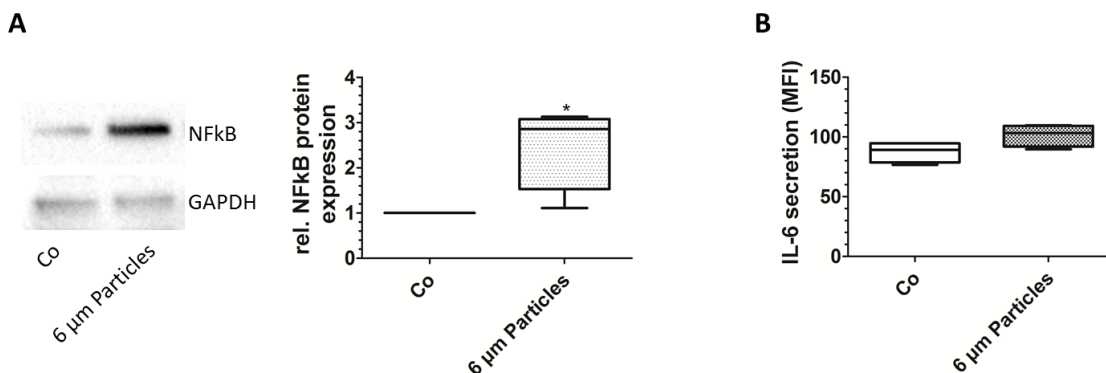


Figure 47: Treatment of MG-63 osteoblasts for 24 h with 6 μ m particles as phagocytosis trigger. (A) Relative NF κ B protein expression determined via western blot with representative western blots and densitometric analyses, (Control (Co) values normalized on 1, n = 4, Mann-Whitney U test, *: P < 0.05). (B) Quantification of Interleukin-6 (IL-6) secretion via luminex assay, (n = 4, Mann-Whitney U test, *: P < 0.05, MFI: mean fluorescence intensity). NF κ B protein amount was clearly elevated after treatment with micro-particles as phagocytosis trigger.

However, MG-63 osteoblasts grown on the micro-pillared topography showed no changes in the NF κ B protein expression after 3, 24 and 96 h of cultivation (Fig. 48), as it was demonstrated for gene expression after 3 and 24 h (Fig. 41).

IL-6 secretion was first tendentially increased during the initial 24 h cultivation, but nevertheless the IL-6 secretion was significantly reduced in osteoblasts grown for 48 and 96 h on the micro-pillars (Fig. 49).

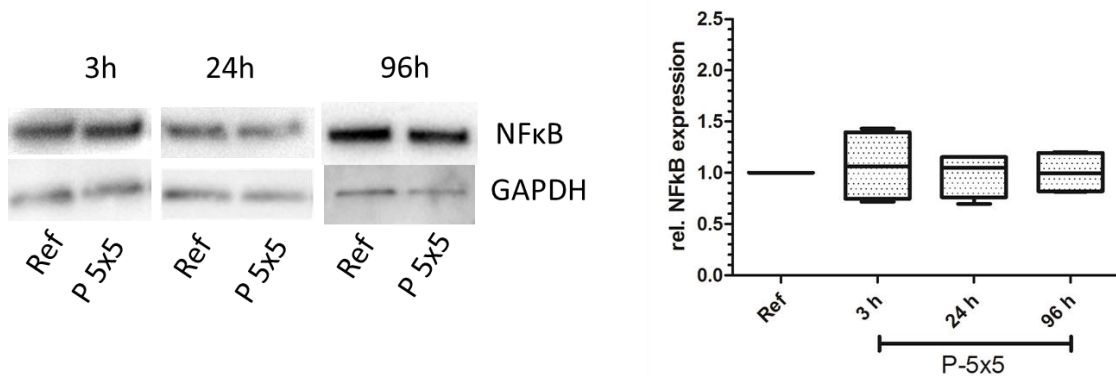


Figure 48: Time-dependent relative NF κ B protein expression in MG-63 osteoblasts after 3, 24 and 96 h cell cultivation on micro-pillared topography (P-5x5) and planar reference (Ref), left representative western blots and right densitometric analyses, (Ref values normalized on 1, n = 4, Mann-Whitney U test). *Micro-pillar topography did not influence NF κ B protein expression during 96 h cultivation time.*

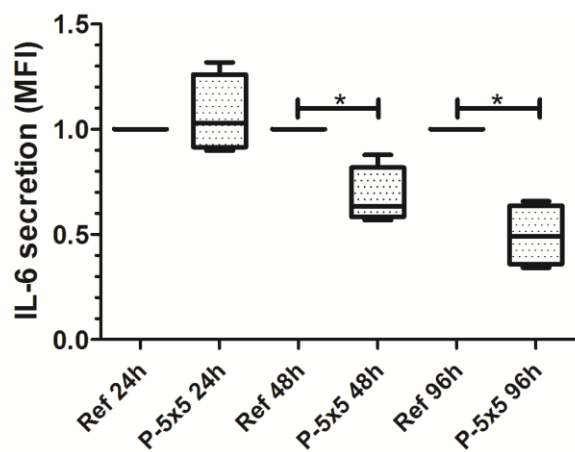


Figure 49: Time-dependent quantification of Interleukin-6 (IL-6) secretion of MG-63 osteoblasts after 24, 48 and 96 h cell cultivation on micro-pillared topography (P-5x5) and planar reference (Ref) via luminex assay, (Ref values normalized on 1, n = 4, Mann-Whitney U test, *: P < 0.05, MFI: mean fluorescence intensity). *IL-6 secretion was reduced after 48 h cell growth on the micro-pillar topography.*

3.9 Micro-pillar coating with plasma-polymerized allylamine (PPAAM)

The homogenous plasma polymer layer of plasma polymerized allylamine (PPAAM) was reported to render the surface more hydrophilic and creates positively charged amino groups on the surface [95]. Therefore, it promotes the initial cell spreading and increased cell mobility. This coating is proved to be a cell adhesive layer [36,95] and osteoblasts can overcome topographically restrictions, if they were cultivated on PPAAM-coated titanium [36]. The micro-pillared topography was coated with PPAAM to enhance the cell-material interaction by increasing the cell adhesion and mobility, to prove the hypothesis of the osteoblastic cells trying to internalize the surface-fixed micro-pillars to increase their surface contact.

In **Fig. 50**, the enhanced initial cell adhesion and spreading after PPAAM-coating is illustrated. The SEM images show widely spread out cells, reaching the bottom of the micro-topography already after 30 min on PPAAM coated pillar surfaces. On the uncoated micro-pillars, the cells exhibited a more spherical form and sit on maximal 4 pillars, whereas on the with PPAAM coated pillars the cells covered more than 4 pillars. After 24 h cultivation, the changes were not so drastic, such as seen after 30 min. The MG-63 osteoblasts on the PPAAM coated micro-pillars were still more spread out with the micro-pillars more imprinted into the cells.

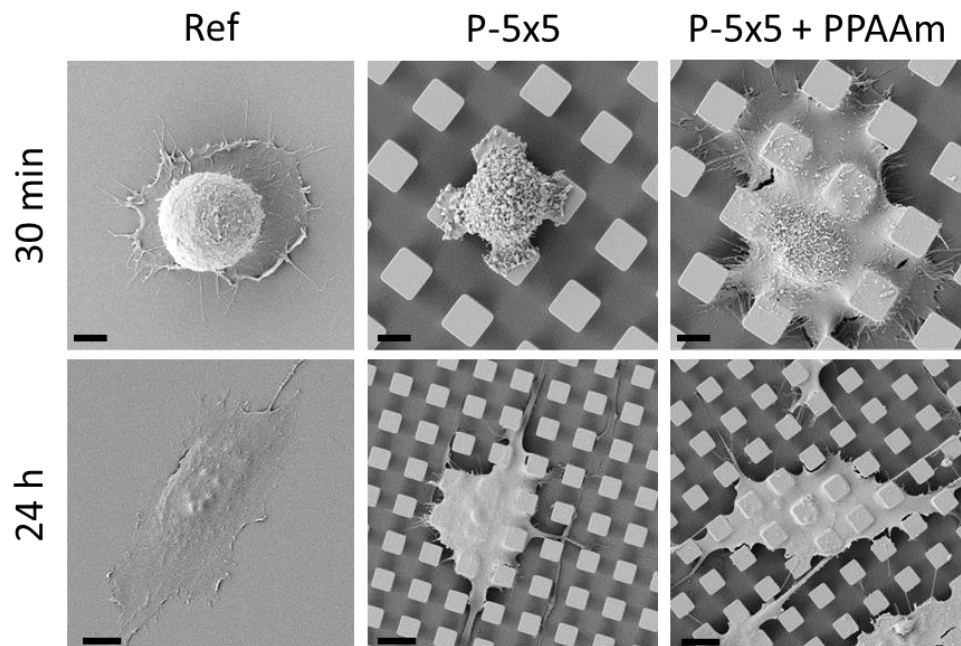


Figure 50: Scanning electron microscopy (SEM) images of MG-63 osteoblasts grown on micro-pillared topography (P-5x5), P-5x5 coated with plasma polymerized allylamine (PPAAM; P-5x5 + PPAAM) and planar reference (Ref) after 30 min (first row) and 24 h (second row) cultivation time, (first row 3,000x magnification and bar 4 µm; second row 1,000x magnification and bar 10 µm, Merlin VP (Carl Zeiss)). PPAAM coating enhanced initial cell spreading on the micro-pillars.

There was the question whether the osteoblasts are still expressing the Cav-1 clusters on the micro-pillar plateaus after coating with PPAAm and therefore having an advantage in cell spreading? Immunofluorescence labeling revealed less Cav-1 cluster formation on the micro-pillar plateaus after PPAAm coating (**Fig. 51**). Just as observed after 72 h on the uncoated micro-pillared topography, the Cav-1 was found more clustered around the pillar walls (**Fig. 24**). The actin cytoskeleton of MG-63 osteoblasts grown for 24 h at PPAAm-coated micro-pillars was accumulated in a ring-like fashion around the micro-pillars, similar to the cells on the uncoated micro-pillars after 72 up to 96 h cultivation time (**Fig. 51+ 52 + 23**). The cell adhesive PPAAm coating boosted the cell spreading including the caveolae-mediated pillar uptake.

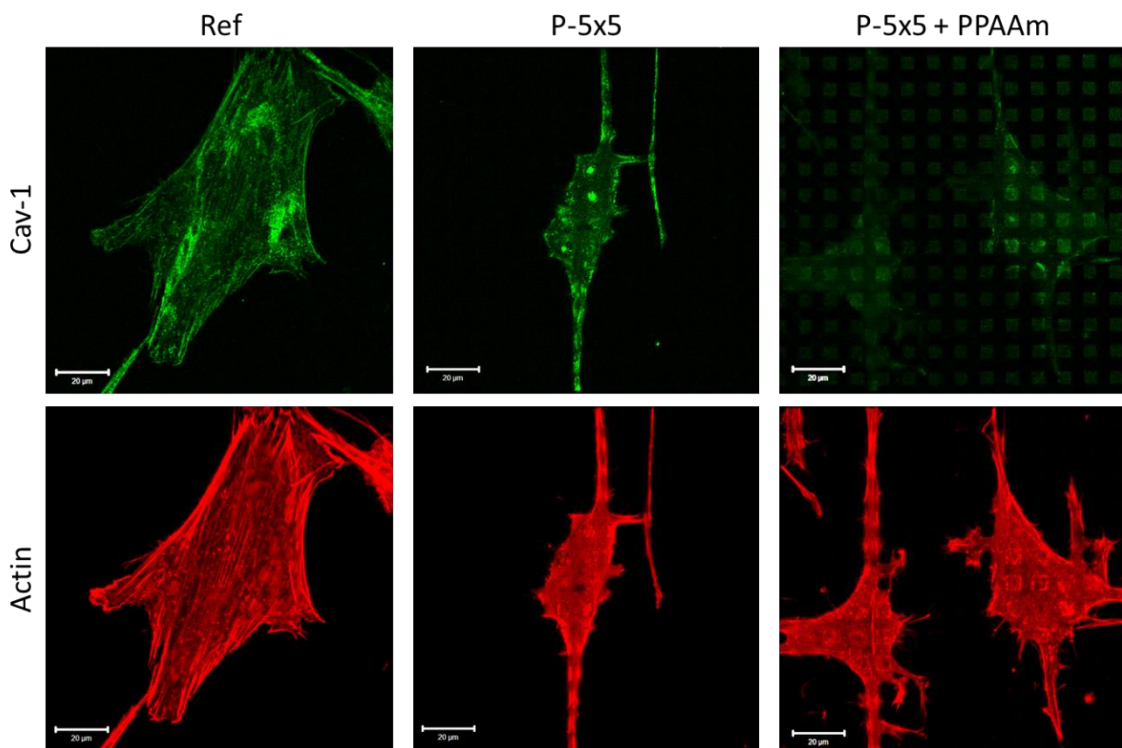


Figure 51: Immunofluorescence images of caveolin-1 (Cav-1, green) and the actin cytoskeleton (red) of MG-63 osteoblasts grown on micro-pillared topography (P-5x5), P-5x5 coated with plasma polymerized allyamine (PPAAm; P-5x5 + PPAAm) and planar reference (Ref) after 24 h, (bars 20 μ m). *Cav-1 clusters and actin filaments were prior located at the pillar edges and walls after PPAAm coating compared to uncoated micro-pillar topography.*

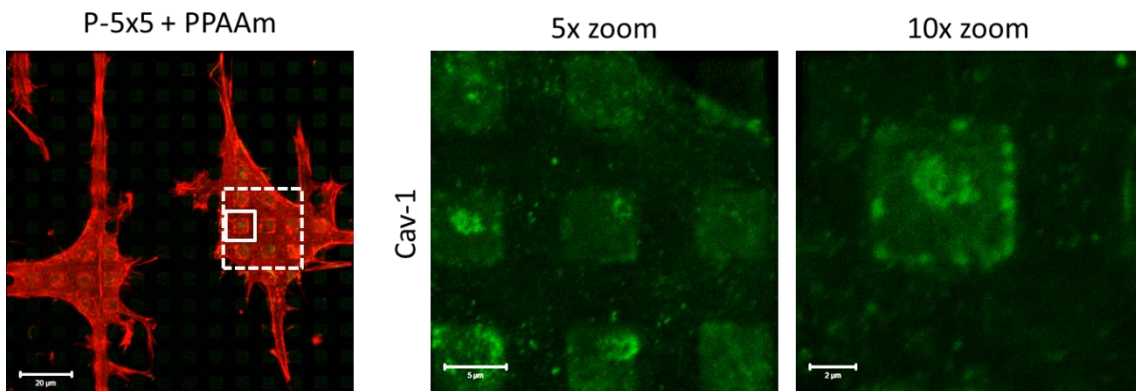


Figure 52: Immunofluorescence staining of caveolin-1 (Cav-1, green) and the actin cytoskeleton (red) in MG-63 osteoblasts grown on micro-pillared topography (P-5x5) coated with plasma polymerized allylamine (PPAAm; P-5x5 + PPAAm) after 24 h cell cultivation, (5x zoom of the marked area with white dashed lines, the continuously white line for the 10x zoom, bars left 20 μ m, 5 μ m for 5x zoom and 2 μ m for 10x zoom). *The actin cytoskeleton and Cav-1 were more shifted to the micro-pillar edges and walls after coating with PPAAm.*

The subsequent question was, if the PPAAm coating, with its advantage of enhanced cell spreading, was influencing beneath the Cav-1 localization also the reduced osteoblast marker expression on the micro-pillared topography? Therefore, the Cav-1 and osteoblast marker gene expression after 24 h cell cultivation on the uncoated and coated micro-pillar topography vs. the planar reference was determined. Cav-1 gene expression was significantly increased on the micro-pillared topography, but after PPAAm coating the Cav-1 gene expression was only tendentially elevated (**Fig. 53a**). The micro-pillars led to significantly reduced gene expression of Col1, FN and OCN (**Fig. 53c-e**), whereas after PPAAm coating these genes were only tendentially decreased or showed no difference to the planar reference. But the gene expression of ALP was significantly diminished on uncoated, as well as PPAAm coated micro-pillars (**Fig. 53b**).

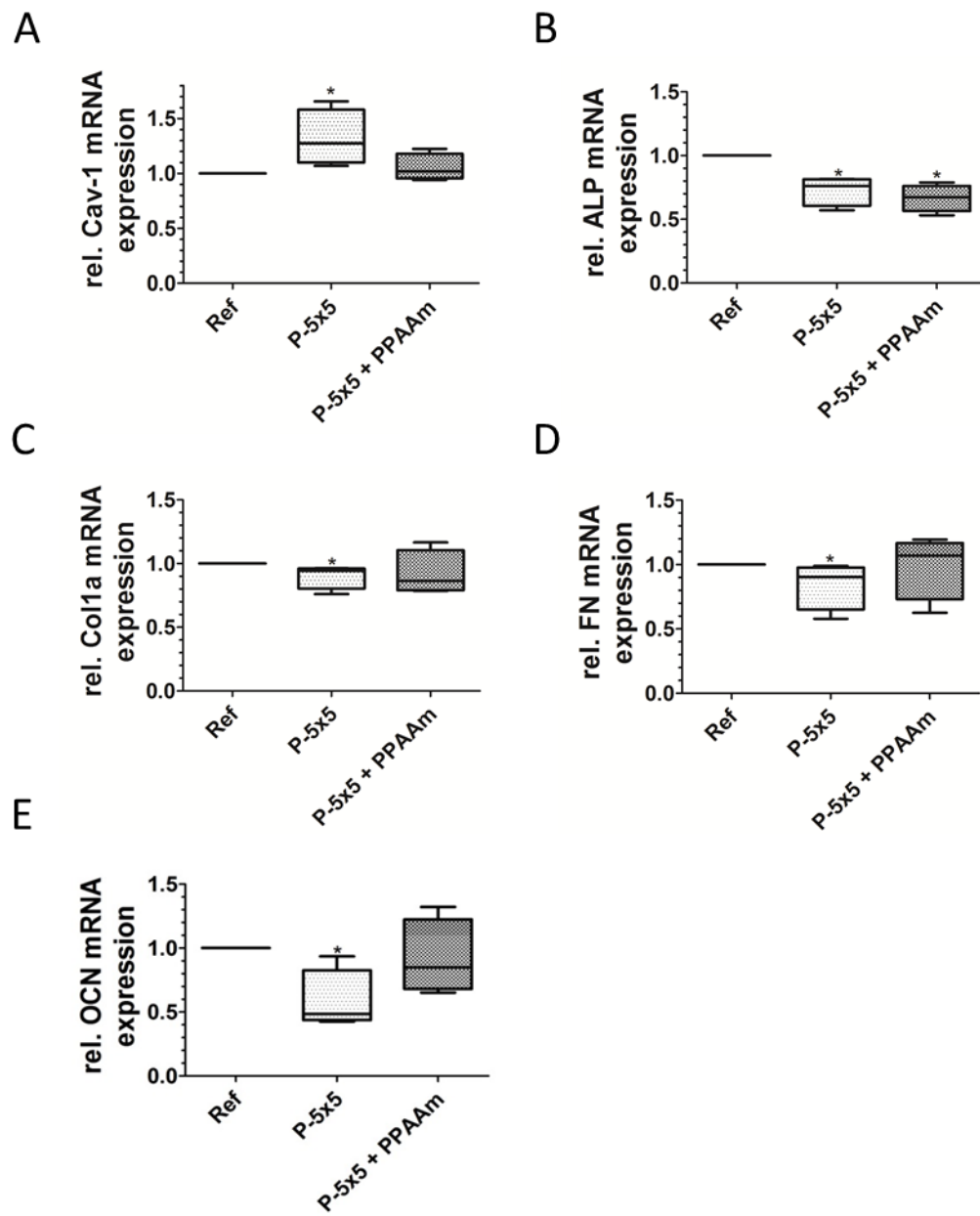


Figure 53: Relative mRNA expression of MG-63 osteoblasts after 24 h cultivation on micro-pillared topography (P-5x5), P-5x5 coated with plasma polymerized allylamine (PPAAm; P-5x5 + PPAAm) and planar reference (Ref). **(A)** caveolin-1 (Cav-1), **(B)** alkaline phosphatase (ALP), **(C)** collagen type I (Col1), **(D)** fibronectin (FN) and **(E)** osteocalcin (OCN), (Ref values normalized on 1, n = 4, Mann-Whitney U test, *: P < 0.05). Micro-pillar topography induced impaired osteoblast marker gene expressions were alleviated after coating with PPAAm, except for ALP.

3.10 Attempted phagocytosis on rough stochastic surfaces

On commercially available corundum-blasted rough titanium (Ti-CB) surfaces, characterized by sharp edges and ridges [7;8], osteoblasts adhered only at the elevations, spanned through the ridges (**Fig. 54**) and exhibited an irregularly distributed actin cytoskeleton (**Fig. 55**). Cav-1 was also predominantly localized in the region of the edges (**Fig. 55**), such as the elevations of the holes and pits created by the blasting process. Cellular ATP and ROS determination of MG-63 osteoblast-like cells on Ti-CB compared with planar, polished titanium surfaces (Ti-P) after 24 h of cultivation showed, analogous to the micro-pillared topographies, a reduced cellular ATP content (**Fig. 56a**) and elevated ROS levels (**Fig. 56b**). In contrast, the ADP content revealed a nearly constant value (**Fig. 56a**), which might a bit attenuates the ATP decrease on the Ti-CB substrates. Interestingly, the cell behavior on Ti-CB was similar to that on the micro-pillared surfaces, as well as after treatment with micro-particles.

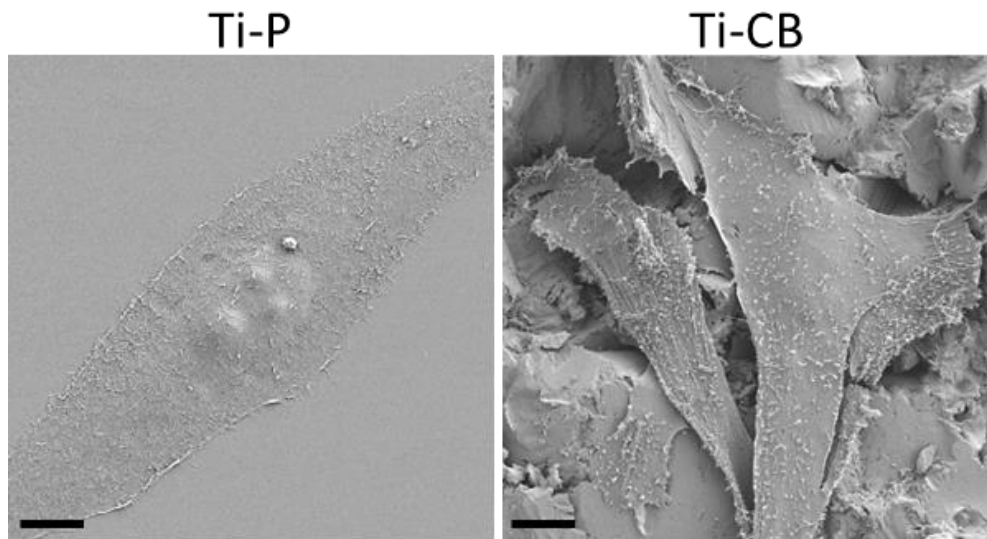


Figure 54: Scanning electron microscopy (SEM) images of MG-63 osteoblasts after for 24 h on corundum blasted (Ti-CB) titanium surfaces compared to polished (Ti-P) titanium surfaces, (1,000x magnification, bars 10 µm, Merlin VP (Carl Zeiss)). *Cells adhered at the elevations on Ti-CB topography.*

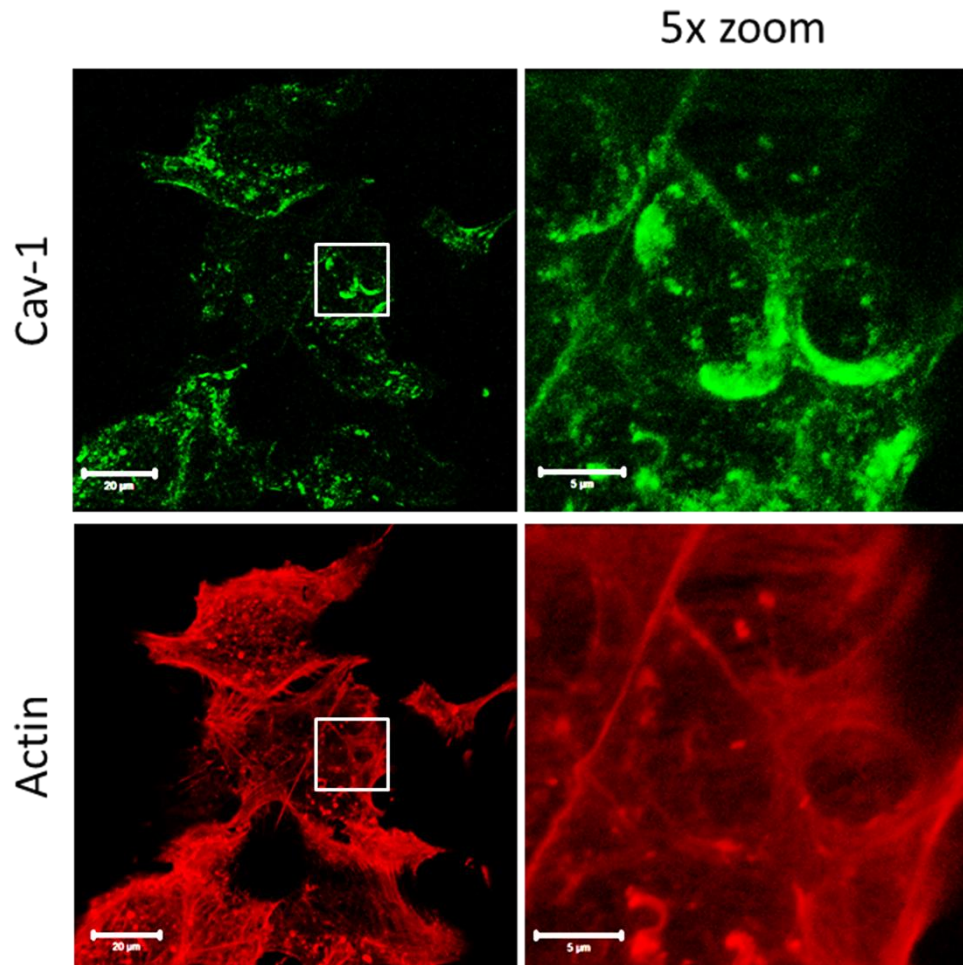


Figure 55: Immunofluorescence images of caveolin-1 (Cav-1, green) and the actin cytoskeleton (red) in MG-63 osteoblasts after 24 h on corundum blasted (Ti-CB) and polished (Ti-P) titanium surfaces, (bar 20 μ m, with 5x zoom of the white lined regions and bar 5 μ m). *Cav-1 and the actin fibers were accumulated in regions of elevations and sharp edges on Ti-CB.*

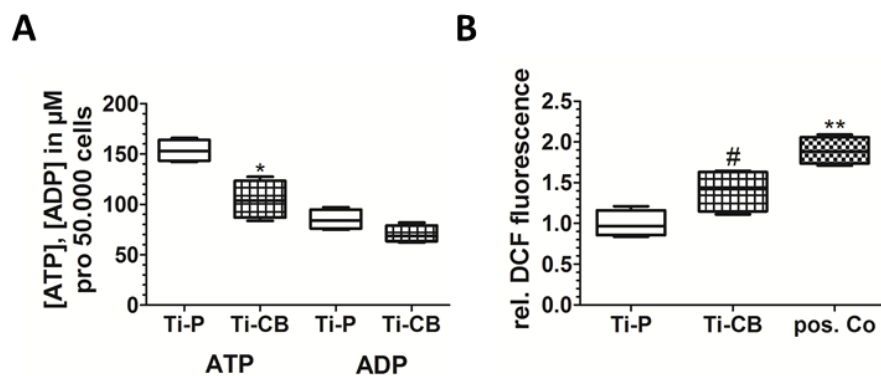


Figure 56: MG-63 osteoblasts cultivation for 24 h on corundum blasted (Ti-CB) and polished (Ti-P) titanium surfaces. **(A)** Intracellular ATP and ADP quantification, ($n = 4$, Mann-Whitney U test, *: $P < 0.05$). **(B)** Reactive oxygen species (ROS) determination by measurement of 2',7'-dichlorofluorescein fluorescence, (treatment with 50 μ M tert-butyl hydrogen peroxide served as positive control, mean value of Ti-P normalized on 1, $n = 4$, Mann-Whitney U test, #: $P = 0.0571$; **: $P < 0.01$). ATP amount decreased and ROS production rose due to of the Ti-CB surface.

4. Discussion

Biomaterial surface topography is known to affect cellular processes, such as cell adhesion, spreading, proliferation or production of extracellular matrix (ECM) proteins. Cells sense and test their underlying surface topography and react to it [25;28], consequently the surface topography influences significantly cell behavior and cell fate [3;9;31;96]. New implant design strategies pursue the development of bioactive surfaces evoking cellular responses, which promote osseointegration [3]. But the complex interplay of the cell-biomaterial interactions are not completely understood, despite increasing cell biological studies. One reason is the highly complex and varied biology of the cellular behavior. In addition, the commonly used stochastic surfaces with their randomized topography, containing a high diversity of surface features, impede the characterization of unique cell responses [97].

For the investigation of unique topography-induced cell changes, regular geometric micro-pillared structures were used as artificial surfaces, extending the work of stochastic surface models [5;6] with the advantage of constant topography variables.

This doctoral thesis base on previous studies of osteoblast interaction with geometric micro-pillared topographies and the found changes in the cells morphology, actin cytoskeleton organization, cell spreading, as well as impaired osteoblast function and ATP-stimulated calcium release [9;10;90;98].

Outstanding was the reorganized actin cytoskeleton and the accompanied decreased osteoblast marker expression on the micro-pillared surfaces.

Therefore, the aim of this thesis was to clarify the interplay of the micro-pillar-induced reorganized actin cytoskeleton with the cellular responses leading to the decreased osteoblast functions to extend the understanding of this specific cell-biomaterial interaction.

As experimental cell culture model, the human osteoblast cell line MG-63 was used. MG-63 osteoblast-like cells have an integrin subunit and phagocytic antigen profile similar to primary human osteoblasts, due to that they have been considered applicable for studying initial cell attachment to surfaces and wear debris phagocytosis [77;99]. Primary human osteoblasts and MG-63 osteoblasts express both the α_2 , α_5 , α_v , β_1 and β_3 integrin subunits [77] as well as various phagocytic surface antigens (i) molecules involved in activation of immune cells, e.g. CD44, (ii) costimulatory proteins participating in antigen presentation, such as CD54, CD80 and CD86, or (iii) molecules associated with cells of the monocytic lineage such as CD10 and CD13 [99]. In addition, preliminary work found similar cellular responses of MG-63 and primary human osteoblasts on titanium probes with stochastically modified surface topography [7;8].

Actin is known to have a primal role in diverse cellular processes and as the essential element of the cytoskeleton, it controls the morphological behavior of cells [24]. The MG-63 osteoblasts exhibited a changed phenotype on the micro-pillar structures [9;10]. The cells spread out on the top of the pillars, only the filopodia reached out to the bottom of the topography. This was opposite to the planar samples (Ref), where the MG-63 cells showed a randomly oriented, flattened phenotype and attachment with the entire cell body to the surface.

There has remained questions after the preliminary studies [9;10;90]:

- (i) Why do the cells rearrange their actin cytoskeleton in this specific manner, although the actin stress fibers could span from one pillar to the next?
- (ii) Why is the cell function disturbed?

4.1 Nucleus deformation and actin organization on micro-pillars

Analysis of the nucleus shape revealed a drastic deformation of the nucleus in cells growing on the micro-pillars. The sinking down and embedding of the pillars by the nucleus may be caused by fewer prominent, thick actin stress fibers localized above the nucleus in the MG-63 cells. Deformation of the cell nucleus by micrometric surface features has been shown to modify gene expression [100;101]. However, Badique and Davidson et al. [101-103] found no changes in gene expression of osteoblast-specific genes (including Col1) in MG-63, SaOs-2 and OHS-4 osteoblast-like cells, despite the deformation of their nuclei caused by growth on micro-pillars. Therefore, only the nucleus deformation might not lead to the impaired osteoblast functions.

The remodeling of the actin cytoskeleton is known to be required for phagocytic processes. The phagocytic domains contain proteins, e.g. AnxA2 or PI3K, which signal cellular movement by coordinated actin polymerization and the extension of the cell membrane over the internalized cargo. Therefore, actin filaments are concentrated in the advancing cup and creating a belt-shaped band that moves over the cargo [67]. This short, clustered actin filament organization was also found at the micro-pillars and led to the hypothesis of the attempted micro-pillar phagocytosis [52;54;67].

For this reason, the cells on the micro-pillars were investigated for different phagocytic pathways, such as the clathrin-mediated and caveolae/lipid raft-mediated phagocytosis. Clathrin localization revealed no alteration on the 5 µm sized pillar surfaces, indicating no clathrin-driven phagocytic pillar uptake. Clathrin coated vesicles are known to be formed by the cell during small-particle endocytosis [25] and with increasing cargo sizes, a shift to a mechanism that involved caveolae-mediated internalization was reported [104].

4.2 Caveolae-mediated phagocytosis of the surface-fixed micro-pillars

Caveolae-mediated phagocytosis: The two major caveolae-components Cav-1 and cholesterol showed a dot-like clustering in the basal osteoblast membrane at the region of the micro-pillar plateaus, after 24 h cultivation time. This phenomenon was not only observed in the human osteoblastic cell line MG-63, but also in the human osteoblastic cell lines SaOs-2 and U-2Os, as well as primary human osteoblasts and fetal osteoblasts. After 72 up to 96 h cultivation time of MG-63 osteoblasts grown on the micro-pillar topography, a shift of the dot-like Cav-1 localization towards surrounding the micro-pillars was observed. This was accompanied by the short filamentous actin, which was then clustered around the pillar walls, hinting a caveolae-mediated phagocytosis of the surface-fixed micro-pillars. SEM images of osteoblasts growing for 72 and 96 h on the micro-pillared topography showed a changed cell morphology compared to the cells after 24 h cultivation on the micro-pillars. These cells did not lie on top of the pillars anymore; instead they reached with the cell body to the bottom of the micro-pillared topography and engulfed the micro-pillars after the extended cultivation time.

Dalby et al. [25] refer an attempted phagocytosis of columns in the nanometer-range by fibroblasts. These fibroblasts had phenotypic similarities to the osteoblasts on the micro-pillars regarding the disrupted actin cytoskeleton, decreased spreading, changes in morphology and filopodia development to probe the surface topography. But the observed nano-column endocytosis was conducted via a clathrin-mediated phagocytosis, an internalization process considered used for small cargos [25;104], instead of caveolae-mediated phagocytosis used for bigger cargos, e.g. the micro-particles or micro-pillars.

Furthermore, Teo et al. [105] reported a phagocytosis of 2 µm poly(methyl methacrylate) pillars by human mesenchymal stem cells, the precursor cell type also for osteoblasts. Primary osteoblasts, as well as MG-63 osteoblast-like cells are able to phagocytize particles in sizes ranging from 0.7 to 10 µm of various compositions (e.g. titanium, titanium-aluminum-vanadium alloy, cobalt-chrome, ceramic, cement and ultrahigh molecular weight polyethylene), all leading to a decreased osteoblastic function by decreased ECM synthesis (including reduced Col1 expression), disorganized actin cytoskeleton, diminished cell spreading and proliferation [60;106-109]. Caveolae formation on the micro-pillar plateaus was confirmed by the dissipation of the dot-like cholesterol clusters after treatment with the lipid raft inhibitor Filipin III [79]. After 24 h cultivation time, the Cav-1 gene expression and Cav-1 phosphorylation were elevated, likewise the Cav-1 protein amount after 96 h cultivation. Upregulation of Cav-1 has been shown to be accompanied by an increase in the number of caveolae [110]. Tyrosine at position 14 (Y14) in the amino acid sequence of Cav-1 undergoes regulated phosphorylation (pCav-1) presumed by integrin-activated Src family kinases. pCav-1 is involved in stabilizing the focal adhesion kinase (FAK) at focal adhesion sites leading to focal adhesions turnover [69;111].

Several components involved in focal adhesion assembly are also important for phagocytosis and result in actin reorganization, e.g. the adapter proteins talin (binds both cytoskeletal and signaling components at focal adhesions) and vinculin (binds to talin and actin) as well as the focal adhesion kinase (FAK) [52]. The localization of pCav-1 at the micro-pillar edges, hinting to cell mobility in these regions, supports the pillar-phagocytosis thesis. Moreover, Cav-1 phosphorylation has been linked to caveolar phagocytosis [61;69].

Micro-pillar plateaus as adhesion sites: Clustering of lipid rafts/caveolae helps establish polarized platforms necessary for cell adhesion and migration [61]. Protein conformation of ECM proteins binding to the surface was reported to be changed in regions of topography edges and corners, e.g. reduced adsorption and higher degree of denatured adsorbed FN. Convex topography structures, such as the pillars edges, display less contact area than concave topography structures, resulting in decreased stabilization of protein-substrate interactions and therefore provoking the reduced adsorption and higher degree of denatured adsorbed FN [31;112]. On the top of the pillars, the membrane curvature is negative, having a concave shaped curve inwards towards the cell cytoplasm, which is unfavorable for the accumulation of adhesion molecules in focal adhesions [32]. Focal adhesion molecules induce a positive membrane curvature (convex shaped membrane, curved outwards towards the cytoplasm) and for this reason, focal adhesion molecules prefer positive membrane curvature for focal adhesion assembly [32] .In summary, convex structures like the pillar edges cause not only reduced adhesion-mediating ECM protein absorption but also unfavorable localization of focal adhesions molecules in the negative membrane curvature (concave shaped membrane).

These effects may explain why the cells require the long time period of around 48 h to overcome the micro-pillar edges. Moreover, the membrane experiences increased membrane tension at the pillared topography [32;105] and phagocytosis is disfavored at regions of high membrane tension [113]. For macrophages, a delayed phagocytosis was reported for slight convex curved or flat particles inducing high membrane tension [114].

The normal size of caveolae is about 50-80 nm [61;62]. Caveolae structures bigger in size emerged on the pillar plateaus indicating a formation of multi-caveolar structures, which might allow a greater expansion of the cell surface. Caveolae are reported to act as mechanotransducers in regions with tension generation [61], such as the tension inducing pillar topographies [32;105]. As a response to increased surface tension, cholesterol accumulated and increased the thickness, as well as stiffness of the membrane lipid bilayers [58;61] on the pillar plateaus. Accordingly, caveolae assembly is important for cell adhesion on topographies with reduced adhesion sites and tension regulation, such as the micro-pillared topography.

However, the caveolae formation could not just be the reason for the establishment of adhesion or tension regulation, because variation of the pillar sizes and spacing (length x width x height x spacing: 1x1x1x1 μm ; 2x2x5x2 μm ; 3x3x5x3 μm) resulting in less tension generation at the pillar regions [32], showed as well a dot-like Cav-1 clustering around and on the pillars after 24 h by MG-63 cells. Caveolae are known to be semi-permanent and stable membrane structures, so the short actin filaments on the pillar plateaus should be nonrelevant to keep the caveolae in a dispersed state [58]. After adhesion and caveolae formation on the micro-pillar plateaus, the cells could develop actin stress fibers for morphological stabilization and thus, there is no more necessity for the caveolae to act as membrane tension regulators. After all, this does not explain why the actin cytoskeleton was constantly fortified as short filaments on the pillars and the pillar edges otherwise than needed for the phagocytic attempt.

Cholesterol and actin stress-fiber formation: Actin stress-fiber formation is regulated by membrane cholesterol through processes that require the small GTPase Rho, the kinases ROCK and Src, as well as Cav-1. Cholesterol depletion was shown to enhance stress fiber formation in osteoblasts by increasing the phosphorylation of Cav-1 via Src-family kinases [115].

In the here presented experiments, a decline of cholesterol in MG-63 osteoblasts on the micro-pillars could be observed by relative quantification of cellular cholesterol content via Filipin III. Increased Cav-1 phosphorylation and expression was also observed, but no actin stress fiber formation. Due to that, the cells must underlie another cellular response, because normally the regulation of synthesis, influx and efflux keeps cellular cholesterol precisely controlled [116].

Enrichment of the lysosome-associated membrane protein CD68 in MG-63 osteoblasts at the pillar plateaus is further evidence of the attempt of micro-pillar phagocytosis by the MG-63 osteoblasts. CD68 serves as a scavenger receptor, which are important for phagocytosis and the delivery of lipids to their proper compartments [59]. CD68 protein amount was shown to be decreased in MG-63 cells on the micro-pillared topography, which might has caused impaired cholesterol delivery, resulting in the reduced cellular cholesterol levels.

In summary, all this findings substantiates the hypothesis of the actin reorganization as short filaments caused by the phagocytosis of the surface-fixed micro-pillars.

Caveolin-1 depletion: For the investigation of the role of Cav-1 in the attempted phagocytosis, siRNA-mediated knock-down of Cav-1 was performed. Depletion of Cav-1 led to decelerated micro-particle phagocytosis but no alteration in the actin cytoskeleton organization in the osteoblasts. In consequence, the altered actin organization around internalized particles, as well as on the micro-pillars was independent of Cav-1 itself.

Cav-1 knock-out mice are reported to survive well without the ability of caveolae-mediated phagocytosis, because internalization can also be accomplished via lipid raft-dependent mechanism [61]. Cav-1 was reported to stabilize caveolae structures, so loss or partially loss of Cav-1 can reduce the phagocytosis efficiency [61;62;64]. A total Cav-1 knock-down could not be established in the MG-63 osteoblast-like cells. In cells, where Cav-1 is abundantly expressed, such as osteoblasts, total attenuation of Cav-1 expression has proven challenging [117]. For the investigation of the actin organization after Cav-1 attenuation in MG-63 osteoblasts on the micro-pillars, only cells expressing nearly no detectable Cav-1 (controlled by immunofluorescence labelling) were considered as representative cells to ensure Cav-1 depletion conditions. For total Cav-1 depletion, osteoblasts isolated from Cav-1 knock-out mice would be the experimental system of choice, but were not available for the experiments during this thesis. The only partially Cav-1 depletion in the MG-63 osteoblast could also explain the reduced and uncompleted phagocytosis of the micro-particles after 24 h, whereas also a shift to other internalization processes, e.g. only lipid raft-mediated phagocytosis, might be possible [61].

Energy-consuming process: Phagocytosis is an active energy-consuming engulfment process with unique actin remodeling [52], which distinguished it from a passive wrapping of the micro-pillars by the cells. In this thesis, the changes of energy metabolism in osteoblasts trying to phagocytize the surface-fixed micro-pillars are reported, e.g. increased ATP-turnover and mitochondrial activity. The increased ATP-turnover is marked with a decrease in ATP amount, while the ADP amount was unaltered. Various cell types, including mouse macrophages and rat pheochromocytoma cells, displayed a decrease in their ATP levels in response to particle treatment as phagocytosis trigger [72]. The actin remodeling during phagocytosis is also a metabolically intense process [114]. ATP synthesis, so energy production in the mitochondria, is correlated with the mitochondrial activity [74;75]. Cells stabilize their energy charge by adjusting the rate of cellular ATP synthesis to the state of energy demand [73]. In consequence of the high energy demand of the micro-pillar phagocytosis, the cells exhibited an enhanced ATP turnover and mitochondrial activity. High mitochondrial activity is associated with ROS generation in the mitochondria [65;75].

Reactive oxygen species (ROS) production: Phagocytosis of particles was reported to increase ROS production in cells [118] and was also observed for our MG-63 osteoblasts treated with particles and grown on the micro-pillared textures. This was accompanied by increased protein expression of ROS-scavenging enzymes, such as catalase or superoxide dismutase. ROS levels could not be measured for cells treated with the 6 µm particles, because the green fluorescence of the particle would interfere with the green fluorescence of the 2,7-dichlorofluorescin (DCF) dye generated by contact with ROS and used for the quantification of ROS.

The measurement of only mitochondrial produced superoxide with MitoSOX™ showed only slight changes induced by the micro-pillared topography. Presumably, the mitochondrial produced and located superoxide got fast eliminated by the ROS-scavenging enzymes or translocated into the cytoplasm. Detection of ROS with DCF measures the overall ROS heterogeneity in the entire cell, not only superoxide in the mitochondria, and might therefore explain the significant elevated ROS determined with DCF in cells on the micro-pillared topography.

In conclusion, the osteoblasts on the micro-pillared topography showed raised energy production after 24 h, which results in higher ROS production and ROS-scavenging enzyme expression, caused by the higher energy demand for the phagocytosis. At the time point, where SEM analysis revealed that the osteoblasts fully engulfed the micro-pillars, the energy metabolism of the osteoblasts showed no significant difference compared to the cells on the planar reference. This indicates a probably finished phagocytic attempt of the surface-fixed pillars after 96 h.

4.3 Micro-particle internalization and inflammatory response

Micro-particle internalization: As a control experiment, treatments of the MG-63 osteoblasts with melamine particles 6 µm in size were performed. MG-63 cells internalized the micro-particles via a caveolae-mediated phagocytosis from their basal side, so surface fixed particles that can be detached by the cells after internalization, as well as free particles from their apical side.

These experiments proved that the osteoblastic cells (i) would be principally able to internalize cargos having the size of the 5x5 µm pillars; (ii) are taking up the micro-particles via a caveolae-mediated phagocytosis; (iii) show similar actin reorganization during particle uptake as observed on the micro-pillared topography; and (iv) are able to internalize more than one big cargo during 24 h.

MG-63 osteoblasts are reported to become saturated with 40-60 particles of 1µm size after 24 h [109]. The micro-particle experiments also revealed that the internalized micro-particles were concentrated and not freely distributed inside the osteoblastic cells. In this way, the cells may reduce the surface-volume ratio of the internalized cargos, which is impossible for the regularly arranged, fixed micro-pillars and may cause the deceleration of the uptake process for up to 96 h.

The internalization of the micro-pillars by the osteoblasts would require a lot of energy and the fixed pillar arrangement does not afford the possibility of concentrating the internalized cargos, as the cells can with particles, and would require a larger membrane expansion during the uptake. These might be reasons for the longer attempted internalization time of the micro-pillars (around 96 h) compared to the micro-particles (24 h).

Phagocytosable particle sizes were stated to be less than 10-15 µm and are reported to be phagocytized by osteoblasts [106;109]. Whereas, bigger structures remain trapped at the surface and are subjects of so-called “frustrated” phagocytosis [119]. Despite the fact, that the used micro-pillars have a much smaller diameter then 10 µm, the presented results show that these structures can also induce a trapped “frustrated” phagocytosis or at least before 96 h of cultivation.

Inflammatory response: NFκB functions, beneath in cell growth and differentiation, also in stress and inflammatory response [3;24;65]. Studies showed that implant wear debris stimulate the expression of the transcription-factor NFκB and pro-inflammatory factors such as interleukin-6 (IL-6), known to recruit monocyte-macrophages or induce osteoclast differentiation activity [49;108;120;121].

Treatment of the MG-63 osteoblasts for 24 h with the 6 µm particles coincided with the increased NFκB protein expression and the stimulated inflammatory response, measured by the IL-6 secretion. Whereas, MG-63 cells grown on the micro-pillared topography revealed no NFκB protein amount changes over the time of 96 h, consequently during the whole attempted micro-pillar phagocytosis phase. In addition, after a tendential increase of IL-6 secretion after 24 h cultivation on the micro-pillars, the IL-6 secretion and therefore the inflammatory response, was significantly decreased.

This was an unexpected cell reaction, because phagocytosis is always correlated with stimulation of the inflammatory response [54]. Nevertheless Wang et al. [122] reported a marked reduce in NFκB expression and inflammatory response in macrophages with Cav-1 overexpression. MG-63 osteoblasts featured a significant rise in Cav-1 protein amount in cells grown on the micro-pillars at the time points of the diminished IL-6 secretion.

Regarding the fact, that only surface contact of macrophage membranes with particles having a non-phagocytosable size was sufficient to trigger an inflammatory response, a much smaller one than the response triggered by completed particle phagocytosis, reflect the sensitivity of these professional phagocytes [109]. The delicate of macrophages was underlined by the study of Linares et al. [123], who showed that during nano-particle treatment macrophages exhibited a slower uptake rate and were more affected in their cell viability compared to osteoblasts, likely because their higher inflammatory response. Osteoblasts, as non-professional phagocytes, showed less sensitivity in inflammatory response, also after particle treatment.

Non-phagocytosable sized particles have no effect on the collagen synthesis in osteoblasts, which is impaired after treatment with phagocytosable sized particles [108;120]. These facts and in addition the overexpression of Cav-1 causing a reduced inflammatory response, might explain the unaltered NFκB protein amount and the abated IL-6 secretion in MG-63 cells after 48 h on the micro-pillars.

However, various NF κ B signaling pathways were reported hitherto, which were regulated differently. The alternative or non-canonical pathway act slow, depend on the NF κ B protein concentration and is activated by pathogen [124] or particle treatment [49]. In contrast, the classical, or canonical, NF κ B pathway is independent of the NF κ B protein concentration and act rapid and transient [124]. This pathway could be involved in the NF κ B signaling induced by the micro-pillared topography. But after all, this supposition needs further investigation of the expression and phosphorylation of I κ B and the p100 subunit of NF κ B. In the classical NF κ B signaling pathway, the I κ B phosphorylation and its subsequent degradation, results in rapid and transient nuclear translocation of NF κ B. The alternative NF κ B pathway relies on phosphorylation-induced proteasome-mediated processing of the p100 subunit to enable the nuclear translocation of NF κ B [124].

4.4 Phosphatidylinositol lipids and their binding protein AnnexinA2

Phosphatidylinositol lipids: The phosphatidylinositol lipids and their turnover, especially by the phosphatidylinositol 3-kinase (PI3K) are crucial for the transducing of internalization signals. PI3K is required for the phagocytosis of micron-sized particles but not for the initial phagosome development because of the sequential turnover of phosphoinositides during the phagosomal formation.

Phagocytic cup extension and early actin polymerization do not require PI3K, but later activities such as the fusion of the phagocytic cup. Phosphatidylinositol-4,5-bisphosphate (PI(4,5)P₂) is located in nascent phagosomes and converted by PI3K to phosphatidylinositol-3,4,5-trisphosphate (PI(3,4,5)P₃) in the late engulfment phase [56;94]. PI(4,5)P₂ is involved in recruiting the actin polymerization machinery, such as Arp2/3, required for actin assembly during phagocytosis by tethering actin-binding proteins [62;53], e.g. AnxA2 [55;57].

Phosphatidylinositol lipids were found to be enriched in regions of the pillar edges in MG-63 osteoblasts after 24 h cultivation on the micro-pillars. Inhibition of the PI3K via LY294002 in MG-63 cells resulted in a decreased micro-particle phagocytosis, accompanied with reduced cell areas after particle phagocytosis under blocked PI3K conditions. Whereas, PI3K inhibition showed no influence on the caveolae formation and actin reorganization in MG-63 cells grown on the micro-pillars. Possibly, because the cells on the micro-pillars never reaches the late engulfment phase due to the fact, that they are never able to fully engulf and closure the micro-pillars because of their surface-fixed position.

Furthermore, it is reported that PI3K inhibition arrests phagocytosis after assembly of the actin-rich cup [53], consequently at stages that were not reached by the MG-63 osteoblasts on the micro-pillars.

PI(3,4,5)P₃ levels rise abruptly in membranes of phagocytic cups to activate enzymes important for the cup closure and indicating a feedback activation of PI3K [53]. MG-63 osteoblasts on the micro-pillared topography revealed a significant decrease in PI3K gene expression after 24 h, at a time point where normal particle phagocytosis was already finished, but the pillar phagocytosis is still forming the phagocytic cup. This decrease in PI3K gene expression might reflect this feedback regulation, because the triggered micro-pillar phagocytosis was more time sophisticated than normal phagocytosis.

Annexin A2 (AnxA2): AnxA2, an actin- and phosphatidylinositol lipid-binding protein, is associated with the organization of lipid rafts at sides of actin recruitment [125], as well as it is reported to induce larger cholesterol cluster formations and stabilize caveolae during their formation [57]. After 3 h of cell cultivation on the micro-pillars, MG-63 osteoblasts exhibited augmented AnxA2 localization in regions of the pillar plateaus, reflecting the AnxA2 property to help form caveolae. After 24 h cell cultivation, the protein amount of AnxA2 was significantly elevated, which might illustrate the essential function of AnxA2 in caveolae stabilization and actin recruitment.

Lipid rafts, as well as caveolae as special form of lipid rafts, contain actin-binding proteins to regulate the actin rearrangements during phagocytosis by binding proteins such as AnxA2 to the in the cell membrane located phosphatidylinositol lipids [57;125]. Annexins are calcium regulated phospholipid-binding proteins, which are not only involved in caveolae formation and actin recruitment to the phagosome [126], but they also play a role in integrating calcium signaling with membrane dynamics during phagosomal maturation [125, 127].

Caveolae regulate calcium signaling pathways by providing a stable platform for the machinery triggering calcium release, thus regulating the spatial organization of calcium entry sites and the delivered amount of calcium to these sites [129]. Therefore, the caveolae also participate in the control the calcium-triggered signals leading to the actin rearrangements during phagocytosis [128;129]. A rise in the cytosolic calcium concentration is an early event that accompanies phagocytosis. It regulates subsequent steps during the phagocytic process and is required for efficient phagosomal maturation [127].

Preliminary research revealed an impaired ATP stimulated calcium ion mobilization and a decreased cytosolic calcium concentration in osteoblasts grown on the micro-pillar topography compared to the cells on the planar reference [10].

These findings might indicate that the cells on the micro-pillar topography had already experienced some calcium oscillation caused by the attempted pillar phagocytosis, which led to a reduced cytosolic calcium concentration, as well as a diminished response of calcium mobilization.

4.5 Integrins and integrin-mediated signaling

Integrins: Beneath phosphatidylinositol lipids, other proteins implicated in phagocytic processes are located in the plasma membrane, e.g. the transmembrane cell adhesion receptors known as integrins. Integrins link the ECM with the actin cytoskeleton and transduce signals from the ECM to the cell. Therefore, clustering of activated $\beta 1$ -integrins results in elevated adhesion strength on reduced surface areas [24;107], which in the case of the micro-pillared topography is presented by the micro-pillar plateaus [130]. The activated $\beta 1$ -integrin was found to be clustered in these regions.

In addition, integrins are known to mediate phagocytosis over a wide range, from uptake of big particles to the capture of smaller cargos, such as collagen fibrils. Phagocytosis is not considered to be a feature of specialized integrins, but rather an extension of their capacity to mediate adhesion, including integrins that mediate binding to ECM components, such as the $\beta 1$ -integrin. Phagocytosis and adhesion rely on the same integrin-mediated regulatory and signaling mechanism [67].

Integrin-mediated FAK activation is further required for the reorganization of the actin cytoskeleton and microtubule stabilization [107]. Tubulin organization in MG-63 cells is not altered by the micro-pillared topography, but the clustered activated integrin may affect the actin organization regarding actin-driven phagocytosis [107].

Integrin-mediated signaling: Integrin signaling pathway is specifically required to activate or maintain caveolae-mediated phagocytosis [131]. Integrin-mediated autophosphorylation of FAK at its tyrosine (Y) 397 (FAK(pY397)) [50] was significantly decreased in MG-63 osteoblasts growing for 24 h on the micro-pillars, while the FAK protein amount was unchanged. This phosphorylation decrease might reflect the reduced adhesion site offered by the micro-pillar plateaus. Reduced autophosphorylation of FAK lead to less accessible binding sites for the Src kinase, which transphosphorylates FAK at its Y861 (FAK(pY861)) resulting in paxillin recruitment to the focal adhesion and connecting them with the actin cytoskeleton. The paxillin binding enables the mature of the focal adhesions and anchorage of the cells with its underlying surface [50;132].

The FAK(pY861) phosphorylation in cells after 24 h on the micro-pillars showed, consistent with the less accessible binding sides for the Src kinase, a decrease in Src kinase mediated FAK(pY861) phosphorylation. Src kinases are also involved in the phosphorylation of other proteins such as Cav-1, leading to focal adhesions turnover and migration instead of focal adhesions maturation and cell anchorage [69;111;133]. The Y14 phosphorylation of Cav-1 is required for the recruitment of Cav-1 to the focal adhesions, where Cav-1 associates with $\beta 1$ -integrins and links the integrins to Src kinases, which regulated in conjugation with FAK focal adhesions turnover, migration and proliferation [68].

MG-63 osteoblasts displayed a decreased Src phosphorylation after 24 h cell cultivation on the micro-pillars, accompanied with reduced Src protein amount. Considering the less accessible binding sites at the FAK, Src might be more implicated in Cav-1 phosphorylation, which was found to be raised in cells grown on the micro-pillars. Consequently, the signaling in the cells grown on the micro-pillars is more associated with cell migration and movement than anchorage of the cells on the micro-pillar topography. The reduced Src kinase protein amount could be explained by the fact that Cav-1 inhibits the Src kinase phosphorylation and expression by binding Src in an inactive conformation [68].

For osteoblasts phagocytizing micro-particles, a decrease in the integrin-mediated autophosphorylation of FAK (FAK(pY397)) was reported [107], which might reflect the cell movement triggered by phagocytosis.

Cells react to exterior force stimuli via various complex signaling pathways, such as the extracellular signal-regulated kinase 1/2 (ERK 1/2) and the nuclear factor κ B (NF κ B) [134]. These signaling proteins are located downstream of the integrin signaling pathway and participate in the regulation of cell growth, differentiation and stress response [3;24;62;64;65;100]. The micro-pillared topography with reduced adhesion sites and resulted tension force generation [32] showed no influences on the gene and protein expression of ERK1/2 and NF κ B in MG-63 osteoblasts.

These findings might indicate that the cells do not react to the micro-pillars just as stamps creating tension force.

4.6 Cell-material surface contact establishment

Plasma membrane reorganization works in concert with the underlying actin cytoskeleton to mediate morphological changes and cell-surface contact [111]. Actin remodeling is especially sensitive to signals that are generated at the membrane-cytoplasm interphase [55]. The actin reorganization at the micro-pillar topography was shown to be characteristic for phagocytosis and not for cells just wrapping over the pillars, because at the mature pillar phagocytosis after 72 up to 96 h, the actin cytoskeleton was concentrated as rings around the micro-pillars.

If the cells would just passively wrap around the micro-pillars, they would not change their energy metabolism and display the unique actin reorganization. Initial cell adhesion (identified 30 min after cell seeding) on the micro-pillars contains settlement of the cells on maximal four pillars. Afterwards, the cells were actively testing the underlying topography with their filopodia. This testing of the underlying topography was first shown by Dalby et al. [25] with fibroblasts exploring nano-sized topography.

Assuming the cells would just passively, non-phagocytizing, elongate and spread at the micro-pillared topography, they would possibly elongate with their lamellipodia extensions between the pillar rows and not span over the pillars. A location between the pillar rows would offer the cells maximal surface contact and adhesion sites. During the cell observations in this study, cells were occasionally observed to be located merely between the pillar rows.

Altogether, this thesis assumes a high energy requirement for the cell's attempted phagocytosis of every single pillar in a fixed position, leading to the question: why do the cells going through the nuisance of the pillar phagocytosis, if it is accompanied with high energy requirements and negative cellular outcome?

A possible explanation for this cell behavior would be given by the fact that osteoblasts are attachment dependent cells, which want to ensure the highest cell-ECM(surface) contact. The maintenance of the osteoblastic function relies on this contact, therefore a certain cell-ECM contact is needed for an adequate osteoblastic cell function [106;107].

Coating of the P-5x5 micro-pillar topography with plasma polymerized allylamine (PPAAm) [85;135] revealed alleviation of the micro-pillar-induced reduction of the osteoblastic markers genes Col1, FN and OCN. After coating the micro-pillars with PPAAm, MG-63 osteoblasts displayed increased initial cell spreading and after 24 h cultivation time, the micro-pillars showed a deeper imprinting into the cells, displayed by the molding of the MG-63 cells into the pillared topography. Cav-1 was found more to be localized in regions of the pillar edges. The actin cytoskeleton was also accumulated around the micro-pillars, pointing to an expedited pillar phagocytosis. This Cav-1 and actin organization was found on the uncoated P-5x5 surfaces not before 48 h cultivation time. PPAAm coating was reported before to be a cell adhesive layer, promoting accelerated cell spreading [36;95].

In conclusion, this confirms the hypothesis of the osteoblasts wanting to create the highest cell-surface contact to maintain their osteoblast specific function, displayed by the production and secretion of ECM proteins.

ALP is involved in the mineralization of the bone ECM, and its gene expression was reduced on the micro-pillared topography, but unaffected after the coating with PPAAm. This leads to the assumption that the reduced ALP gene expression on the micro-pillared topography is not caused by lessened cell-surface interaction and more by the phagocytic process. If a process requires high energy demands, such as phagocytosis, other energy expenditures must be abated [73], e.g. the expression of proteins, such as ALP, which are redundant in case the cells produce less ECM or occupied with establishing sufficient cell-ECM contact.

Especially considering, that high energy demands are placed on osteoblasts not only during phagocytosis, but also at the production of the ECM, by expressing and secreting ECM proteins [136].

Unfortunately, the PPAAm coating exhibits autofluorescence, especially in the green channel. This would interfere with quantitative immunofluorescence analysis on these structures; therefore the mitochondrial activity could not be measured. Additionally, the PPAAm coating does not allow the trypsinization of the cells in a vital state from the micro-pillared surfaces due to its high cell-attractive characteristics. MG-63 cells on PPAAm were 1.5 times more resistant to a shear stress compared to cells on uncoated titanium [137]. For that reason, the cellular cholesterol amount, intracellular ADP and ATP amount and ROS generation could not be investigated.

4.7 Stochastic rough surfaces and commercial implant designs

Roughening of Ti is used for commercial implant surface modification. The rough implant topography can increase the contact surface with the bone by providing more surface sites for osseointegration, thus a better biomechanical interlocking between bone and implant [3;19;39;138].

One standard method for roughening the Ti surface is by blasting the Ti surface with corundum particles (Ti-CB) thereby creating irregularly distributed sharp edges and elevation, having a roughness value (R_a : mean of the peak-to-valley measurements of a surface) of $R_a = 6 \mu\text{m}$ [8;139].

Previous studies reported a reduced mineralization rate in osteoblasts on Ti-CB, hence a decreased osteoblast function, after the first 24 h of cultivation. In addition, the actin cytoskeleton was rearranged in short filament clusters, as well as the $\beta 1$ -integrin and the focal adhesions adapter protein vinculin were found in clusters at the region of sharp edges and elevation [7;8].

Osteoblasts at Ti-CB surfaces adhered only at the elevations, and therefore the cell morphology was similar to the MG-63 osteoblasts cultured on the micro-pillar topography, as well as their actin cytoskeleton distribution, $\beta 1$ -integrin and vinculin clustering at the elevations [9].

Cav-1 localization analysis in MG-63 osteoblasts on Ti-CB revealed an accumulation of Cav-1 in the regions of the irregularly distributed actin cytoskeleton on the elevations. Furthermore, the MG-63 osteoblast exhibited an increased ATP turnover and ROS generation after 24 h on the Ti-CB surfaces. These responses were also observed for the osteoblasts on the micro-pillared topography as well as after treatment with micro-particles as phagocytosis trigger. Finally leading to the conclusion, that osteoblastic cells might not only attempt to phagocytize the geometric micro-pillars but also the elevations on stochastic rough surfaces to ensure the highest cell-ECM contact to maintain the osteoblastic function [106;107].

Micro-roughness of bone-replacing implants is a controversial factor and the mechanisms effecting cell behavior on micro-rough topographies remain still unclear. One possible reason is the lack of systematic studies investigating the changed physicochemical properties, e.g. surface energy or surface chemistry, dependent on the different micro-roughness structures or modifications. Also problematically is a consistent definition of the surface roughness of the many various rough topographies. The most widely used parameter to characterize the roughness is the R_a value, which determines the average peak-to-valley-height. But this value does not consider the type of topography, such as the spacing between the irregularities, or the different shapes, e.g. ridges, holes, pores, curvature of valleys and especially the sharpness of the peaks. Therefore, the comparison of the various data is difficult [3].

Some studies reported positive influences by micro-roughness on osteoblasts, such as exhibiting a more differentiated phenotype by increased alkaline phosphatase activity and osteocalcin expression [23;30]. In addition, micro-roughness was reported to generate an osteogenic micro-environment through higher production of prostaglandin E₂ as well as transforming growth factor $\beta 1$ and an enhanced production of natural physiological resembling bone matrix in combination with reduced osteoclast activity [3;140].

However, others had reported negative effects of the surface micro-roughness on osteoblasts, such as lower cell numbers, diminished cell spreading and proliferation as well as reduced expression of the osteoblast marker alkaline phosphatase [134;140-142]. Cells growing on rough surfaces showed changes in their cell physiology, such as the integrin expression [7;34] and formation of vinculin-containing focal adhesion sites [139]. Nebe et al. [112;139] revealed not only a topography-induced integrin and vinculin expression in osteoblasts, but also showed that the underlying topography affect the actin cytoskeleton at various stochastic rough surfaces, e.g. machined, vacuum plasma sprayed, blasted with glass spheres or corundum particles, all are commercially used as implant surface modifications.

After all, osseointegration is reported to be enhanced on rougher surfaces rather than on smooth ones, because it offers a higher surface area and therefore more sites for bone fixation [140].

Implants, containing a micro-rough surface, have the disadvantage of releasing wear debris particles with an average size of 1 μm . In consequence, these wear debris have a phagocytosable size and have the potential to elicit an inflammatory response, as well as weaken the surrounding osteoblasts in their function [48;143;144].

In vivo studies documented attenuated osteoblast function and integration strength due to co-cultivation with titanium particles. Inhibition of osteoblastic cell function by phagocytosis of wear debris or topography-features reduces bone formation and decreases osseointegration [106-108].

Anselme et al. [145] reported that human osteoblasts prefer surfaces with moderate micro-roughness but with a low level of repeatability concerning their orientation, adhesion and proliferation.

According to the knowledge gathered in this thesis, surfaces that offer the osteoblastic cells insufficient ECM interaction area, and consequently induce internalization processes, lead to a decrease in the cells' osteoblastic function. These osteoblasts exhibit impaired biomaterial interaction during the first phase of osseointegration, which would lead to a decrease in acceptance and success of an implant [3;19;39;140]. Thus the commonly used stochastically structured implants, used in orthopedic surgery, should avoid any topographical heights inducing phagocytosis preventing the successful ingrowth.

Micro-pillar topographies, ineligible as implant design, allow modulation of cytoskeletal arrangements. They affect adhesion, proliferation, as well as induce differentiation of osteoblasts [9;90;102;105]. This topography may provide another way of eliciting responses that could be exploited for research tools and medical materials. Due to this geometrical arrangement of surface features, we could reveal the reason why cells organize their actin cytoskeleton around the elevations leading to the reduced cell function.

The discovered phagocytosis of the surface-fixed micro-pillars might be advantageous for implant designs in the area of drug delivery, i.e. pillars composed of a degradable material that engulfs a drug reservoir. This drug would be internalized by the cells after the initial adhesion to the implant surface and could then boost the bone formation (e.g. 1,25-dihydroxyvitamin D3) or release an antibiotic to fight bacterial infection [3].

A study by Unadkat et al. used mathematical algorithms to design randomized libraries of micron-sized surface topographies for high-throughput screening of cell-topography interactions. They found novel surface topographies that were able to induce osteogenic differentiation of mesenchymal stem cells. In addition, they could correlate topographical parameters to cellular responses, e.g. that nodules or spheroids enhance osteogenic differentiation [146]. Consequently, certain micron-sized surface topographies could be used as bioactive surface topographies but these contain no sharp edges or rectangular structures such as the micro-pillars.

Only disordered and nano-sized geometric topographies have been reported to benefit the implant ingrowth [100;105]. Hence implant designs containing pillars in nano-size range might be advantageous, contrary to micron-size, for attenuating the osteoblast function and osseointegration. Nano-sized features might offer the increased surface area, as well as adhesion sides required for bone interlocking. But the smaller surface features might lead to less phagocytic efforts, so then less stressed cells.

Within the context of the development of new bioactive implant designs, the artificial micro-structured pillar topography used here, highlights the importance of the cell-material contact area for the osteoblasts in maintaining their specific osteoblastic function and how this contact can manipulate the cell reactions. Besides, the geometric micro-pillared structure was proven to serve as artificial topography in the analysis of topography-induced cell responses by standardizing the order and diameters of the micro-topography.

5. Summary

In cell-biomaterial interaction, knowledge of the dependence of cell behavior on topographical features is relevant for designing implant surfaces. Cells are sensitive to their underlying topography and especially micro-topography offers cues that evoke large ranges of cell responses, but the complex interplay is not completely understood. The overall question of this thesis was why cells organize their actin cytoskeleton in a mimicry fashion on the geometric micro-pillar topographies?

The performed experiments discovered an attempted caveolae-mediated phagocytosis of the surface-fixed micro-pillars ($1 \times 1 \times 1 \mu\text{m}$ up to $5 \times 5 \times 5 \mu\text{m}$) by human MG-63 osteoblastic cells, which explained the local actin rearrangement. This attempt to phagocytize the cubic elevations of the Ti surface results in higher energy requirements for the cells, as indicated by enhanced ATP metabolism and mitochondrial activity, leading to increased intracellular reactive oxygen species (ROS) generation and finally to impaired osteoblast function, characterized by a decreased expression of osteoblast marker proteins such as collagen, fibronectin, osteocalcin or alkaline phosphatase. Similar cell responses regarding the actin cytoskeleton, energy metabolisms and osteoblast function were also observed for the osteoblasts treated with micro-particles as phagocytosis trigger. Osteoblasts growing on stochastic rough Ti surfaces, modified by corundum blasting and commercially used as implant surfaces, showed analogous cell responses regarding the ATP metabolism, ROS production as well as Cav-1 and actin organization. These results indicate as well a phagocytosis of the elevated surface structures, such as edges, ridges or spikes. Osteoblasts, as attachment dependent cells, try to establish the highest surface-cell contact to maintain their osteoblast specific function. Therefore, they attempt to internalize the micro-rough, as well as micro-pillared topography features. Coating of the micro-pillared topography with the cell-adhesive layer PAAm resulted in an accelerated micro-pillar uptake by the osteoblasts and a less impaired osteoblast specific cell function.

Within the context of the development of new bioactive implant designs, the artificial micro-structured pillar topography used here highlights the importance of the cell-material contact area for the osteoblasts in maintaining their specific osteoblastic function and how this contact can manipulate the cell reactions. Altogether, bone-replacing implant biomaterials should provide (i) sufficient contact area without micron-sized elevations, that induce internalization processes by the osteoblastic cells and consequently impair their osteoblastic function and (ii) enough surface sides or area to provide a good mechanical fixation of the implant in the native bone, possibly via macro-roughness in dimensions greater than one cell.

Zusammenfassung

Ausführliche Erkenntnisse über die Zellphysiologie an Biomaterialgrenzflächen sind bedeutend für die Weiterentwicklung von Implantaten. Biomaterialoberflächen, insbesondere deren Mikro-Topographie, beeinflussen viele zellbiologische Prozesse, deren komplexe Zusammenhänge immer noch nicht vollständig aufgeklärt wurden. Die vorliegende Arbeit befasste sich mit der Aufklärung des Phänomens, dass Mikro-Pfostentopographien eine Umorganisation des Aktinzytoskeletts in humanen Osteoblasten bewirken. Es konnte gezeigt werden, dass humane MG-63 Osteoblasten an der Oberfläche-fixierte Mikro-Pfosten ($1 \times 1 \times 1 \mu\text{m}$ bis $5 \times 5 \times 5 \mu\text{m}$) durch Caveolae-vermittelte Phagozytose internalisieren. Diese Phagozytose bewirkte die lokale Umorganisation des Aktinzytoskeletts und induzierte einen gesteigerten Energieverbrauch (gekennzeichnet durch erhöhte ATP-Metabolisierung und mitochondrialer Aktivität sowie der Bildung reaktiver Sauerstoffspezies(ROS)). Dies wiederum resultierte in einer beeinträchtigten Expression von Proteinen, welche spezifisch für die Osteoblastfunktion sind, wie u.a. Collagen, Fibronektin, Osteocalcin oder Alkalische Phosphatase. Ähnliche zelluläre Reaktionen bezüglich des Aktinzytoskeletts, des Energiestoffwechsels und der Osteoblastenfunktion wurden bei Mikro-Partikel-phagozytierenden Osteoblasten gefunden. Auch auf rauem, stochastisch strukturiertem Titan, modifiziert mittels Korundstrahlen, waren analoge Zellantworten hinsichtlich der ATP-Metabolisierung, ROS-Produktion sowie Cav-1 und Aktinzytoskelettorganisation zu beobachten. Diese Ergebnisse weisen ebenso auf eine Phagozytose der Oberflächentopographie aus spezifischen Kanten, Graten und Spitzen bestehend dieser bereits kommerziell verwendeten Implantatoberflächen hin. Osteoblasten sind adhärente Zellen. Für die Aufrechterhaltung ihrer Osteoblastenfunktion sind sie bestrebt, den größtmöglichen Zell-Kontakt zur Materialoberfläche herzustellen, weshalb sie versuchen, sowohl die Erhöhungen der rauen Mikro-Strukturierung, als auch die geometrischen Mikro-Pfosten zu internalisieren. Eine Beschichtung der Mikro-Pfosten mit dem zelladhäsiven Plasmapolymer PPAAm begünstigt die Zelladhäsion sowie -ausbreitung und führte dadurch zu einer verbesserten Osteoblastenfunktion. Die gezeigten Zellreaktionen auf den verwendeten, artifiziellen Mikro-Pfostentopographien unterstreichen die Bedeutung der Zell-Material-Kontaktfläche für die Erhaltung der Osteoblastenfunktion. Zusammenfassend führen diese Ergebnisse zu folgenden Ansprüchen an ein Knochenersatz-Implantat: (i) ausreichend Kontaktfläche für die Zellen ohne Erhöhungen wie Spitzen oder scharfe Kanten im Mikrometer-Bereich, um Internalisierungsprozesse und folglich zu einer Beeinträchtigung der Osteoblastenfunktion zu verhindern, sowie (ii) die Gestaltung einer Makro-Rauheit in größeren Dimensionen als die der Zellen, um eine gute mechanische Fixierung des Implantates im Knochen zu gewährleisten.

References

- [1] Kim SH, Gaiser S, Meehan JP. Epidemiology of primary hip and knee arthroplasties in germany: 2004 to 2008. *J Arthroplasty* 2012;27(10):1777-1782. Doi:10.1016/j.arth.2012.06.017
- [2] https://www.hkk.de/fileadmin/doc/broschueren_flyer/sonstiges/20131129_hkk_Gesundheitsreport_Knie-Hueft-Tep.pdf (09.03.2016)
- [3] Bacakova L, Filova E, Parizek M, Ruml T, Svorcik V. Modulation of cell adhesion, proliferation and differentiation on materials designed for body implants. *Biotech Adv* 2011;29:739-767. Doi:10.1016/j.biotechadv.2011.06.004
- [4] Wilson CJ, Clegg RE, Leavesley DI, Pearcy MJ. Mediation of Biomaterial-cell interactions by adsorbed proteins: a review. *Tissue Eng* 2005;11(1/2):1-18. Doi:10.1089/ten.2005.11.1
- [5] Wennerberg A, Albrektsson T. Effects of titanium surface topography on bone integration: a systematic review. *Clin Oral Implants Res* 2009;4:172-184. Doi:10.1111/j.1600-0501.2009.01775.x
- [6] Jäger M, Zilkens C, Zanger K, Krauspe R. Significance of nano- and microtopography for cell-surface interactions in orthopaedic implants. *J Biomed Biotechnol* 2007;8:69036-69055. Doi:10.1155/2007/69036
- [7] Lüthen F, Lange R, Becker P, Rychly J, Beck U, Nebe B. The influence of surface roughness of titanium on $\beta 1$ - and $\beta 3$ -integrin adhesion and the organization of fibronectin in human osteoblastic cells. *Biomaterials* 2005;26:2423-2440. Doi:10.1016/j.biomaterials.2004.07.054
- [8] Diener A, Nebe B, Lüthen F, Becker P, Beck U, Neumann HG, Rychly J. Control of focal adhesion dynamics by material surface characteristics. *Biomaterials* 2005;26(4):383-392. Doi:10.1016/j.biomaterials.2004.02.038
- [9] Matschelewski C, Staehlke S, Loeffler R, Lange R, Chai F, Kern DP, Beck U, Nebe BJ. Cell architecture – cell function dependencies on titanium arrays with regular geometry. *Biomaterials* 2010;31:5729-5740. Doi:10.1016/j.biomaterials.2010.03.073
- [10] Staehlke S, Koertge A, Nebe B. Intracellular calcium dynamics dependent on defined microtopographical features of titanium. *Biomaterials* 2015;46:48-57. Doi:10.1016/j.biomaterials.2014.12.016
- [11] Clarke B. Normal bone anatomy and physiology. *Clin J Am Soc Nephrol* 2008;3:131–139. Doi:10.2215/CJN.04151206
- [12] Boskey AL. Bone composition: relationship to bone fragility and antiosteoporotic drug effects. *BoneKey Reports* 2013;2(447):1-11. Doi:10.1038/bonekey.2013.181
- [13] Bilezikian JP, Raisz LG, Rodan GA. Principles of bone biology. Academic Press 2008, 3rd edition, ISBN 978-0-12-098652-1.
- [14] Deal S. Potential new drug targets for osteoporosis. *Nat Clin Pract Rheum* 2009;5:20-27. Doi:10.1038/ncprheum0977
- [15] Williams DF. The williams dictionary of biomaterials. Liverpool University Press 1999, ISBN 0853237344.
- [16] Williams DF. On the nature of biomaterials. *Biomaterials* 2009;30:5897-909. Doi:10.1016/j.biomaterials.2009.07.027

- [17] Schmidt CS, Baier JM. A cellular vascular tissues: natural biomaterials for tissue repair and tissue engineering. *Biomaterials* 2000;21:2215-2231. Doi:10.1016/S0142-9612(00)00148-4
- [18] Griffith LG. Emerging design principles in biomaterials and scaffolds for tissue engineering. *Ann NY Acad Sci.* 2002;961:83-95. Doi:10.1111/j.1749-6632.2002.tb03056.x
- [19] Puleo DA, Nanci A. Understanding and controlling the bone implant interface. *Biomaterials* 1999;20:2311-2321.
- [20] Gristina AG, Naylor P, Myrvik Q. Infections from biomaterials and implants: a race for the surface. *Med Prog Technol* 1988;14:205-224.
- [21] Uggeri J, Guizzardi S, Scandroglio R, Gatti R. Adhesion of human osteoblasts to titanium: A morpho-functional analysis with confocal microscopy. *Micron* 2010;41(3):210-219. Doi:10.1016/j.micron.2009.10.013
- [22] Nebe JB, Lüthen F, Lange R, Beck U. Interface interactions of osteoblasts with structured titanium and the correlation between physicochemical characteristics and cell biological parameters. *Macromol Biosci* 2007;7:567-578. Doi:10.1002/mabi.200600293
- [23] Zinger O, Zhao G, Schwartz Z, Simpson J, Wieland M, Landolt D, Boyan B. Differential regulation of osteoblasts by substrate microstructural features. *Biomaterials* 2005;26(14):1837-1847. Doi:10.1016/j.biomaterials.2004.06.035
- [24] Biggs MJP, Richards RG, Dalby MJ. Nanotopographical modification: a regulator of cellular function through focal adhesions. *Nanomedicine: NBM* 2010;6:619-633. Doi:10.1016/j.nano.2010.01.009
- [25] Dalby MJ, Berry CC, Riehle MO, Sutherland DS, Agheli H, Curtis ASG. Attempted endocytosis of nano-environment produced by colloidal lithography by human fibroblasts. *Exp Cell Res* 2004;295:387-394. Doi:10.1016/j.yexcr.2004.02.004
- [26] Shalabi MM, Gortemaker A, Van't Hof MA, Jansen, Creugers NHJ. Implant surface roughness and bone healing: a systematic review. *J Dent Res* 2006;85(6):496-500. Doi:10.1177/154405910608500603
- [27] Dalby MJ, Riehle MO, Johnstone H, Affrossman S, Curtis ASG. Investigating the limits of filopodial sensing: a brief report using SEM to image the interaction between 10 nm high nano-topography and fibroblast filopodia. *Cell Biol Int* 2004;28:229-236. Doi:10.1016/j.cellbi.2003.12.004
- [28] Anselme K, Bigerelle M. Role of materials surface topography on mammalian cell response. *Int Mat Rev* 2011;56(4):243-266. Doi:10.1179/1743280411Y.0000000001
- [29] Schwartz Z, Raines AL, Boyan BD. The effect of substrate microtopography on osseointegration of titanium implants. In: Ducheyene P, Healy KE, Hutmacher DW, Grainger DW, Kirkpatrick CJ. *Comprehensive Biomaterials* 2011;6:343-352.
- [30] Schwartz Z, Olivares-Navarrete R, Wieland M, Cochran DL, Boyan BD. Mechanisms regulating increased production of osteoprotegerin by osteoblasts cultured on microstructured titanium surfaces. *Biomaterials* 2009;30:3390-396. Doi:10.1016/j.biomaterials.2009.03.047
- [31] Elter P, Lange R, Beck U. Atomic force microscopy studies of the influence of convex and concave nanostructures on the adsorption of fibronectin. *Colloids Surf B Biointerfaces*. 2012;89:139-146. Doi:10.1016/j.colsurfb.2011.09.021.
- [32] Kabaso D, Gongadze E, Perutkova S, Matschegowski C, Kralj-Iglic V, Beck U, van Rienen U, Iglic A. Mechanics and electrostatics of the interactions between osteoblasts and titanium surface. *Comput Meth Biomech Biomed Eng* 2011;14(05):469-482 (2011). Doi:10.1080/10255842.2010.534986

- [33] Wilson CJ, Clegg RE, Leavesley DI, Pearcy MJ. Mediation of biomaterial-cell interactions by adsorbed proteins: a review. *Tissue Eng* 2005;11:1-18. Doi:10.1089/ten.2005.11.1
- [34] Anselme K. Osteoblast adhesion on biomaterials. *Biomaterials* 2000;21:667-681. Doi:10.1016/S0142-9612(99)00242-2
- [35] von der Mark K, Park J. Engineering biocompatible implant surfaces Part II: Cellular recognition of biomaterial surfaces: Lessons from cell-matrix interactions. *Process in Materials Science* 2013;58:327-381. Doi:10.1016/j.pmatsci.2012.09.002
- [36] Rebl H, Finke B, Lange R, Weltmann KD, Nebe JB. Impact of plasma chemistry versus titanium surface topography on osteoblast orientation. *Acta Biomater* 2012;8(10):3840-51. Doi:10.1016/j.actbio.2012.06.015
- [37] Duske K, Koban I, Kindel E, Schröder K, Nebe JB, Holtfreter B, Jablonowski L, Weltmann K-D, Kocher T. Atmospheric plasma enhances wettability and cell spreading on dental implant metals. *J Clin Periodontol* 2012;39:400-407. Doi:10.1111/j.1600-051X.2012.01853.x.
- [38] Duske K, Jablonowski L, Koban I, Matthes R, Holtfreter B, Sckell A, Nebe JB, von Woedtke T, Weltmann KD, Kocher T. Cold atmospheric plasma in combination with mechanical treatment improves osteoblast growth on biofilm covered titanium discs. *Biomaterials* 2015;52:327-334. Doi:10.1016/j.biomaterials.2015.02.035
- [39] Schwartz Z, Boyan BD. Underlying mechanisms at the bone-biomaterial interface. *J Cell Biochem* 1994;56:340-347. Doi:10.1002/jcb.240560310
- [40] Garcia AJ. Get a grip: integrins in cell-biomaterial interactions. *Biomaterials* 2005;26:7525-7529. Doi:10.1016/j.biomaterials.2005.05.029
- [41] Wang Z, Telci D, Griffin M. Importance of syndecan-4 and syndecan-2 in osteoblast cell adhesion and survival mediated by a tissue transglutaminase-fibronectin complex. *Exp Cell Res* 2011;317:367-381. Doi:10.1016/j.yexcr.2010.10.015
- [42] Humphries JD, Byron A, Humphrie MJ. Integrin ligands at a glance. *J Cell Sci* 2006;119:3901-3903. Doi:10.1242/jcs.0309
- [43] Kanchanawong P, Shtengel G, Pasapera AM, Ramko EB, Davidson MW, Hess HF, Waterman CM. Nanoscale architecture of integrin-based cell adhesions. *Nature* 2010;468:580-586. Doi:10.1038/nature09621
- [44] Case LB, Waterman CM. Integration of actin dynamics and cell adhesion by a three-dimensional, mechanosensitive molecular clutch. *Nat Cell Biol* 2015;17(8):956-963. Doi:10.1038/ncb3191
- [45] Harburger DS, Calderwood DA. Integrin signaling at a glance. *J Cell Sci* 2006;122:159-163. Doi:10.1242/jcs.0180
- [46] <http://www.reading.ac.uk/nitricoxide/intro/migration/focal%20adhesion.jpg> (09.03.2016)
- [47] Hyzy SL, Olivares-Navarrete R, Hutton DL, Tan C, Boyan BD, Schwartz Z. Microstructured titanium regulates interleukin production by osteoblasts, an effect modulated by exogenous BMP-2. *Acta Biomat* 2013;9:5821-5829. Doi:10.1016/j.actbio.2012.10.030
- [48] Chiu R, Goodman SB. Biological response of osteoblasts and osteoprogenitors to orthopaedic wear debris. Out of Osteogenesis, Prof. Yunfeng Lin, InTech 2012; ISBN: 978-953-51-0030-0.
- [49] Fritz EA, Jacobs JJ, Glant TT, Roebuck KA. Chemokine IL-8 induction by particulate wear debris in osteoblasts is mediated by NF-κB. *J Ortho Res* 2005;23:1249-1257. Doi:10.1016/j.orthres.2005.03.013

- [50] Geiger B, Bershadsky A, Pankov R, Yamada KM. Transmembrane extracellular matrix-cytoskeleton crosstalk. *Nat Rev Mol Cell Biol* 2001;2:793-805. Doi:10.1038/35099066
- [51] Dominguez R, Holmes KC. Actin structure and function. *Annu Rev Biophys* 2011;40:169-186. Doi:10.1146/annurev-biophys-042910-155359
- [52] May RC, Machesky LM. Phagocytosis and the actin cytoskeleton. *J Cell Sci* 2001;114:1061-1077.
- [53] Swanson JA. Shaping cups into phagosomes and micropinosomes. *Nat Rev Mol Cell Biol* 2008;9:639-649. Doi:10.1038/nrm2447
- [54] Doherty GJ, McMahon HT. Mechanisms of endocytosis. *Annu. Rev. Biochem.* 2009;78:857-902. Doi:10.1146/annurev.biochem.78.081307.110540
- [55] Janmey PA, Lindberg U. Cytoskeletal regulation: rich in lipids. *Nat Rev Mol Cell Biol* 2004;5:658-666. Doi:10.1038/nrm1434
- [56] Gillooly DJ, Simonsen A, Stenmark H. Phosphoinositides and phagocytosis. *J Cell Biol* 2001;155:15-17. Doi:10.1083/jcb.200109001
- [57] Drücker P, Pejic M, Galla HJ, Gerke V. Lipid segregation and membrane budding induced by peripheral membrane binding protein annexin A2. *J Biol Chem* 2013;288(34):24764-24776. Doi:10.1074/jbc.M113.474023
- [58] Viola A, Gupta N. Tether and trap: regulation of membrane-raft dynamics by actin-binding proteins. *Nat Rev Immunol* 2007;7:889-896. Doi:10.1038/nri2193
- [59] Song L, Lee C, Schindler C. Depletion of the murine scavenger receptor CD68. *J Lipid Res* 2011;52:1542-1550. Doi:10.1194/jlr.M015412
- [60] Heinemann DEH, Lohmann C, Siggelkow H, Alves F, Engel I, Köster G. Human osteoblast-like cells phagocytose metal particles and express the macrophage marker CD68 in vitro. *J Bone Joint Surg* 2000;82(B):283-289.
- [61] Parton RG, del Pozo MA. Caveolae as plasma membrane sensors, protectors and organizers. *Nat Rev Mol Cell Biol* 2013;14:98-112. Doi:10.1038/nrm3512
- [62] Pelkmans L, Helenius A. Endocytosis via caveolae. *Traffic* 2002;3:311-320. Doi:10.1034/j.1600-0854.2002.30501.x
- [63] Fielding CJ, Fielding PE. Relationship between cholesterol trafficking and signaling in rafts and caveolae. *Biochim Biophys Acta* 2003;1610:219-228. Doi:10.1016/S0005-2736(03)00020-8
- [64] Parton RG, Simons K. The multiple faces of caveolae. *Nat Rev Mol Cell Biol* 2007;8:185-194. Doi:10.1038/nrm2122
- [65] Wauquier F, Leotoing L, Coxam V, Guicheux J, Wittrant Y. Oxidative stress in bone remodeling and disease. *Trends Mol Med* 2009;15(10):468-477. Doi:10.1016/j.molmed.2009.08.004
- [66] Jacobs MD, Harrison SC. Structure of an IkBa/NFkB complex. *Cell* 1998;95:749-758. Doi:10.1016/S0092-8674(00)81698-0
- [67] Dupuy AG, Caron E. Integrin-dependent phagocytosis – spreading from microadhesion to new concepts. *J Cell Sci* 2008;121:1773-1783. Doi:10.1242/jcs.018036

- [68] Li S, Couet J, Lisanti MP. Src tyrosine kinase, G-alpha subunits and H-Ras share a common membrane-anchored scaffolding protein, caveolin: caveolin binding negatively regulates the auto-activation of Src tyrosine kinases. *J Biol Chem* 1996;271:29182-29190.
- [69] Nethe M, Hordijk PL. A model for phosphor-caveolin-1 driven turnover of focal adhesions. *Cell Adh Migr* 2011;5(1):59-64. Doi:10.4161/cam.5.1.13702
- [70] <https://www.qiagen.com/geneglobe/static/images/Pathways/Integrin%20Pathway.jpg> (09.03.2016)
- [71] Ereciflkska M, Wilson DF. Regulation of cellular energy metabolism. *J Membrane Biol* 1982;70:1-14.
- [72] Borregaard N, Herlin T. Energy metabolism of human neutrophil during phagocytosis. *J Clin Invest* 1982;70:550-557.
- [73] Ataullakhanov FI, Vitvitsky VM. What determines the intracellular ATP concentration. *Biosci Reports* 2002;22:501-511. Doi:10.1023/A:1022069718709
- [74] Chen LB. Mitochondrial membrane potential in living cells. *Ann Rev Cell Biol* 1988;4:155-181.
- [75] Adam-Vizi A, Chinopoulos C. Bioenergetics and the formation of mitochondrial reactive oxygen specis. *Trends in Pharmacol Sci* 2006;27(12):639-645. Doi:10.1016/j.tips.2006.10.005
- [76] He C, Jiang S, Jin H, Chen S, Lin G, Yoa H, Wang X, Mi P, Ji Z, Lin Y, Lin Z, Liu G. Mitochondrial electron transport chain identified as a novel molecular target of SPIO nanoparticles mediated cancer-specific cytotoxicity. *Biomaterials* 2016;83:102-114. Doi:10.1016/j.biomaterials.2016.01.010
- [77] Czekanska EM, Stoddart MJ, Richards RG, Hayes JS. In search of an osteoblast cell model for in vitro research. *Eur Cell Mat* 2012;24,1-17.
- [78] Alberts B, Johnson A, Lewis J, Raff M, Roberts K, Walter P. *Molekularbiologie der Zelle*. Wiley-VCH Verlag, 4. Auflage, 2003, ISBN 978-3527304929.
- [79] Schnitzer JE, Oh PO, Pinney E, Allard J. Filipin-sensitive caveolae-mediated transport in endothelium: reduced transcytosis, scavenger endocytosis, and capillary permeability of selected macromolecules. *J Cell Biol* 1994;127(5):1217-1232.
- [80] Lie YS, Petropoulos CJ. Advances in quantitative PCR technology: 5' nuclease assays. *Curr Opin Biotechnol* 1998, 9:43-48. Doi:10.1016/S0958-1669(98)80082-7
- [81] Bradford MM. Rapid and sensitive method for the quantitation of microgram quantities of protein utilizing the principle of protein-dye binding. *Anal Biochem* 1976;72:248-254.
- [82] Laemmli UK. Cleavage of structural proteins during the assembly of the head of bacteriophage T4. *Nature* 1970, 227:680-685.
- [83] Towbin H, Staehelin T, Gordon J. Electrophoretic transfer of proteins from polyacrylamide gels to nitrocellulose sheets: Procedure and some applications. *Proc Natl Acad Sci* 1979;76(9):4350-4354.
- [84] Houser B. Bio-Rad's Bio-Plex® suspension array system, xMAP technology overview. *Arch Physiol Biochem* 2012;118(4):192-196. Doi:10.3109/13813455.2012.705301
- [85] Izant JG, Weintaub H. Inhibition of thymidine kinase gene expression by anti-sense RNA: a molecular approach to genetic analysis. *Cell* 1984;36:1007-1015.

- [86] Reers M, Smith TW, Chen LB. Mitochondrial membrane potential monitored by JC-1 dye. *Methods Enzymol* 1995;260:406-414.
- [87] Ali SF, LeBel CP, Bondy SC. Reactive oxygen species formation as a biomarker of methylmercury and trimethyltin neurotoxicity. *Neurotoxicology* 1991;13(3):637-648.
- [88] Boyce FM, Buchner NL. Baculovirus-mediated gene transfer into mammalian cells. *PNAS* 1996;93:2348-2352.
- [89] Wilson T. Confocal Microscopy. s.l. : Academic Press, London, ISBN-10: 0127572708, 1990. S. 1-64.
- [90] Matschegewski C, Staehlke S, Birkholz H, Lange R, Beck U, Engel K, Nebe JB. Automatic actin filament quantification of osteoblasts and their morphometric analysis on microtextured silicon-titanium arrays. *Materials* 2012;15:11776-1195. Doi:10.3390/ma5071176
- [91] Nagao G, Ishii K, Hirota K, Makino K, Terada H. Role of lipid rafts in phagocytic uptake of polystyrene latex microspheres by macrophages. *Anticancer Res* 2010;30:3167-3176.
- [92] Fire A, Xu SQ, Montgomery MK, Kostas SA, Driver SE, Mello CC. Potent and specific genetic interference by double-stranded RNA in *Caenorhabditis elegans*. *Nature* 1989;391:806-811. Doi:10.1038/35888
- [93] Pelkmans L, Helenius A. Endocytosis via caveolae. *Traffic* 2002;3:311-320. Doi:10.1034/j.1600-0854.2002.30501.x
- [94] Araki N, Johnson MT, Swanson JA. A role for phosphoinositide 3-kinase in the completion of macropinocytosis and phagocytosis by macrophages. *J Cell Biol* 1996;135(5):1249-1260. Doi:10.1083/jcb.135.5.1249
- [95] Finke B, Luethen F, Schroeder K, Mueller PD, Bergemann C, Frant M, Ohl A, Nebe BJ. The effect of positively charged plasma polymerization on initial osteoblastic focal adhesion on titanium surfaces. *Biomaterials* 2007;28:4521-4534. Doi:10.1016/j.biomaterials.2007.06.028
- [96] Ismail FSM, Rohanizadeh R, Atwa S, Mason RS, Ruys AJ, Martin PJ, Bendavid A. The influence of surface chemistry and topography on the contact guidance of MG63 osteoblast cells. *J Mater Sci: Mater Med* 2007;(18):705-714.
- [97] Lange R, Lüthen F, Nebe B, Rychly J, Beck U. Mathematical correlation between biomaterial and cellular parameters-Critical reflection of statistics. *Biomol Eng* 2007;24:526-530. Doi:10.1016/j.bioeng.2007.08.002
- [98] Nebe JB, Finke B, Koertge A, Rebl H, Staehlke S. Geometrical micropillars combined with chemical surface modifications-Independency of actin filament spatial distribution in primary osteoblasts. *Mat Sci Forum* 2014;783-786:1320-1325. Doi:10.4028/MSF.783-786.1320
- [99] Diaz-Rodrigues L, Gracia-Martinez O, Arroyo-Morales M, Reyes-Botella C, Ruiz C. Antigenic phenotype and phagocytic capacity of MG-63 osteosarcoma line. *Integr Physiol: Ann NY Acad Sci* 2009;1173:46-54. Doi:10.1111/j.1749-6632.2009.04950.x
- [100] McNamara LE, Burchmore R, Riehle MO, Herzyk P, Biggs MJP, Wilkinson CDW, Curtis ASG, Dalby MJ. The role of microtopography in cellular mechanotransduction. *Biomaterials* 2012;33:2835-2847. Doi:10.1016/j.biomaterials.2011.11.047
- [101] Davidson PN, Fromique O, Marie PJ, Hasirci V, Reiter G, Anselme K. Topographically induced self-deformation of the nuclei of cells: dependence on cell type and proposed mechanisms. *J Mater Sci: Mater Med* 2010;21:936-946. Doi:10.1007/s10856-009-3950-7

- [102] Badique F, Stamov DR, Davidson PM, Veuillet M, Reiter G, Freund JN, Franz CM, Anselme K. Directing nuclear deformation on micropillared surfaces by substrate geometry and cytoskeleton organization. *Biomaterials* 2013;34:2991-3001. Doi:10.1016/j.biomaterials.2013.01.018
- [103] Davidson PM, Özcelik H, Hasirci V, Reiter G, Anselme K. Microstructured surfaces cause severe but non-detrimental deformation of the nucleus. *Adv Mater* 2009;21:3586-3590. Doi:10.1002/adma.200900582
- [104] Rejman J, Oberle V, Zuhorn IS, Hoeckstra D. Size-dependent internalization of particles via the pathways of clathrin- and caveolae-mediated endocytosis. *Biochem J* 2004;377:159-169. Doi:10.1042/BJ20031253
- [105] Teo BKK, Goh SH, Kustandi TS, Loh WW, Low HY, Yim EKF. The effect of micro and nanotopography on endocytosis in drug and gene delivery systems. *Biomaterials* 2011;32:9866-9875. Doi:10.1016/j.biomaterials.2011.08.088
- [106] Choi MG, Koh HS, Kluess D, O'Connor D, Mathur A, Truskey GA, Rubin J, Zhou DXF, Sung KLP. Effects of titanium particle size on osteoblast functions in vitro and in vivo. *PNAS* 2005;102(12):4578-4583. Doi:10.1073/pnas.0500693102
- [107] Saldana L, Vilaboa N. Effects of micrometric titanium particles on osteoblast attachment and cytoskeleton architecture. *Acta Biomater* 2010;6:1649-1660. Doi:10.1016/j.actbio.2009.10.033
- [108] Yao J, CS-Szabo G, Jacobs J, Kuettner K, Glant T. Suppression of osteoblast function by titanium particles. *J Bone Joint Surg Am* 1997;79(1):107-112.
- [109] Vermes C, Glant TT, Hallab NJ, Fritz EA, Roebuck KA, Jacobs JJ. The potential role of the osteoblast in the development of periprosthetic osteolysis. *J Arthroplasty* 2001;16(8):95-100. Doi:10.1054/arth.2001.28719
- [110] Abrami L, Fivaz M, Kobayashi T, Kinoshita T, Parton RG, van der Goot FG. Cross-talk between caveolae and glycosylphosphatidylinositol-rich domains. *J Biol Chem* 2001;276(33):30729-30736. Doi:10.1074/jbc.M102039200
- [111] Head BP, Patel HH, Insel PA. Interaction of membrane/lipid rafts with the cytoskeleton: Impact on signaling and function. *Biochimica et Biophysica Acta* 2014;1838:532-545. Doi:10.1016/j.bbamem.2013.07.018
- [112] Nebe JGB, Luethen F, Lange R, Beck U. Cellular activity and biomaterial's surface topography. *Mat Sci Forum* 2007;539-543:517-522. Doi:10.4028/MSF.539-543.517
- [113] Sinha B, Köster D, Ruez R, Gonnord P, Bastiani M, Abankwa D, Stan RV, Butler-Browne G, Vedie B, Johannes L, Morone N, Parton RG, Raposo G, Sens P, Lamaze C, Nassoy P. Cells respond to mechanical stress by rapid disassembly of caveolae. *Cell* 2010;144:402-413. Doi:10.1016/j.cell.2010.12.031
- [114] Champion JA, Mitragotri S. Role of target geometry in phagocytosis. *PNAS* 2006;103(13):4930-4934. Doi:10.1073_pnas.0600997103
- [115] Qi M, Liu Y, Freeman MR, Solomon KR. Cholesterol-regulated stress fiber formation. *J Cell Biochem* 2009;106:1031-1040. Doi:10.1002/jcb.22081
- [116] Simons K, Ikonen E. How cells handle cholesterol. *Science* 2000;290:1721-1726. Doi:10.1126/science.290.5497.1721
- [117] Case N, Ma M, Sen B, Xie Z, Gross TS, Rubin J. Beta-catenin levels influence rapid mechanical responses in osteoblasts. *J Biol Chem* 2008;283:29196-29205. Doi:10.1074/jbc.M801907200
- [118] Jeong YS, Oh WK, Kim S, Jang J. Cellular uptake, cytotoxicity, and ROS generation with silica/conducting polymer core/shell nanospheres. *Biomaterials* 2011;32:7217-7225. Doi:10.1016/j.biomaterials.2011.06.020

- [119] Dostert C, Petrilli V, van Bruggen R, Steele C, Mossman BT, Tschopp J. Innate immune activation through Nalp3 inflammasome sensing of asbestos and silica. *Science* 2008;320: 674-677. Doi:10.1126/science.1156995
- [120] Vermes C, Roebuck KA, Chandrasekaran R, Dobai JG, Jacobs JJ, Glant TT. Particulate wear debris activates protein tyrosine kinase and nuclear factor κB, which down-regulates type I collagen synthesis in human osteoblasts. *J Bone Miner Res* 2000;15:1756-1765. Doi:10.1359/jbm.2000.15.9.1756
- [121] Vermes C, Chandrasekaran R, Jacobs JJ, Galante JO, Roebuck KA, Glant TT. The effects of particulate wear debris, cytokines, and growth factors on the functions of MG-63 osteoblasts. *J Bone Joint Surg Am* 2001;83(2):201-211.
- [122] Wang XM, Kim HP, Song R, Choi AMK. Caveolin-1 confers anti-inflammatory effects in murine macrophages via the MKK3/p38 MAPK pathway. *Am J Respir Cell Mol Biol* 2006;34:434-442. Doi:10.1165/rcmb.2005-0376OC
- [123] Linares J, Matesanz MC, Vila M, Feito MJ, Goncalves G, Vallet-Regi M, Marques PAAP, Portoles MT. Endocytic mechanisms of graphene oxide nanosheets in osteoblasts, hepatocytes and macrophages. *ACS Appl Mater Interfaces* 2014;6:13697-13706. Doi:10.1021/am5031598
- [124] Sun SC. Non-canonical NF-κB signaling pathway. *Cell Res* 2011;21:71-85. Doi:10.1038/cr.2010.177
- [125] Gerke V, Creutz CE, Moss SE. Annexins: linking Ca²⁺ signaling to membrane dynamics. *Nat Rev Mol Cell Biol* 2005;6:449-461. Doi:10.1038/nrm1661
- [126] Patel DM, Ahmed SF, Weiss DG, Gerke V, Kuznetsov SA. Annexin A1 is a new linker between actin filaments and phagosomes during phagocytosis. *J Cell Sci* 2011;124:578-588. Doi:10.1242/jcs.076208
- [127] Nunes P, Demaurex N. The role of calcium signaling in phagocytosis. *J Leukocyte Biol* 2010;88:57-68. Doi:10.1189/jlb.0110028
- [128] Pani B, Singh BB. Lipid rafts/caveolae as microdomains of calcium signaling. *Cell Calcium* 2009;45(6):325-633. Doi:10.1016/j.ceca.2009.02.009
- [129] Isshiki M, Anderson RGW. Function of caveolae in Ca²⁺ entry and Ca²⁺-dependent signal transduction. *Traffic* 2003;4:717-723. Doi:10.1034/j.1600-0854.2003.00130.x
- [130] Bittig AT, Matschegowski C, Nebe JB, Stähle S, Uhrmacher AM. Membrane related dynamics and the formation of actin in cells growing on micro-topographies: a spatial computational model. *BMC System Biol* 2014;8(106):1-19. Doi:10.1186/s12918-014-0106-2
- [131] Pelkmans L, Fava E, Grabner H, Hannus M, Habermann B, Krausz E, Zerial M. Genome-wide analysis of human kinases in clathrin- and caveolae/raft-mediated endocytosis. *Nature* 2005;436(7):78-86. Doi:10.1038/nature03571
- [132] Fletcher DA, Mullins RD. Cell mechanics and the cytoskeleton. *Nature* 2011;463:485-492. Doi:10.1038/nature0890
- [133] Gottlieb-Abraham E, Shvartsman DE, Donaldson JC, Ehrlich M, Gutman O, Martin GS, Henis YI. Src-mediated caveolin-1 phosphorylation affects the targeting of active Src to specific membrane sites. *Mol Biol Cell* 2013;24:3881-3895. Doi:10.1091/mbc.E13-03-0163
- [134] Vogel V, Sheetz M. Local force and geometry sensing regulate cell functions. *Nat Rev Mol Cell Bio* 2006;7:265-275. Doi:10.1038/nrm1890
- [135] Rebl H, Finke B, Ihrke R, Rothe H, Rychly J, Schoeder K, Nebe BJ. Positively charged material surfaces generated by plasma polymerized allylamine enhance vinculin mobility in vital human osteoblasts. *Adv Eng Mat* 2010;12:356-364. Doi:10.1002/adem.200980070

- [136] Komarova SV, Ataullakhanov FI, Globus RK. Bioenergetics and mitochondrial transmembrane potential during differentiation of cultured osteoblasts. *Am J Physiol Cell Physiol* 2000;279:1220-1229.
- [137] Gabler C, Zietz C, Göhler R, Fritsche A, Lindner T, Haenle M, Finke B, Meichsner J, Lenz S, Frerich B, Lüthen F, Nebe JB, Bader R. Evaluation of osseointegration of titanium alloyed implants, *Int J Mol Sci* 2014;15:2454-246. Doi:10.3390/ijms15022454
- [138] Ehrenfest DMD, Coelho PG, Kang BS, Sul YT, Albrektsson T. Classification of osseointegrated implant surfaces: materials, chemistry and topography. *Trends in Biotechnol* 2010;28(4):198-206. Doi:10.1016/j.tibtech.2009.12.003
- [139] Nebe JGB, Luethen F, Lange R, Beck U. Interface interactions of osteoblasts with structured titanium and the correlation between physicochemical characteristics and cell biological parameters. *Macromol Biosci* 2007;7:567-578. Doi:10.1002/mabi.200600293
- [140] Schwartz Z, Raz P, Zhao G, Barak Y, Tauber M, Yao H, Boyan BD. Effect of micrometer-scale roughness of the surface of Ti6Al4V pedicle screws in vitro and in vivo. *J Bone Joint Surg Am* 2008;90:2485-98. Doi:10.2106/JBJS.G.00499
- [141] Zhao L, Mei S, Chu PK, Zhang Y, Wu Z. The influence of hierarchical hybrid micro/nano-textured titanium surface with titania nanotubes on osteoblast functions. *Biomaterials* 2010;31:5072-5082. Doi:10.1016/j.biomaterials.2010.03.014
- [142] Sader MS, Balduino A, de Soares A, Brorjevic R. Effect of three distinct treatments of titanium surface on osteoblast attachment, proliferation, and differentiation. *Clin Oral Implants Res* 2005;16(6):667-675. Doi:10.1111/j.1600-0501.2005.01135.x
- [143] Lohmann CH, Schwartz Z, Köster G, Jahn U, Buchhorn GH, MacDougall MJ, Casasola D, Liu Y, Sylvia VL, Dean DD, Boyan BD. Phagocytosis of wear debris by osteoblasts affects differentiation and local factor production in a manner dependent on particle composition. *Biomaterials* 2000;21:551-561. Doi:10.1016/S0142-9612(99)00211-2
- [144] Maloney WJ, Smith RL, Schmalzried TP, Chiba J, Huene D, Rubash H. Isolation and characterization of wear particles generated in patients who have had failure of hip arthroplasty without cement. *J Bone Joint Surg Am* 1995;77:1301-1310.
- [145] Anselme K, Bigerelle M, Noël B, Iost A, Hardouin P. Effect of grooved titanium substratum on human osteoblastic cell growth. *J Biomed Mater Res* 2002;60(4):529-540. Doi:10.1002/jbm.10101
- [146] Unadkat HV, Hulsmans M, Cornelissen K, Papenburg BJ, Truckenmüller RK, Carpenter AE, Wessling M, Post GF, Uetz M, Reinders MJT, Stamatialis D, van Blitterswijk CA, de Boer J. An algorithm-based topographical biomaterials library to instruct cell fate. *PNAS* 2011;108(40):16565-16570. Doi:10.1073/pnas.1109861108

Appendix

Acknowledgements

Mein besonderer Dank gilt Frau Prof. Dr. Barbara Nebe für die Möglichkeit der Anfertigung dieser Dissertation mit der äußerst interessanten Aufgabenstellung, sowie für der fachlichen Betreuung und Begleitung während dieser Dissertation.

Frau Prof. Dr. Ursula van Rienen, sowie den weiteren Betreuern des DFG Graduiertenkollegs *welisa*, danke ich für die einzigartigen interdisziplinären Diskussionen, welche ein fachlich exzellentes Umfeld für das Anfertigen der Dissertation baten.

Mein herzlichen Dank gilt den Kollegen des AB Zellbiologie für das gute Laborklima und die stetige Hilfsbereitschaft. Dabei möchte ich mich besonders Frau Dr. Petra Müller für die anregenden Problemlösungen und Ratschläge sowie das stetige Interesse bedanken. Weiterhin möchte ich auch Frau Petra Seidel, Frau Dr. Henrike Rebl, Frau Dr. Claudia Bergemann und Frau Dr. Susanne Stähle für allezeit unterstützende und aufmunternde Worte sowie den vielen anregenden Gesprächen danken.

Den Mitarbeitern von Elektronenmikroskopischen Zentrum Herr Dr. Marcus Frank, Wolfgang Labs und Gerhard Fulda danke ich für die technische Unterstützung bei den REM-Aufnahmen. Weiterhin möchte ich mich bei Norbert Zichner (TU Chemnitz) und Frau Dr. Cornelia Prinz (DOT GmbH) für die Bereitstellung der Titanproben, sowie Frau Dr. Birgit Finke (INP Greifswald) für die Beschichtung der Titanproben bedanken.

Ein besonderer Dank gilt der Deutschen Forschungsgemeinschaft (DFG) für die finanzielle Unterstützung zum Anfertigen meiner Dissertation im Rahmen des DFG-Graduiertenkollegs *welisa* 1505/2.

Abschließend bedanke ich mich von ganzem Herzen bei meiner Familie und Freunden, die mich stets in jeglicher Form unterstützt haben.

Statutory declaration

I declare that I have authored this thesis independently, that I have not used other than the declared sources / resources, and that I have explicitly marked all material which has been quoted either literally or by content from the used sources.

Rostock, 21.03.2016

Caroline Mörke

Eidesstattliche Erklärung

Hiermit versichere ich, dass ich die vorliegende Arbeit selbstständig angefertigt und ohne fremde Hilfe verfasst habe, keine außer den von mir angegebenen Hilfsmitteln und Quellen dazu verwendet habe und die den benutzten Werken inhaltlich und wörtlich entnommenen Stellen als solche kenntlich gemacht habe.

Das bearbeitete Thema wurde von mir weder schon früher im Rahmen einer anderen Arbeit behandelt noch bisher einer anderen Fakultät als Arbeit vorgelegt.

Rostock, 21.03.2016

Caroline Mörke

Publications and Lectures

Journal Publications

- **Moerke, C.**, Mueller, P. and Nebe, B., 2016. Attempted caveolae-mediated phagocytosis of surface-fixed micro-pillars by human osteoblasts. *Biomaterials*, 10(76), pp. 102-114.
Doi:10.1016/j.biomaterials.2015.10.030 (IF 8.61)
- **Moerke, C.**, Mueller, P. and Nebe, B., 2016. Data supporting attempted caveolae-mediated phagocytosis of surface-fixed micro-pillars by human osteoblasts. *Data in Brief*, 7, pp. 177-182.
Doi:10.1016/j.dib.2016.02.023 (IF 0.22)
- **Mörke, C.**, Finke, B., Schnabelrauch, M., Anselme, K. and Nebe, J.B., 2014. Impact of the chemistry of geometrically designed titanium on cell behavior and alignment. *BioNanoMat*, 15, pp. 22.
Doi:10.1515/bnm-2014-9003
- Nebe, B., **Moerke, C.**, Staehlke, S., Finke, B., Schnabelrauch, M., Anselme, K., Helm, C.A., Frank, M., Rebl, H., 2016. Complex cell physiology on topographically and chemically designed material surfaces. *Materials Science Forum*, submitted.

Abstracts and Posters

- Stählke, S., **Mörke, C.**, Kunz, F., Körtge, A., Nebe, J.B. 2013, Analyse der Zellarchitektur-Zellfunktions-Beziehung in Osteoblasten auf definierter Mikrostruktur. 2nd Research Workshop of the University of Rostock.
- **Mörke, C.**, Stählke, S. and Nebe, B., 2014. Influence of geometric micro-pillared structures on the cell physiology of MG-63 osteoblast-like cells. International Meeting of the German Society for Cell Biology, Regensburg, Abstract book p. 81.
- **Mörke, C.**, Finke, B., Schnabelrauch, M., Anselme, K., Körtge, A., Weltmann, K.D. and Nebe B.J., 2014, Impact of the chemistry of geometrically designed titanium on cell behavior and alignment. *Biointerface*, Redwood City (CA, USA), Abstract book p. 10.
- **Mörke, C.**, Finke, B., Schnabelrauch, M., Anselme, K. and Nebe, J.B., 2014. Impact of the chemistry of geometrically designed titanium on cell behavior and alignment. Annual Meeting of the German Society of Biomaterials, Dresden, *BioNanoMat*, 15, pp. 22. Doi:10.1515/bnm-2014-9003
- **Mörke, C.**, Finke B., Dubs, M., Airoudj, A., Roucoules, V., Körtge, A., Nestler, P., Duske, K., Schnabelrauch, M., Anselme, K., Helm, C.A. and Nebe, J.B. 2015. Influence of chemically modified micro-grooved titanium on osteoblast alignment. 5th International Symposium Interface of Biology of Implants, Warnemünde, Abstract book pp. 91-92.
- Truong, T.D., **Mörke, C.**, Nebe, B. and van Rienen, U., 2015. Numerical study on actin filament patterns on various micro-structured pillar arrays. 5th International Symposium Interface of Biology of Implants, Warnemünde, Abstract book pp. 73-74.
- **Mörke, C.**, Stählke, S. and Nebe, J.B., 2015. Defined micro-topographical features interfere with osteoblast cell physiology. 4. Workshop "Neue Horizonte für metallische Biomaterialien", Geesthacht, Abstract book p. 30.

- **Moerke, C.** and Nebe, J.B., 2015. Caveolae formation in osteoblasts membranes on structured titanium surfaces - an attempted phagocytosis of micro-pillars. 4th Workshop on Biomaterials and their Interactions with Biological Membranes, Salou (Spain), Abstract book p. 27.
- **Moerke, C.** and Nebe, J.B. 2015, Phagocytotic processes on biomaterial surfaces with sharp edged elevations. 3rd Research Workshop of the University of Rostock.
- **Moerke, C.**, Rebl, H., Staehlke, S., Frank, M., Nebe, J.B. 2016, Attempted phagocytosis of titanium surface micro-structures by osteoblasts. Euro Bio-Inspired Materials, Potsdam, PO-28.
- **Moerke, C.**, Staehlke, S. and Nebe, J.B. 2016, Micro-topographical surface features interfere with osteoblast cell signaling. World Biomaterial Congress, Montreal (Canada).

Lectures

- **Cell Biology Seminar, 12.09.2013, Rostock**
Aminopeptidases in BRIN-DB11 insulinoma cells
- **9th Welisa Workshop, 20.11.2013, Wustrow**
Evaluation of the influence of topographic and chemical surface properties on the cell biology of osteoblast-like cells
- **Life Light Matter graduate network meeting, 24.01.2014, Rostock**
Evaluation of the influence of topographic and chemical surface properties on the cell biology of osteoblast-like cells
- **10th Welisa Workshop, 11.06.2014, Hasenwinkel**
Impact of chemical surface modifications of geometrical groove structures on the cell elongation
- **Jahrestagung der Deutschen Gesellschaft für Biomaterialien 2014, 06.-08.11.2014, Dresden**
Impact of the chemistry of geometrically designed titanium on cell behavior and alignment (short communication)
- **11th Welisa workshop, 26.11.2014, Rostock**
Cell interaction with micro-pillared surfaces -attempted caveolae-mediated pillar endocytosis by MG63 human osteoblasts
- **Cell Biology Seminar, 22.01.2015, Rostock**
Osteoblasts on micro-pillared topographies
- **Life Light & Matter graduate network meeting, 23.01.2015, Rostock**
Cell morphology on micro-grooved titanium
- **12th Welisa Workshop, 13.04.2015, Wustrow**
Comparison of osteoblast behavior on micro-pillared and corundum blasted Ti surfaces
- **13th Welisa Workshop, 05.11.2015, Gremmelin**
Cell signaling in osteoblasts during their attempted phagocytosis of micro-pillars
- **Life Light & Matter graduate network meeting, 22.01.2016, Rostock**
Spiky surface micro-structures provoke phagocytosis in human osteoblasts
- **Euro Bio-Inspired Material Conference 2016, 22.02.2016, Potsdam**
Attempted phagocytosis of titanium surface micro-structures by osteoblasts (short communication)